Emulation and Simulation of Polarization Dependent Loss and Polarization Mode Dispersion in Optical Fibre Communication Systems

Liu, Yangzi

Award date:
2019

Awarding institution:
University of Bath

Emulation and Simulation of Polarization Dependent Loss and Polarization Mode Dispersion in Optical Fibre Communication Systems

submitted by

Yangzi Liu

for the degree of Doctor of Philosophy

of the

University of Bath

Department of Electronic and Electrical Engineering

February 2019

ABSTRACT

Polarization becomes a severe obstacle in optical fibre transmission systems when the bit rate increases. Polarization affects the system performance in two ways: polarization mode dispersion (PMD) and polarization dependent loss (PDL). As PMD has been researched for decades, there are a few methods to compensate the distortion caused by it. However, even though PDL was considered a minor issue to be compared with PMD, the combined effects between PDL and PMD distorts the PMD statistics from its theoretical distribution.

In order to study the PDL statistics distribution over time and long transmission distance in laboratorial environment, it is essential to have a reliable PDL source which is able to generate similar results to the real optical fibre communication systems. As it is not economical to build an emulator with an ultra-long fibre link in a laboratory, a simulation model was developed as an alternative approach to accomplish the mission. To confirm the algorithm of the simulation model works properly, a PDL emulator for short fibre links can be built as a comparison.

In this thesis, a PDL emulator is designed with computer-driven polarization controllers and single mode fibre. The measurement results show that the generated PDL obeys Maxwellian distribution when it is expressed in dB, as expected. This was achieved with just a few polarization controllers. By adjusting the combination of the polarization controllers with different lengths of fibre links, it has been found that the positioning of polarization components can affect the PDL statistics results, even if the total length of the fibre link and the number of the involved polarization components remain the same. The results suggest that with a fixed initial state of polarization, the PDL variance reaches a minimum

when each of the fibre lengths is approximately equal.

The simulation model is developed based on the approach of the Mueller matrix which is described later in the thesis. It is used to examine the statistics of PDL to be compared with the measurement from the emulator for short fibre link, in order to confirm it is reliable for long distance simulation. After that, it is extended to simulate a long distance transmission system.

A simulation model for pulse propagation has also been developed. It is used to investigate the effects of polarization in fibre communication systems. The simulation focuses on the signal attenuation caused by chromatic dispersion, nonlinear effects and polarization. The approach of optical phase conjugation (OPC) is also applied to compensate for the attenuation. Results show that the pulse widening caused by chromatic dispersion and nonlinear effects can be recovered by OPC. However, due to randomness, the signal distortion caused by polarization cannot be recovered with OPC.

The pulse simulation model was altered to study the impact on signal-to-noise ratio caused by the combined effect of PMD and thermal noise. An optical eye diagram was formed and the results showed that PMD contributes horizontally reducing the eye width and noise contributes vertically reducing the eye height. A numerical approach was provided to reduce the pulse jitter caused by PMD and it worked well to increase eye width.

The pulse simulation model was also altered to study the combined effects of PMD and nonlinearity. The results showed that polarization mode dispersion can distort the pulse shape which partly prevents the optical phase conjugation's function recovering the pulse spreading from nonlinearity. The results also showed the similarity between the combined effects of PMD and PDL and the combined effect of fibre nonlinearity and PMD. That leads to an conclusion that the combined effect of PMD and PDL can be achieved with the combined effect of PMD and nonlinearity followed by an attenuator.

ACKNOWLEDGEMENTS

I would like to acknowledge my supervisors Dr. Peter Shepherd, Dr. Duncan Allsopp and Dr. Robert Watson for the support, guidance and advice they gave me during the whole project.

I would like to acknowledge my parents and my wife for the support on finance, the understanding and the encouragement.

I would also like to acknowledge all of my friends for friendship, support and encouragement.

ABBREVIATIONS

DGD	Differential group delay.
GPIB	General purpose interface bus
MCVD	Modified chemical vapour deposition
NLS	Nonlinear Schrödinger equation.
OPC	Optical phase conjugation.
PC	Polarization controllers.
PDL	Polarization dependent loss.
PMD	Polarization mode dispersion.
PMF	Polarization-maintaining fibre.
SMF	Single mode fibre.
SOP	State of polarization.
TLS	Turnable laser source.
WDM	Wavelength-division multiplexing.

CONTENTS

LIST OF FIGURES

LIST OF TABLES

CHAPTER 1

INTRODUCTION

1.1 Motivation

The invention of optical fibre in 1955 made high-bandwidth data transmission over ultra-long distance commercially practical. It was developed in 1970 by Corning Glass Works, with attenuation low enough for communication purposes (about 20 dB/km), and at the same time GaAs semiconductor lasers were developed that were compact and therefore suitable for transmitting light through fibre optic cables for long distances [1].

The first commercial fibre-optic communications system was developed after some research from 1975, with an operating wavelength around 0.8 μm, GaAs semiconductor lasers was used. The bit rate of this first-generation communication system was 45 Mbit/s, with repeater spacing of up to 10 km. On 22 April 1977, the first live telephone traffic was sent through fibre at 6 Mbit/s by General Telephone and Electronics in Long Beach, California [2].

The second generation of commercial fibre-optic communication was developed in the early 1980s, with an operating wavelength of 1.3 μm. The laser source was made from InGaAsP semiconductor. At the beginning, the systems were limited by multi-mode fibre dispersion, until 1981 when the single-mode fibre was found to make a great improvement on system performance. However,

there was still the limitation that it was difficult to develop the practical connectors that were capable of working with single mode fibre. By 1987, these systems were operating at bit rates of up to 1.7 Gb/s with repeater spacing up to 50 km [3, 4].

Third-generation fibre-optic systems had a operating wavelength of 1550 nm and a loss figure of about 0.2 dB/km. The production of Indium Gallium Arsenide and the development of the Indium Gallium Arsenide photodiode by Nahory [5] made a huge contribution to this. The earlier difficulties with pulse-spreading were solved by using dispersion-shifted fibres designed to have minimal dispersion at 1550 nm or by limiting the laser spectrum to a single longitudinal mode. By this time InGaAsP semiconductor lasers were used at this wavelength. These developments described above eventually allowed this generation to operate commercially at 2.5 Gbit/s with repeater spacing in excess of 100 km [6].

In order to reduce the need for repeaters, optical amplification was used in the fourth generation [7]. Meanwhile, wavelength-division multiplexing was used to increase data capacity [8] . These two improvements doubled the system capacity every 6 months from 1992 to 2001, until a bit rate of 10 Tb/s was reached [9]. The record was beaten again in 2006, when a bit-rate of 14 Tbit/s was reached over a single 160 km line using optical amplifiers [10].

The fifth generation of fibre-optic communications focused on the techniques of extending the wavelength range over which a WDM system can operate. The conventional wavelength window, known as C band, covers the wavelength range 1530-1570 nm. The fibre has a low-loss window, which extended the range to 1300-1650 nm [11]. At the same time, the propagation of optical soliton pulses which preserve their shape by counteracting the effects of dispersion caused by the nonlinear effects of the fibre, was demonstrated [12].

With the development of optical fibre communication systems, multiple solutions of signal attenuation compensation caused by fibre loss, nonlinearity and chromatic dispersion have been well researched. From this, polarization has become one of the most significant obstacles to modern communications, especially for high rate transmissions [13, 14]. Polarization changes happen because of the asymmetry of optical fibre factors on the two orthogonal axes, such as asymmetry

of dispersion parameters which causes polarization mode dispersion (PMD) and asymmetry in loss parameters which causes polarization dependent loss (PDL). The effect of PMD and PDL in optical fibre transmission systems is that signals will become more distorted as the bit rate increases, and leads to an increased bit error rate.

PMD introduces modal dispersion and is usually associated with single mode fibres. It is measured in picoseconds per square root of kilometre ($ps/\sqrt{km}$) as it is proportional to the square root of the length of the fibre. In early experiments PMD was found in the range from 0.05 to 1.0 $ps/\sqrt{km}$ [15]. The causes of PMD are birefringence or differential group delay.

PMD becomes the major limiting factor in optical transmission systems when bit rates exceed 10 Gb/s [16], and this makes problems more severe (as high as $10ps/\sqrt{km}$ in the 1980s, compared with a value of $0.1ps/\sqrt{km}$ in present-day fibre systems).

As PMD is a significant obstacle to fibre communication systems, it has been well researched for more than three decades and many measurement and compensation technologies have been developed. On the other hand, compared with PMD, PDL is less important so has not attracted as much attention. However, due to the facts that PDL reduces the signal-to-noise ratio and interacts with PMD[17, 18], it will improve the system performance if it can be reasonably reduced.

1.2 Aims

The fibre length of the real communication systems can be ultra long, such as hundreds or thousands kilometres, between city and city, country and country, even continent and continent. It is impossible to build an emulator to study the PDL statistical distribution like that. However, it is possible to build a system involving short lengths of fibre, and it can be used to emulate PDL statistics. After confirming that the PDL statistical result matches the theoretical result from previous research, a computer model can be built with the emulator design, to simulate the PDL statistics in longer distance systems.

An ideal practical PDL emulator should have these features: (i) low loss and low connection loss; (ii) high stability and repeatability; (iii) fast control speed; (iv) accurate statistical distributions [19]. As PDL has been researched less than PMD, there are not many PDL emulator designs that can be used as reference. However, PMD emulators can be considered as a point of reference as they can provide the state of polarization (SOP) variance needed and they have been well researched.

A fairly well-known early design of PMD emulator can be constructed with a series of polarization controllers (PC), connected by sections of polarization-maintaining fibres (PMF), see Fig. 1-1. The original design requires at least 13 sets of polarization controllers (it is desirable to enlarge the number of polarization controllers to over 30). Further designs reduced the cost by replacing some of the polarization controllers with more polarization maintaining fibres, with randomly fixed angles between each span of PMF [20]. See Fig. 1-2.

Figure 1-1: *Early design of polarization emulator*

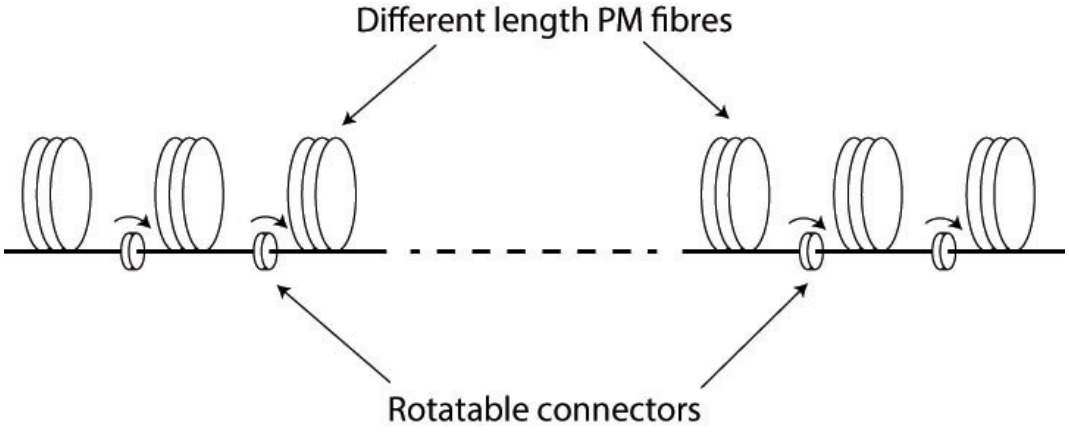

Figure 1-2: *Set up of I. T. Lima's emulator, with 15 polarization controllers [20].*

Various all-order PMD emulation schemes have been demonstrated with early configurations using for example, from twisted fibre sections [21], motor-driven rotatable crystals [22], to more recent designs including a micro-heater and a PMF based emulator [23], a tunable emulator using variable differential group delay (DGD) elements [24] and a coherent programmable PMD source [25].

In this thesis, the aim was to build a novel PDL emulator with fewer elements and have lower cost to achieve similar performance. The newly designed emulator is able to produce reliable PDL effects in the systems, and it can be easily adjusted to emulate the effect of multiple PDL components.

The other aim of this thesis is to study the impact of polarization on digital signalling, and to study the combined effects of polarization and other factors, such as noise and nonlinearity. A proper simulation model will be programmed to achieve these targets. With this simulation model, the mitigating the of polarization effects will also be studied.

1.3 Novel Contributions

In this thesis, a polarization dependent loss (PDL) emulator is built with computer-driven polarization controllers and single mode fibres (SMF). The results show

that it works reliably on generating PDL statistics obeying Maxwellian distribution. The novelty lies in the substantial reduction of polarization controllers required while maintaining required performance and behaviour.

By adjusting the combination of the polarization controllers with different lengths of fibre links, it has been found that the positioning of polarization components (polarization controllers in this case) can affect the PDL statistics, even if the total length of the fibre link and the number of the involved polarization components remain the same. This is possibly because that when PDL components are equally distributed, there is a bigger chance they will self-mitigated the effects which reduce the PDL output eventually. This will be further discussed in later chapterl. The results show that with a fixed initial state of polarization, the PDL variance reaches a minimum when each of the fibre lengths is approximately equal.

A new simulation model has had to be developed to enable the comparison of simulation and emulation results. It was used to examine the statistics of PDL and compared with the measurement from the emulator for a short fibre link in the first instance. Based on the agreement of these results, it has been extended to simulate long distance transmission system. The results from the long distance simulation have found to compare favourably with other published results.

A signal simulation model was also developed to study how a pulse-shaped signal propagates through an optical fibre communication systems. It was also extended to form an optical eye diagram to evaluate the impact to the signal-to-noise ratio caused by the combined effect of polarization mode dispersion and thermal noise. A numerical approach was provided to mitigate the effect of polarization mode dispersion.

This signal simulation model was also extended to study the combined effect of nonlinearity and polarization mode dispersion. The results demonstrated that polarization mode dispersion can distort the pulse shape to partly prevent the optical phase conjugator from recovering the pulse spreading from nonlinearity. The results also showed the similarity between the combined effects of PMD and PDL and the combined effect of fibre nonlinearity and PMD. That leads to

an conclusion that the combined effect of PMD and PDL can be achieved with the combined effect of PMD and nonlinearity followed by an attenuator.

1.4 Thesis Organisation

Chapter 2 introduces the background about the ray model of waveguiding and the derivation of lightwave propagation equation from Maxwell's equations.

Chapter 3 introduces the academic background about optical fibre communication systems which includes the signal attenuation and compensation, polarization mode dispersion and polarization dependent loss.

Chapter 4 describes the methodology this thesis applied, which includes both of the emulator building and simulation coding. To explain how the emulator works, there is a description of the experimental equipment used, the software and the emulator design. To describe the simulation model, critical algorithms are introduced, such as the Monte Carlo method and Split-step Fourier method.

Chapter 5 describes the emulation set-up. This includes emulator calibration, short-term testing, long-term testing and the final emulation. Chapter 5 describes the simulation design, which includes optical pulse propagation with split-step Fourier method and PDL simulation with the Mueller matrix method.

Chapter 6 shows the results comparison of the simulation and emulation. The PDL simulator model was also altered to simulate the scenario of long-distance transmission systems. A pulse simulation model was also programmed to simulate signal propagation over long-distance transmission systems.

Chapter 7 uses the altered signal simulator programmed in Chapter 6 to study the digital signalling. An optical eye diagram was formed, to be used to research the impacts of polarization and thermal noise. A numerical approach was provided to reduce the impact from polarization mode dispersion.

Chapter 8 uses the altered signal simulator programmed in Chapter 6 to study the combined effects of nonlinearity and polarization mode dispersion. Simulations were run in two directions. The first set of simulation focused on how the increased polarization mode dispersion (accumulated over distance increasing) affected the systems. The second set of simulation focused on how the input power affected the systems.

Chapter 9 concludes the research of this thesis and offers some ideas about the continuous research directions to the following researchers.

There is no independent chapter for literature review, as the relevant background literatures were reviewed in each of those chapters.

1.5 Summary

This chapter described the motivation and aim of this research. It listed the novel contributions of the thesis and described the organisation of this thesis.

CHAPTER 2

FUNDAMENTALS OF GUIDED WAVE OPTICS

This chapter reviews the underpinning theory used in the later modelling development. Waveguiding theory helps understanding the basic concept of lightwave propagation through fibre. Maxwell's equations is the foundation of the derivation of the nonlinear lightwave propagation equations, which is the key factor of optical signal simulation.

2.1 Ray Model of Waveguiding

The propagation of a light ray can be treated according to the laws of geometrical optics in a homogeneous change-free media [26]. Because of the fact that a transparent, dielectric medium with a refractive index higher than its surroundings would act as a lightwave guide, a ray model can be built to describe the light waveguiding.

2.1.1 Snell's Law

Refraction at an interface between uniform media of different refractive indexes is governed by Snell's law, which is illustrated in Fig. 2-1. Here a ray of light passes from a medium of higher refractive index n_1 into a medium of lower refractive index n_2. For $0 < \theta < \theta_c$ and $0 < \theta' < \pi/2$, there is

$$n_1 \sin\theta = n_2 \sin\theta', \tag{2.1}$$

where θ and θ' are the angles between incidence and refraction, defined in Fig. 2-1. The angle $\theta = \theta_c$ is defined as the critical angle, which leads to $\theta' = \pi/2$, thus

$$n_1 \sin\theta_c = n_2 \tag{2.2}$$

By keeping increasing θ, when $\theta > \theta_c$ the ray of light would be completely reflected at the boundary, leading to the result of no losses. This is defined as total internal reflection.

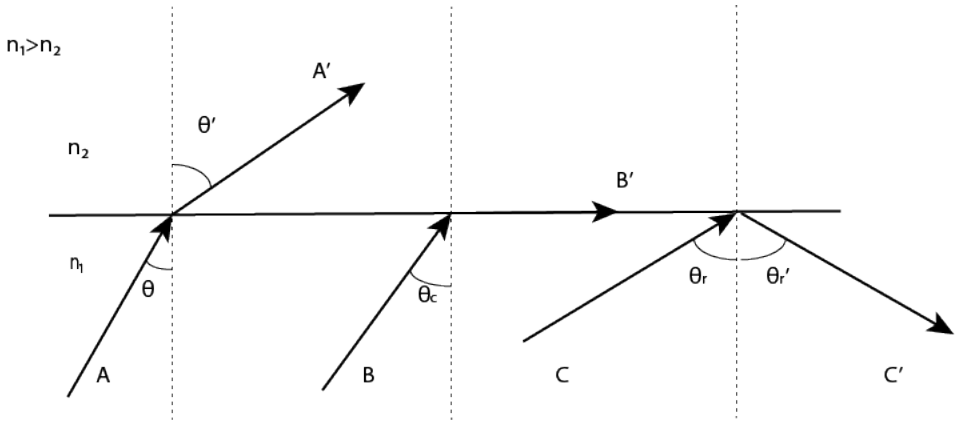

Figure 2-1: *Snell's Law*

2.1.2 Numerical Aperture

Consider a cylindrical glass fibre consisting of an inner core with refractive index n_1, and an outer cladding with refractive index n_2, where $n_1 > n_2$, the cross-section of which is shown in Fig. 2-2. The end face of the fibre is cut at right

angles to the fibre axis. A ray of light enters the end face from the outside (air), with a refractive index n_a. In Fig. 2-2, AA' is an axial ray; BB' is the critical ray for total internal reflection at the interface; ray path CC' is too oblique to reflect at the interface, and passes out into the cladding. The ray of light will propagate unattenuated along the fibre by means of multiple internal reflections provided that the angle of incidence onto the interface between the core and the cladding, θ, is greater than the critical angle θ_c. This requires that the angle of obliqueness to the axis, $\phi = \pi/2 - \theta$ is less than $\phi_m = \pi/2 - \theta_c$. Also, the angle of incidence α is required to be less than a certain value α_m.

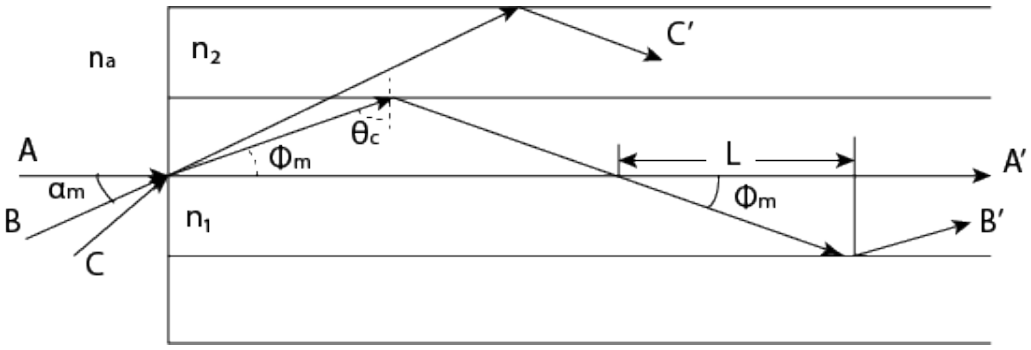

Figure 2-2: *Lightwave propagation in optical fibre.*

Assuming $n_a = 1$ and applying Snell's Law, there is

$$\sin\alpha = n_1 \sin\phi = n_1 \cos\theta, \tag{2.3}$$

For the critical ray, there is

$$\sin\alpha_m = n_1 \sin\phi_m = n_1 \cos\theta_c \tag{2.4}$$

Recalling Eq. (2.3), there is

$$\cos\theta_c = \frac{(n_1^2 - n_2^2)^{1/2}}{n_1} \tag{2.5}$$

which leads to

$$\sin\alpha_m = (n_1^2 - n_2^2)^{1/2} \tag{2.6}$$

By defining

$$\Delta n = n_1 - n_2 \tag{2.7}$$

$$n = \frac{n_1 + n_2}{2} \tag{2.8}$$

then there is

$$\sin \alpha_m = (2n\Delta n)^{1/2} \tag{2.9}$$

It can be seen that the greater the value of α_m, the greater is the proportion of the light incident onto the end face that can be collected by the fibre and be propagated by total internal reflection. The product $n_a \sin \alpha_m$ is defined as the numerical aperture (NA) of the fibre [27], where n_a is the refractive index of the medium surrounding the fibre. Recalling we typically assume $n_a = 1$, yields

$$(NA) = \sin \alpha_m = (2n\Delta n)^{1/2} \tag{2.10}$$

2.1.3 Multipath Time Dispersion

Consider a small diffuse light source, in which the power radiated per unit solid angle in a direction at an angle θ to the surface is given by

$$I(\theta) = I_0 \cos \theta \tag{2.11}$$

where I_0 is the initial power. The total power, ϕ_0, emitted by the source can be calculated by integrating $I(\theta)$ over all forward directions,

$$\phi_0 = \int_0^{\pi/2} (I_0 \cos\theta)(2\pi)(\sin\theta) d\theta \tag{2.12}$$

$$= -2\pi I_0 [\frac{1}{2} \cos^2 \theta]_{\theta=0}^{\pi/2} \tag{2.13}$$

$$= \pi I_0 \tag{2.14}$$

Considering the power from such a source can be only collected by an adjacent fibre for angles of incidence no greater than α_m, the collectable power ϕ is

$$\phi = \int_0^{\alpha_m} (I_0 \cos\theta)(2\pi)(\sin\theta)d\theta \tag{2.15}$$

$$= -\pi I_0[\cos^2\theta]_{\theta=0}^{\alpha_m} \tag{2.16}$$

$$= \pi I_0 \sin^2\alpha_m \tag{2.17}$$

$$= \phi_0(NA)^2 \tag{2.18}$$

Therefore, it follows that $\phi/\phi_0 = (NA)^2 = 2n\Delta n$.

In order to increase the collectable power, it is clear that it is necessary to increase both n and Δn. The first thought is to use fibre with high refractive index core and without any cladding, in which total internal reflection will occur at the boundary of the core. However, there are two problems with this approach. First, an electromagnetic disturbance, as known as the evanescent wave, will penetrate the reflecting interface, when the lightwave suffers total internal reflection. This will lead to a significant fraction of power coupling out of the fibre, to cause high attenuation.

Second, even though the lightwave has already propagated through the fibre within total internal reflection, not all of the rays in the launched lightwave propagate along the axis. Some of them propagate with angles to the axis, such as BB' in Fig. 2-2. As the velocity of the lightwave propagation in the medium is given by

$$v = c/n_1 \tag{2.19}$$

where n_1 is the refractive index of the medium. The time of the lightwave propagating through the axial distance L is

$$T_0 = \frac{n_1 L}{c} \tag{2.20}$$

while the propagation time of the ray with the critical angle is

$$T' = \frac{n_1 L}{c\cos\phi_m} = \frac{n_1 L}{c\sin\theta_c} = \frac{n_1^2 L}{n_2 c} \tag{2.21}$$

As they are launched together, they will arrive with a time delay ΔT

$$\Delta T = T' - T_0 = \frac{n_1}{n_2}\frac{L}{c}\Delta n, \tag{2.22}$$

and a pulse will spread during propagation by an amount given by

$$\frac{\Delta T}{L} = \frac{n_1}{n_2}\frac{\Delta n}{c} \tag{2.23}$$

This is known as the multipath time dispersion. This figure for an unclad fibre can be quite large, which leads to signal distortion, such as short pulses become broadened or spread in time [28, 29].

2.1.4 Step-index Fibre

Due to these two problems, a second option is to clad the core with glass having a slightly lower refractive index, known as step-index fibre [29, 30], as shown in Fig. 2-3. There are three effects of this idea:

(i) the attenuation can be greatly reduced if the cladding is high quality and of sufficient thickness to contain the evanescent wave;
(ii) time dispersion can be reduced;
(iii) the light gathering power of the fibre will be reduced.

When $\Delta n \ll n$, the time dispersion of the fibre can be approximated by $\Delta T/L \backsimeq \Delta n/c$.

If taking the typical value as $n = 1.45$ and $\Delta n = 0.02$, the numerical aperture $(NA) = 0.241$, the acceptance angle $\alpha_m = 14°$, the fraction of the optical power from a diffuse source is $(NA)^2 = 5.8\%$, and the time dispersion of the fibre is $67ns/km$.

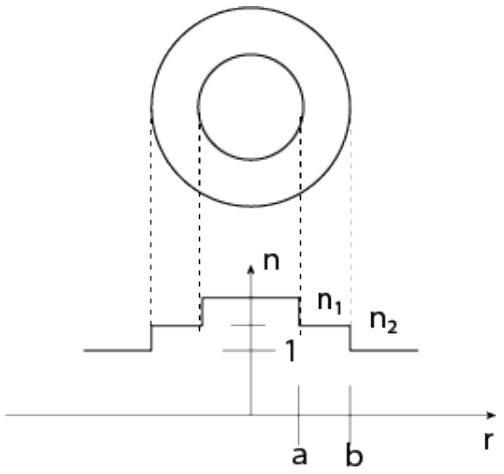

Figure 2-3: *Step-index Fibre.*

2.2 Maxwell's Equations

Maxwell's Equations are a set of four equations which is used to describe the world of electromagnetic phenomena. In particular, these equations are used to describe how electric and magnetic fields propagate, interact, and how they are influenced by objects. Maxwell's equations are [31]

$$\boldsymbol{\nabla} \times \boldsymbol{E}(\boldsymbol{r}, t) = -\frac{\partial}{\partial t}\boldsymbol{B}(\boldsymbol{r}, t) \tag{2.24}$$

$$\boldsymbol{\nabla} \times \boldsymbol{H}(\boldsymbol{r}, t) = \frac{\partial}{\partial t}\boldsymbol{D}(\boldsymbol{r}, t) + \boldsymbol{J}(\boldsymbol{r}, t) \tag{2.25}$$

$$\boldsymbol{\nabla} \cdot \boldsymbol{D}(\boldsymbol{r}, t) = \rho(\boldsymbol{r}, t) \tag{2.26}$$

$$\boldsymbol{\nabla} \cdot \boldsymbol{B}(\boldsymbol{r}, t) = 0 \tag{2.27}$$

In these equations, $\boldsymbol{E}$ represents the electric field vector and $\boldsymbol{H}$ represents the magnetic field vector. $\boldsymbol{D}$ represents the electric flux density vector which is related to $\boldsymbol{E}$ by $\boldsymbol{D} = \epsilon\boldsymbol{E}$, and $\boldsymbol{B}$ represents the magnetic flux density which is related to $\boldsymbol{H}$ by $\boldsymbol{B} = \mu\boldsymbol{H}$ [31]. The terms ϵ and μ represent the permeabilities of medium in $\boldsymbol{E}$ and $\boldsymbol{H}$ respectively. The electric current density is represented by $\boldsymbol{J}$ and ρ represents the volume electric charge density.

By considering non-magnetic media with no free charges only, Maxwell's equa-

tions can be simplified to

$$\boldsymbol{\nabla} \times \boldsymbol{E}(\boldsymbol{r}, t) = -\frac{\partial}{\partial t}\boldsymbol{B}(\boldsymbol{r}, t) \tag{2.28}$$

$$\boldsymbol{\nabla} \times \boldsymbol{B}(\boldsymbol{r}, t) = \mu_0 \frac{\partial}{\partial t}\boldsymbol{D}(\boldsymbol{r}, t) \tag{2.29}$$

$$\boldsymbol{\nabla} \cdot \boldsymbol{D}(\boldsymbol{r}, t) = 0 \tag{2.30}$$

$$\boldsymbol{\nabla} \cdot \boldsymbol{B}(\boldsymbol{r}, t) = 0 \tag{2.31}$$

These coupled equations describe the evolution in position and time of electric and magnetic fields.

2.2.1 Helmholtz Equation

In order to derive the equation which describes the optical signal propagation, $\boldsymbol{B}$ can be eliminated by combining Eq. (2.29) and using $\boldsymbol{D} = \epsilon\boldsymbol{E} + \boldsymbol{P}$ where $\boldsymbol{P}$ is the polarization and can take into account any nonlinear effects, which leads to

$$\boldsymbol{\nabla} \times \boldsymbol{B} = \mu_0\epsilon\frac{\partial}{\partial t}\boldsymbol{E} + \mu_0\frac{\partial}{\partial t}\boldsymbol{P} \tag{2.32}$$

By taking the curl of both sides of Eq. (2.28), there is

$$\boldsymbol{\nabla} \times \boldsymbol{\nabla} \times \boldsymbol{E} = -\frac{\partial}{\partial t}(\boldsymbol{\nabla} \times \boldsymbol{B}) \tag{2.33}$$

which can be also written as

$$\boldsymbol{\nabla}(\boldsymbol{\nabla} \cdot \boldsymbol{E}) - \boldsymbol{\nabla}^2\boldsymbol{E} = -\frac{\partial}{\partial t}(\boldsymbol{\nabla} \times \boldsymbol{B}) \tag{2.34}$$

By combining this with Eq. (2.32), there is

$$\boldsymbol{\nabla}(\boldsymbol{\nabla} \cdot \boldsymbol{E}) - \boldsymbol{\nabla}^2\boldsymbol{E} = -\mu_0\epsilon\frac{\partial^2}{\partial t^2}\boldsymbol{E} - \mu_0\frac{\partial^2}{\partial t^2}\boldsymbol{P} \tag{2.35}$$

As $\boldsymbol{\nabla} \cdot \boldsymbol{E} = 0$ in a homogeneous change-free media, and by recalling $\mu_0 \epsilon = 1/c^2$ where c is the speed of light in vacuum, Eq. (2.35) can be simplified to

$$\boldsymbol{\nabla}^2 \boldsymbol{E} - \frac{1}{c^2} \frac{\partial^2}{\partial t^2} \boldsymbol{E} = \mu_0 \frac{\partial^2}{\partial t^2} \boldsymbol{P} \tag{2.36}$$

By assuming (**i**) the polarization response of the material is instantaneous and (**ii**) the nonlinearity is weak enough to be treated perturbatively, which means

$$\boldsymbol{P} = \epsilon(\chi^{(1)} \boldsymbol{E} + \chi^{(2)} \boldsymbol{E}^2 + \chi^{(3)} \boldsymbol{E}^3 + \cdots) = \boldsymbol{P}_{linear} + \boldsymbol{P}_{nonlinear} \tag{2.37}$$

The precise value of the linear part of the polarization depends on the frequency, which can be expressed in the frequency domain as $\boldsymbol{P}_{linear}(\omega) = \epsilon \chi^{(1)}(\omega) \boldsymbol{E}(\omega)$. Eq. (2.36) can be expressed in the frequency domain by recalling that for harmonic time variations $\dfrac{\partial}{\partial t} \rightarrow j\omega$

$$(\boldsymbol{\nabla}^2 + \frac{\omega^2}{c^2}(1 + \chi^{(1)})) \boldsymbol{E}'(\omega) = -\mu_0 \omega^2 \boldsymbol{P}_{nonlinear} \tag{2.38}$$

when the nonlinear effect is negligible $\boldsymbol{P}_{nonlinear} = 0$ in Eq. (2.38) can be neglected, so Eq. (2.15) can be re-written as

$$(\boldsymbol{\nabla}^2 + \frac{\omega^2}{c^2}(1 + \chi^{(1)})) \boldsymbol{E}'(\omega) = 0 \tag{2.39}$$

where $\boldsymbol{E}'(\omega) = \int_{-\infty}^{\infty} \boldsymbol{E} \exp(j\omega t) dt$.

As $\chi^{(1)}$ is in the frequency domain, which is in general complex, and the frequency dependent dielectric constant ε is defined as $\varepsilon = 1 + \chi^{(1)}$, ε is in general complex as well. Its real and imaginary parts can be related to the refractive index n and the absorption coefficient α respectively, which is defined as $\varepsilon = (n + i\alpha c/2\omega)^2$.

Because of the low optical losses in fibres in the wavelength region of interest, the imaginary part of ε is small enough in comparison to the real part to

be ignored, to make $\varepsilon = 1 + \chi^{(1)} \approx n^2$. Then Eq. (2.38) can be rewritten as

$$\boldsymbol{\nabla}^2 \boldsymbol{E}' + \frac{\omega^2}{c^2} n^2 \boldsymbol{E}' = 0 \tag{2.40}$$

Eq. (2.40) is called the Helmholtz equation, whose solutions when applied to optical fibre are defined as fibre modes [32].

2.2.2 Fibre Modes

Optical fibre is a flexible, transparent fibre made by drawing glass (silica) or plastic, and wrapped by multiple layers of materials, as shown in Fig. 2-4. Typically, it includes a transparent core (layer 1 in Fig. 2-4) surrounded by a transparent cladding material (layer 2 in Fig. 2-4) with a lower index of refraction. Light is kept in the core by the phenomenon of total internal reflection which causes the fibre to act as a waveguide. Both core and cladding are protected by the buffer (layer 3 in Fig. 2-4) from damage and moisture. The jacket (layer 4 in Fig. 2-4) provides a protective robust outer layer [33].

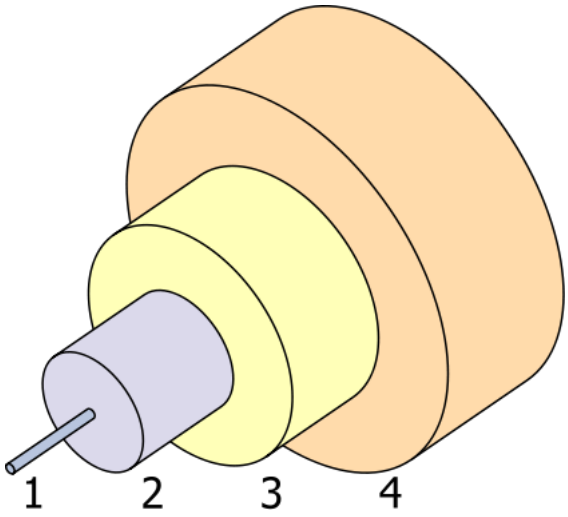

Figure 2-4: *Step-index Fibre [33].*

A number of guided modes can be supported by optical fibres at any frequency.

The spatial distribution of these modes $\boldsymbol{E}(r,\omega)$ is a solution of the Eq. (2.40). Because of the cylindrical symmetry of fibres, Eq. (2.40) can be expressed in cylindrical coordinates ρ, ϕ and z as [34]

$$\frac{\partial^2 \boldsymbol{E}}{\partial \rho^2} + \frac{1}{\rho}\frac{\partial \boldsymbol{E}}{\partial \rho} + \frac{1}{\rho^2}\frac{\partial^2 \boldsymbol{E}}{\partial \phi^2} + \frac{\partial^2 \boldsymbol{E}}{\partial z^2} + n^2 k_0^2 \boldsymbol{E} = 0 \tag{2.41}$$

where $k_0 = \omega/c = 2\pi/\lambda$. Similarly, for the magnetic field

$$\frac{\partial^2 \boldsymbol{H}}{\partial \rho^2} + \frac{1}{\rho}\frac{\partial \boldsymbol{H}}{\partial \rho} + \frac{1}{\rho^2}\frac{\partial^2 \boldsymbol{H}}{\partial \phi^2} + \frac{\partial^2 \boldsymbol{H}}{\partial z^2} + n^2 k_0^2 \boldsymbol{H} = 0 \tag{2.42}$$

Both $\boldsymbol{E}$ and $\boldsymbol{H}$ satisfy Maxwell's equation, so only two components out of six are independent. By choosing $\boldsymbol{E}_z$ and $\boldsymbol{H}_z$ as the independent components, $\boldsymbol{E}_\rho$, $\boldsymbol{E}_\phi$, $\boldsymbol{H}_\rho$ and $\boldsymbol{H}_\phi$ can be expressed in terms of $\boldsymbol{E}_z$ and $\boldsymbol{H}_z$. Exploiting the geometry of an optical fibre, wave equation for $\boldsymbol{E}_z$ can be solved to a very good approximation by using the method of separation of variables, resulting in the following general form for the amplitude of electric field:

$$\boldsymbol{E}_z(r,\omega) = A(\omega)F(\rho)\exp(\pm jm\phi)\exp(j\beta z) \tag{2.43}$$

where A is a normalization constant, β is the propagation constant, m is an integer and $F(\rho)$ is the solution of

$$\frac{\partial^2 \boldsymbol{F}}{\partial \rho^2} + \frac{1}{\rho}\frac{\partial \boldsymbol{F}}{\partial \rho} + (n^2 k_0^2 - \beta^2 - \frac{m^2}{\rho^2})F = 0 \tag{2.44}$$

where

$$n = \begin{cases} n_1, \rho \leq a \\ n_2, \rho > a \end{cases}$$

The solution of Eq. (2.44) is in term of Bessel functions [35], and its general solution inside the core can be written as

$$F(\rho) = C_1 J_m(\kappa\rho) + C_2 N_m(\kappa\rho) \tag{2.45}$$

where J_m is the Bessel function, N_m is the Neumann function, and

$$\kappa = (n_1^2 k_0^2 - \beta^2)^{1/2} \tag{2.46}$$

The constants C_1 and C_2 are determined using the boundary conditions. As $N_m(\kappa\rho)$ has a singularity at $\rho = 0$, $C_2 = 0$ for a physically meaningful solution. The constant C_1 can be absorbed in A appearing in Eq. (2.43). Therefore,

$$F(\rho) = J_m(\kappa\rho), \rho \leq a \tag{2.47}$$

In the cladding region, the concept of electromagnetic power guidance implies solutions should decay exponentially for large ρ. The modified Bessel function K_m represents such a solution. Therefore,

$$F(\rho) = K_m(\gamma\rho), \rho \geq a \tag{2.48}$$

where $\gamma = (\beta^2 - n_2^2 k_0^2)^{1/2}$.

The magnetic field component $\boldsymbol{H}_z$ can be obtained by following the same procedure. Because of the boundary condition, the tangential components of $\boldsymbol{E}$ and $\boldsymbol{H}$ are continuous across the core-cladding interface. It requires that $\boldsymbol{E}_z$, $\boldsymbol{H}_z$, $\boldsymbol{E}_\phi$ and $\boldsymbol{H}_\phi$ have the same value when $\rho = a$ is approached from inside or outside the core. The equality of these field components at $\rho = a$ leads to an eigenvalue equation whose solutions determine the propagation constant β for the fibre modes. With the relation of

$$\kappa^2 + \gamma^2 = (n_1^2 - n_2^2)k_0^2, \tag{2.49}$$

the eigenvalue equation can be written as

$$\left[\frac{J'_m(\kappa a)}{\kappa J_m(\kappa a)} + \frac{K'_m(\gamma a)}{\gamma K_m(\gamma a)}\right]\left[\frac{J'_m(\kappa a)}{\kappa J_m(\kappa a)} + \frac{n_2^2}{n_1^2}\frac{K'_m(\gamma a)}{\gamma K_m(\gamma a)}\right] = \left(\frac{m\beta k_0(n_1^2 - n_2^2)}{a n_1 \kappa^2 \gamma^2}\right)^2 \tag{2.50}$$

where a prime denotes differentiation with respect to the argument [29, 36, 37].

Single-Mode Condition

The number of modes supported by a specific fibre at a given wavelength depends on its design parameters, namely the core radius a and the difference between

the refractive indexes of the core (n_1) and the cladding (n_2), ie. $n_1 - n_2$. An important parameter for each mode is its cut-off frequency. This frequency is determined by the condition $\gamma = 0$. The value of κ when $\gamma = 0$ for a given mode determines the cut-off frequency from Eq. (2.49). It is useful to define a normalized frequency V by the relation [34]

$$V = \kappa_c a = k_0 a (n_1^2 - n_2^2)^{1/2}, \qquad k_0 = \frac{2\pi}{\lambda} \tag{2.51}$$

where κ_c is obtained from Eq. (2.49) by setting $\gamma = 0$.

A single-mode fibre supports only the HE_{11} mode, also referred to as the fundamental mode. All other modes are beyond cut-off if the parameter $V < V_c$, where V_c is the smallest solution of $J_0(V_c) = 0$ or $V_c \approx 2.405$. The cut-off wavelength λ_c for single-mode fibres can be obtained by using $k_0 = 2\pi/\lambda_c$ and $V = 2.405$ in Eq. (2.51). For a typical value $n_1 - n_2 = 0.005$ for the index difference, $\lambda_c = 1.2\mu m$ for $a = 4\mu m$, indicating that such a fibre supports a single mode only for $\lambda > 1.2\mu m$. In practice, the core radius should be below $5\mu m$ for a fibre to support a single mode for wavelengths in the visible region.

Fundamental Mode

The field distribution $\boldsymbol{E}(\boldsymbol{r}, t)$ corresponding to the HE_{11} mode has three non-zero components E_ρ, E_ϕ and E_z, or in Cartesian coordinates E_x, E_y and E_z. Among these, either E_x or E_y dominates. Therefore, to a good degree of approximation, the fundamental fibre mode is linearly polarized in either x or y direction depending on whether E_x or E_y dominates. In this respect, even a single-mode fibre is not truly single mode because it can support two modes of orthogonal polarizations. The notation LP_{mn} is sometimes used to denote the linearly polarized modes, which are approximate solutions of Eq. (2.41). The fundamental mode HE_{11} corresponds to LP_{01} in this notation [29].

The two orthogonally polarized modes of a single-mode fibre are degenerate (i.e., they have the same propagation constant) under ideal conditions. In practice, irregularities such as random variations in the core shape and size along the

fibre length break this degeneracy slightly, mix the two polarization components randomly, and scramble the polarization of the incident light as it propagates down the fibre. Assuming that the incident light is polarized along a principal axis, the electric field for the fundamental fibre mode HE_{11} is approximately given by

$$\boldsymbol{E}(\boldsymbol{r},\omega) = \widehat{x}A(\omega)F(x,y)\exp[j\beta(\omega)z] \tag{2.52}$$

where $A(\omega)$ is a normalization constant. The transverse distribution inside the core is found to be

$$F(x,y) = J_0(\kappa\rho), \rho \leq a, \tag{2.53}$$

where $\rho = (x^2+y^2)^{1/2}$ is the radial distance. Outside the fibre core, the field decays exponentially as

$$F(x,y) = (a/\rho)^{1/2}J_0(\kappa a)\exp[-\gamma(\rho-a)], \rho \geq a \tag{2.54}$$

The propagation constant $\beta(\omega)$ is obtained by solving the eigenvalue equation. Its frequency dependence results not only from the frequency dependence of n_1 and n_2 but also from the frequency dependence of κ. The former is referred to as material dispersion while the latter is called waveguide dispersion.

The modal distribution $F(x,y)$ is cumbersome in practice, so the fundamental fibre mode is often approximated by a Gaussian distribution of the form [34]

$$F(x,y) \approx \exp[-(x^2+y^2)/w^2] \tag{2.55}$$

where the width parameter w is determined by fitting the exact distribution to a Gaussian form or by following a variational procedure.

2.2.3 Pulse Propagation Equation and Nonlinear Schrödinger Equation

In order to derive a basic equation in which both types of dispersion and nonlinear effects are included, it is necessary to start with the wave equation. Recalling Eq. (2.36) and Eq. (2.37), the wave equation is written as

$$\boldsymbol{\nabla}^2\boldsymbol{E} - \frac{1}{c^2}\frac{\partial^2}{\partial t^2}\boldsymbol{E} = \mu_0\frac{\partial^2}{\partial t^2}\boldsymbol{P}_{linear} + \mu_0\frac{\partial^2}{\partial t^2}\boldsymbol{P}_{nonlinear} \tag{2.56}$$

where there are [38]

$$\boldsymbol{P}_{linear}(\boldsymbol{r},t) = \varepsilon_0 \int_{-\infty}^{t} \chi^{(1)}(t-t') \cdot \boldsymbol{E}(\boldsymbol{r},t')dt' \tag{2.57}$$

$$\boldsymbol{P}_{nonlinear}(\boldsymbol{r},t) \approx \varepsilon_0 \int_{-\infty}^{t} dt_1 \int_{-\infty}^{t} dt_2 \int_{-\infty}^{t} dt_3 \times \chi^{(3)}(t-t_1, t-t_2, t-t_3) \tag{2.58}$$

$$\vdots \boldsymbol{E}(\boldsymbol{r},t_1)\boldsymbol{E}(\boldsymbol{r},t_2)\boldsymbol{E}(\boldsymbol{r},t_3) \tag{2.59}$$

Nonlinear Pulse Propagation

In order to solve Eq. (2.56), it is necessary to simplify it by making several assumptions. First, $\boldsymbol{P}_{nonlinear}$ is treated as a small perturbation to $\boldsymbol{P}_{linear}$. This is proper because nonlinear changes in the refractive index are $< 10^{-6}$ in practice [34]. Second, the optical field is assumed to maintain its polarization along the fibre length so that a scalar approach is valid. Last, the optical field is assumed to be quasi-monochromatic, i.e., the pulse spectrum, centred at ω_0 , is assumed to have a spectral width $\Delta\omega$ such that $\Delta\omega/\omega_0 \ll 1$. Since $\omega_0 \sim 10^{-15}s^{-1}$, the last assumption is valid for pulses as short as 0.1 ps. In the slowly varying envelope approximation adopted here, it is useful to separate the rapidly varying part of the electric field in the form

$$\boldsymbol{E}(\boldsymbol{r},t) = \frac{1}{2}\widehat{x}[E(\boldsymbol{r},t)\exp(-j\omega_0 t) + c.c.] \tag{2.60}$$

where $\widehat{x}$ is the polarization unit vector and $\boldsymbol{E}(\boldsymbol{r},t)$ is a slowly varying function of time (relative to the optical period) and *c.c.* stands for complex conjugate. Similarly, the polarization components can be expressed as

$$\boldsymbol{P}_{linear}(\boldsymbol{r},t) = \frac{1}{2}\widehat{x}[P_{linear}(\boldsymbol{r},t)\exp(-j\omega_0 t) + c.c.] \tag{2.61}$$

$$\boldsymbol{P}_{nonlinear}(\boldsymbol{r},t) = \frac{1}{2}\widehat{x}[P_{nonlinear}(\boldsymbol{r},t)\exp(-j\omega_0 t) + c.c.] \tag{2.62}$$

Combining Eq. (2.57) and Eq. (2.61) yields

$$P_{linear}(\boldsymbol{r},t) = \varepsilon_0 \int_{-\infty}^{\infty} \chi^{(1)}_{\chi\chi}(t-t')E(\boldsymbol{r},t')\exp[j\omega_0(t-t')]dt' \tag{2.63}$$

$$= \frac{\varepsilon_0}{2\pi} \int_{-\infty}^{\infty} \tilde{\chi}^{(1)}_{\chi\chi}(\omega)\tilde{E}(\boldsymbol{r},\omega-\omega_0)\exp[-j(\omega-\omega_0)t]d\omega \tag{2.64}$$

where $\tilde{E}(\boldsymbol{r},\omega)$ is the Fourier transform of $E(\boldsymbol{r},t)$ [34].

The nonlinear component $P_{nonlinear}(\boldsymbol{r},t)$ can be obtained by combining Eq. (2.58) and Eq. (2.62). Considerable simplification occurs if the nonlinear response is assumed to be instantaneous so that the time dependence of $\chi^{(3)}$ in Eq. (2.58) is given by the product of three delta functions of the form $\delta(t-t_1)$. Eq. (2.58) then can be simplified to

$$\boldsymbol{P}_{nonlinear}(\boldsymbol{r},t) = \varepsilon_0 \chi^{(3)} \vdots \boldsymbol{E}(\boldsymbol{r},t)\boldsymbol{E}(\boldsymbol{r},t)\boldsymbol{E}(\boldsymbol{r},t) \tag{2.65}$$

By combining Eq. (2.60), Eq. (2.65) and Eq. (2.62), the nonlinear component can be re-written as

$$P_{nonlinear}(\boldsymbol{r},t) \approx \varepsilon_0 \varepsilon_{nonlinear} E(\boldsymbol{r},t) \tag{2.66}$$

where the nonlinear contribution to the dielectric constant is defined as

$$\varepsilon_{nonlinear} = \frac{3}{4}\chi^{(3)}_{\chi\chi\chi\chi}|E(\boldsymbol{r},t)|^2 \tag{2.67}$$

$\varepsilon_{nonlinear}$ is treated as a constant during the derivation of the propagation equation. The approach is proper in the view of the slowly varying envelope approximation and the perturbative nature of $P_{nonlinear}$. By substituting Eq. (2.60), (2.61) and (2.62) into Eq. (2.56), the Fourier transform $\tilde{E}(r,\omega-\omega_0)$ is found to satisfy the Helmholtz equation

$$\nabla^2\tilde{E} + \varepsilon(\omega)k_0^2\tilde{E} = 0 \tag{2.68}$$

where

$$\varepsilon(\omega) = 1 + \tilde{\chi}^{(1)}_{\chi\chi}(\omega) + \varepsilon_{nonlinear} \tag{2.69}$$

Eq. (2.68) can be solved by using the method of separation of variables. Assuming a solution of the form

$$\tilde{E}(\boldsymbol{r},\omega-\omega_0) = F(x,y)\tilde{A}(z,\omega-\omega_0)\exp(j\beta_0 z) \tag{2.70}$$

where $\tilde{A}(z,\omega)$ is a slowly varying function of z and β_0 is the wave number to be determined later, Eq. (2.68) leads to the following two equations for $F(x,y)$ and $\tilde{A}(z,\omega)$

$$\frac{\partial^2 F}{\partial x^2} + \frac{\partial^2 F}{\partial y^2} + [\varepsilon(\omega)k_0^2 - \tilde{\beta}^2]F = 0, \tag{2.71}$$

$$2j\beta_0 \frac{\tilde{A}}{z} + (\tilde{\beta}^2 - \beta_0^2)\tilde{A} = 0 \tag{2.72}$$

The dielectric constant $\varepsilon(\omega)$ in the equation above can be approximated by

$$\varepsilon = (n + \Delta n)^2 \sim n^2 + 2n\Delta n \tag{2.73}$$

where the small perturbation Δn is given by

$$\Delta n = n_2|E|^2 + \frac{j\tilde{\alpha}}{2k_0} \tag{2.74}$$

The equation of $F(x,y)$ can be solved using first-order perturbation theory [39]. We first replace ε with n^2 and obtain the modal distribution $F(x,y)$, and the corresponding wave number $\beta(\omega)$. For a single-mode fibre, $F(x,y)$ corresponds to the modal distribution of the fundamental fibre mode HE_{11} given by Eq. (2.53) and (2.54), or by the Gaussian approximation (2.55). Then the effect of Δn is included in Eq. (2.71). In the first-order perturbation theory, Δn does not affect the modal distribution $F(x,y)$. However, the eigenvalue $\tilde{\beta}$ becomes

$$\tilde{\beta}(\omega) = \beta(\omega) + \Delta\beta \tag{2.75}$$

where

$$\Delta\beta = \frac{k_0 \int\int_{-\infty}^{\infty} \Delta n|F(x,y)|^2 dxdy}{\int\int_{-\infty}^{\infty} |F(x,y)|^2 dxdy} \tag{2.76}$$

Recalling Eq. (2.60) and (2.70), the electric field $\boldsymbol{E}(\boldsymbol{r},t)$ can be written as

$$\boldsymbol{E}(\boldsymbol{r},t) = \frac{1}{2}\widehat{x}\{F(x,y)A(z,t)\exp[j(\beta_0 z - \omega_0 t)] + c.c.\} \tag{2.77}$$

where $A(z,t)$ is the slowly varying pulse envelope. The Fourier transform $\tilde{A}(z,\omega-\omega_0)$ of $A(z,t)$ can be written as

$$\frac{\partial \tilde{A}}{\partial z} = j[\beta(\omega) + \Delta\beta - \beta_0]\tilde{A} \tag{2.78}$$

By taking the inverse Fourier transform of Eq. (2.78), the propagation equation of $A(z,t)$ in the time domain can be obtained. However, an exact functional form of $\beta(\omega)$ is rarely known. The approach is to expand $\beta(\omega)$ in a Taylor series about the carrier frequency ω_0 as

$$\beta(\omega) = \beta_0 + (\omega-\omega_0)\beta_1 + \frac{1}{2}(\omega-\omega_0)^2\beta_2 + \frac{1}{6}(\omega-\omega_0)^3\beta_3 + \cdots \tag{2.79}$$

where

$$\beta_m = (\frac{d^m\beta}{d\omega^m})_{\omega=\omega_0}, (m = 1, 2, \cdots) \tag{2.80}$$

If the spectral width $\Delta\omega \ll \omega_0$, the cubic and higher-order terms in this expansion are generally negligible. By substitute Eq. (2.79) into Eq. (2.78) and taking the inverse Fourier transform by using

$$A(z,t) = \frac{1}{2\pi}\int_{-\infty}^{\infty} \tilde{A}(z,\omega-\omega_0)\exp[-j(\omega-\omega_0)t]d\omega \tag{2.81}$$

The term $\omega-\omega_0$ is replaced by the differential operator $j(\partial/\partial t)$ in the Fourier transform operation. This yields

$$\frac{\partial A}{\partial z} = -\beta_1\frac{\partial A}{\partial t} - \frac{j\beta_2}{2}\frac{\partial^2 A}{\partial t^2} + j\Delta\beta A \tag{2.82}$$

The term with $\Delta\beta$ includes the effect of fibre loss and nonlinearity. By using Eqs. (2.74) and (2.76), $\Delta\beta$ can be evaluated and substituted in (2.82). The result is

$$\frac{\partial A}{\partial z} + \beta_1\frac{\partial A}{\partial t} + \frac{j\beta_2}{2}\frac{\partial^2 A}{\partial t^2} + \frac{\alpha}{2}A = j\gamma|A|^2A \tag{2.83}$$

where α is the loss figure and the nonlinear parameter γ is defined as

$$\gamma = \frac{n_2\omega_0}{cA_{eff}} \tag{2.84}$$

where A_{eff} is the effective core area [34].

Nonlinear Schrödinger Equation

Equation (2.83) needs to be modified for ultra-short optical pulse (width is close to or <1 ps). The spectral width of such pulses becomes large enough that several approximations made in the derivation become invalid. The most important limitation turns out to be the neglect of the Raman effect. For pulses with a wide spectrum (>0.1 THz), the Raman gain can amplify the low-frequency components of a pulse by transferring energy from the high-frequency components of the same pulse. This phenomenon is called intra-pulse Raman scattering. As a result of it, the pulse spectrum shifts toward the low-frequency (red) side as the pulse propagates inside the fibre, a phenomenon referred to as the self-frequency shift [40]. The physical origin of this effect is related to the delayed nature of the Raman (vibrational) response.

Starting with Eq. (2.58), non-resonant, incoherent (intensity-dependent) nonlinear effects can be included by assuming the following functional form for the third-order susceptibility [41]

$$\chi^{(3)}(t-t_1, t-t_2, t-t_3) = \chi^{(3)} R(t-t_1)\delta(t-t_2)\delta(t-t_3) \tag{2.85}$$

where $R(t)$ is the nonlinear response function normalized in a manner similar to the delta function. By substituting Eq. (2.85) in Eq. (2.58) the nonlinear polarization is given by

$$\boldsymbol{P}_{nonlinear}(\boldsymbol{r}, t) = \varepsilon_0 \chi^{(3)} \boldsymbol{E}(\boldsymbol{r}, t) \int_{-\infty}^{t} R(t-t_1) |\boldsymbol{E}(\boldsymbol{r}, t_1)|^2 dt_1 \tag{2.86}$$

where it is assumed that the electric field and the induced polarization vectors point along the same direction. The upper limit of integration in Eq. (2.86) extends only up to t because the response function $R(t-t_1)$ must be zero for $t_1 > t$ to ensure causality.

In the frequency domain, $\tilde{E}$ is found to satisfy [42]

$$\nabla^2\tilde{E} + n^2(\omega)k_0^2\tilde{E} = -jk_0\alpha + \chi^{(3)}\frac{\omega^2}{c^2} \int_{-\infty}^{\infty}\int_{-\infty}^{\infty}\tilde{R}(\omega-\omega_1)\times\tilde{E}(\omega_1,z)\tilde{E}(\omega_2,z)\tilde{E}*(\omega_1+\omega_2-\omega,z)d\omega_1 d\omega_2 \tag{2.87}$$

where $\tilde{R}$ is the Fourier transform of R. The terms on the right-hand side can be treated as a small perturbation and first obtaining the modal distribution by neglecting them.

Defining the slowly-varying amplitude $A(z,t)$ as in Eq. (2.77), the pulse evolution inside a single-mode fibre can be given by [43]

$$\frac{\partial A}{\partial z}+\frac{\alpha}{2}A+\beta_1\frac{\partial A}{\partial t}+\frac{j\beta_2}{2}\frac{\partial^2 A}{\partial t^2}-\frac{\beta_3}{6}\frac{\partial^3 A}{\partial t^3} = j\gamma(1+\frac{j}{\omega_0}\frac{\partial}{\partial t})(A(z,t)\int_{-\infty}^{\infty}R(t')|A(z,t-t')|^2dt') \tag{2.88}$$

For pulses wide enough to contain many optical cycles (widths> 10 fs), Eq. (2.88) can be simplified by using a Taylor-series expansion, namely

$$|A(z,t-t')|^2 \simeq |A(z,t)|^2 - t'\frac{\partial}{\partial t}|A(z,t)|^2 \tag{2.89}$$

The approximation is reasonable if the pulse envelope evolves slowly along the fibre. Defining the first moment of the nonlinear response function as

$$T_R \equiv \int_{-\infty}^{\infty}tR(t)dt = f_R\int_{-\infty}^{\infty}th_R(t)dt = f_R\frac{d(Im\tilde{h}_R)}{d(\Delta\omega)}|_{\Delta\omega=0} \tag{2.90}$$

and noting that $\int_0^{\infty}R(t)dt = 1$, Eq. (2.87) can be approximated by

$$\frac{\partial A}{\partial z}+\frac{\alpha}{2}A+\frac{j\beta_2}{2}\frac{\partial^2 A}{\partial t^2}-\frac{\beta_3}{6}\frac{\partial^3 A}{\partial t^3} = j\gamma(|A|^2A+\frac{j}{\omega_0}\frac{\partial}{\partial T}(|A|^2A)-T_RA\frac{\partial|A|^2}{\partial T}) \tag{2.91}$$

Eq. (2.91) is well known as the Nonlinear Schrödinger Equation (NLS). For the pulse of width $T_0 > 5$ ps, the parameters $(\omega_0T_0)^{-1}$ and T_R/T_0 become small enough (<0.001) that the last two terms can be neglected. As the contribution of the third-order dispersion term is also quite small for such pulses (as long as the

carrier wavelength is not too close to the zero-dispersion wavelength), the NLS can be simplified to

$$j\frac{\partial A}{\partial z} + \frac{j\alpha}{2}A - \frac{\beta_2}{2}\frac{\partial^2 A}{\partial t^2} + \gamma(|A|^2 A) = 0 \tag{2.92}$$

2.3 Summary

In this chapter, the ray waveguide model was discussed to help understanding how lightwave propagated through optical fibre. In addition, the lightwave propagation function was derived from the basic Maxwell's equation, which will be used later to program the simulation model for optical pulse propagation in this thesis.

CHAPTER 3

OPTICAL COMMUNICATION SYSTEMS

3.1 Signal Distortion

Optical communication typically involves communication over a distance using variations in the intensity or phase of the light (laser for most of the cases) as the means to carry information. Messages are encoded by the transmitter into optical signals, which propagate through optical fibre to the receivers. The transmitted signals will then be decoded at the receiver. Ideally, the decoded signal will remain the same as the original signal.

However, due to the character of optical fibre and the variability of the deployed environment, the signal will be distorted and attenuated during propagation. The main factors of signal attenuation include loss, chromatic dispersion, noise, nonlinearities, and polarization. Without proper compensation of each of these factors, the signals will be too distorted to be reliably decoded.

3.1.1 Fibre Loss

Power loss during transmission of signal inside the fibre is an important fibre parameter in optical communication. If P_0 is the launched power at the input of a fibre with a length of L, the received power P_T is given by

$$P_T = P_0 \exp(-\alpha L) \tag{3.1}$$

where the attenuation constant α is a measure of total fibre losses from all sources. It is customary to express α in units of dB/km using the relation

$$\alpha_{dB} = -\frac{10}{L} \log(\frac{P_T}{P_0}) = 4.343\alpha \tag{3.2}$$

where Eq.3.1 was used to relate α_{dB} and α [44].

Fibre losses depend on the wavelength of the light beam. Fig. 3-1 shows the loss spectrum of a fibre made by modified chemical vapour deposition (MCVD) process [45]. This fibre exhibits a minimum loss of about $0.2dB/km$ near $1.55\mu m$. Losses are considerably higher at shorter wavelengths, reaching a level of a few dB/km in the visible region. However, compared to most of other materials, such as traditional copper cables, the loss of optical fibre is still incredibly low.

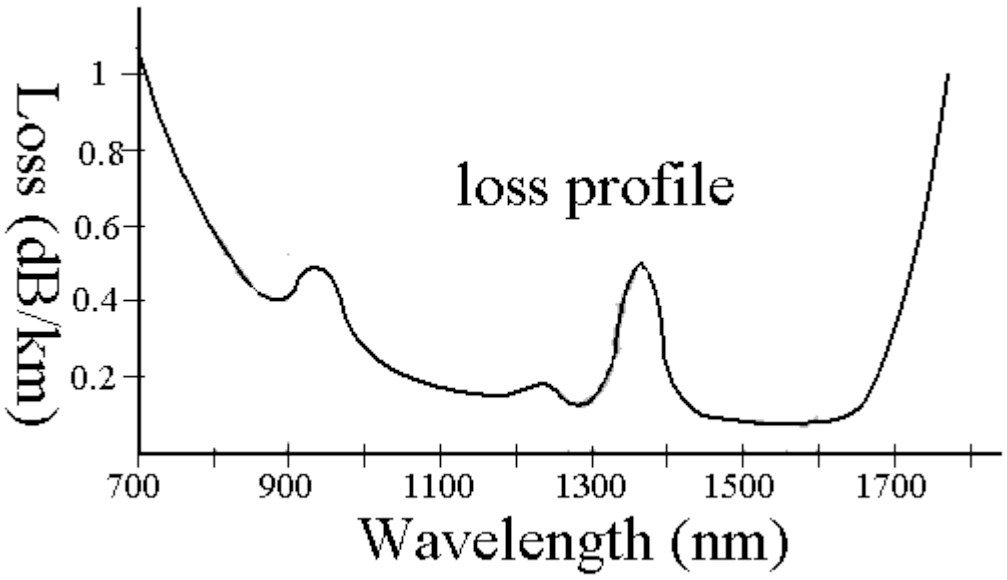

Figure 3-1: *Measured loss spectrum of a single-mode fibre. Dashed curve shows the contribution resulting from Rayleigh scattering [45]*

.

3.1.2 Chromatic Dispersion

When an electromagnetic wave interacts with the bound electrons of a dielectric, the medium response, in general, depends on the optical frequency ω. This property, referred to as chromatic dispersion, becomes manifest through the frequency dependence of the refractive index $n(\omega)$. On a fundamental level, the origin of chromatic dispersion is related to the characteristic resonance frequencies at which the medium absorbs the electromagnetic radiation through oscillations of bound electrons.

Fibre dispersion plays a critical role in the propagation of short optical pulses because different spectral components associated with the pulse travel at different speeds given by $c/n(\omega)$. Even when the nonlinear effects are not important, dispersion-induced pulse broadening can be detrimental for optical communication systems. In the nonlinear regime, the combination of dispersion and nonlinearity can result in a qualitatively different behaviour. Mathematically, the effects of fibre dispersion are accounted for by expanding the mode-propagation constant β in a Taylor series about the frequency ω_0 at which the pulse spectrum is centred:

$$\beta(\omega) = n(\omega)\frac{\omega}{c} = \beta_0 + \beta_1(\omega - \omega_0) + \frac{1}{2}\beta_2(\omega - \omega_0)^2 + \cdots \tag{3.3}$$

where

$$\beta_m = (\frac{d^m\beta}{d\omega^m})_{\omega=\omega_0} \quad (m{=}0,1,2,\cdots) \tag{3.4}$$

The parameters β_1 and β_2 are related to the refractive index n and its derivatives through the relations

$$\beta_1 = \frac{1}{V_g} = \frac{n_g}{c} = \frac{1}{c}(n + \omega\frac{dn}{d\omega}), \tag{3.5}$$

$$\beta_2 = \frac{1}{c}(2\frac{dn}{d\omega} + \omega\frac{d^2n}{d\omega^2}), \tag{3.6}$$

where n_g is the group index and V_g is the group velocity [46]. Physically speaking, the envelope of an optical pulse moves at the group velocity while the parameter β_2 represents dispersion of the group velocity and is responsible for pulse broadening. The phenomenon is known as the group-velocity dispersion (GVD), and β_2 is the GVD parameter [47].

3.1.3 Noise

A simple communication system is the cascade of information source, transmitter, channel (or channels in wavelength-division multiplexing systems), receiver and information user. The transmitter modulates or encodes information supplied by the source into a signal form suitable to the channel. The channel conveys the signal over the space intervening between the transmitter and receiver, the receiver demodulates or decodes the signal into a form suitable for the user.

Randomness or unpredictability can enter a communication system in two ways: the information generated by the source is not be completely predictable,and the communication link may be randomly disturbed. It is in fact a fundamental tenet of information theory that the output of a source must be unpredictable to some degree in order to impart information at all; if the source output were completely predictable, the user could, without communication from the source, state at any instant the entire future output of the source. Disturbances in the communication link can occur in many ways. Both the transmitter and receiver can add noise. If the channel is a radio channel, it can, for example, add atmospheric noise, galactic noise, or man-made interference. In addition, it might be subject to a randomly variable multipath propagation mode which causes a single transmitted signal to appear as a multiplicity of interfering signals at the receiver [48, 49].

Even though the signal and noise in a communications system are random, the behaviour of that system can be determined to a considerable degree if various average properties of the signals and noise are known. Such properties might include the average intensity or power, the distribution of power with frequency, and the distribution of the instantaneous amplitude. The determination of the relations among the various average properties falls into the domain of probability theory and statistics.

3.1.4 Nonlinearities

Like other dielectrics, the response of optical fibre to light becomes nonlinear for intense electromagnetic fields. The origin of the nonlinear response is related to

anharmonic motion of bound electrons under the influence of an applied field. As a result, the total polarization $\mathbf{P}$ induced by electric dipoles is not linear in the electric field $\mathbf{E}$, but satisfies the more general relation as described in Eq. (2.37) [38, 50, 51, 52], In general, $\chi^{(k)}$ is a tensor of rank $k+1$. The linear susceptibility $\chi^{(1)}$ represents the dominant contribution to $\mathbf{P}$. Its effects are included through the refractive index n and the attenuation coefficient α. The second-order susceptibility $\chi^{(2)}$ is responsible for such nonlinear effects as second-harmonic generation and sum-frequency generation [38].

3.2 Polarization in Fibre Communication

Like other vector waves, light can oscillate with more than one orientation. An optical wave of arbitrary polarization can be represented as the superposition of two orthogonally polarized modes. Therefore, a single-mode fibre actually supports two degenerate modes which are orthogonally polarized. These two modes are indistinguishable and have the same propagation constants in an ideal fibre, due to the cylindrical symmetry of the waveguide. However, in real communication systems, perfectly symmetrical fibres do not exist. Even if the technology is able to produce sections of perfectly symmetrical fibres, the environmental conditions in the deployed area can break up the symmetry, for example, stress, bending, twisting and temperature [53].

Certain environmental conditions such as variations in the temperature and stresses in the fibres can change the refractive index of the fibres [54]. When the temperature increases, the refractive index varies over all wavelengths which results in varying wavelength speeds. The refractive indices on x-axis and y-axis are different from each other due to the asymmetry of fibre core in the real situation. Thus the refractive index will have a different value across what can be defined as the horizontal and vertical axis of the fibre core. This difference in the refractive index will result in two orthogonal states of polarization. This will cause birefringence in which the light gets split up into a fast axis (n_x) and a slow axis (n_y), when a ray of light enters a fibre. This phenomenon is also known as double refraction [55]. The birefringence effect is illustrated in Fig. 3-2.

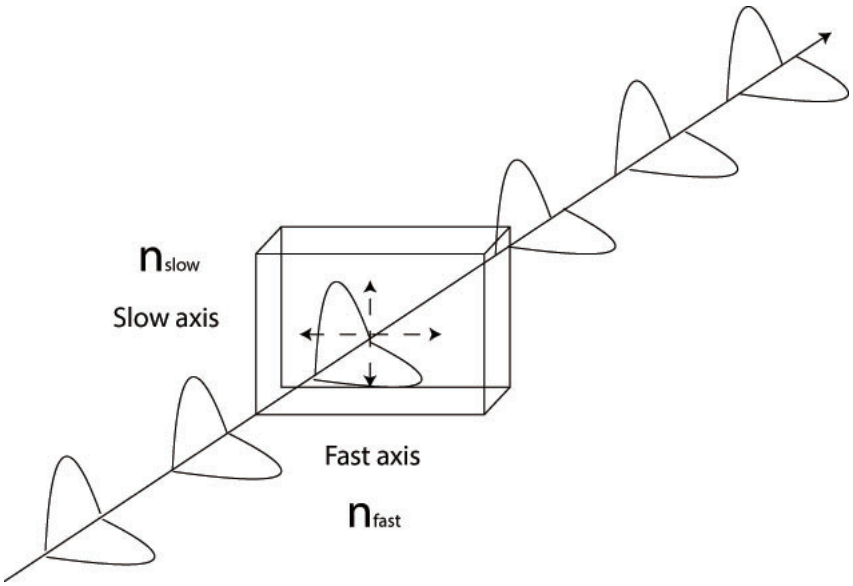

Figure 3-2: *Birefringence Effect [56].*

3.2.1 Polarization Mode Dispersion

The equation for birefringence in terms of difference in the refractive index is given as

$$\Delta\beta = \beta_s - \beta_f \tag{3.7}$$

where $\beta_s = 2\pi n_s/\lambda$ is the phase constant of the slow axis and $\beta_f = 2\pi n_f/\lambda$ is the phase constant of the fast axis.

The birefringence effect of the fibre will cause Differential Group Delay (DGD) between the two polarization states (see Fig. 3-3). The DGD is the difference in propagation time delay between the two polarization states. This differential time delay between the propagation modes is called the first order Polarization Mode Dispersion (PMD). Since this delay depends on the frequency and varies over the bandwidth another dispersion factor arises. This will cause further pulse spreading resulting in second order PMD.

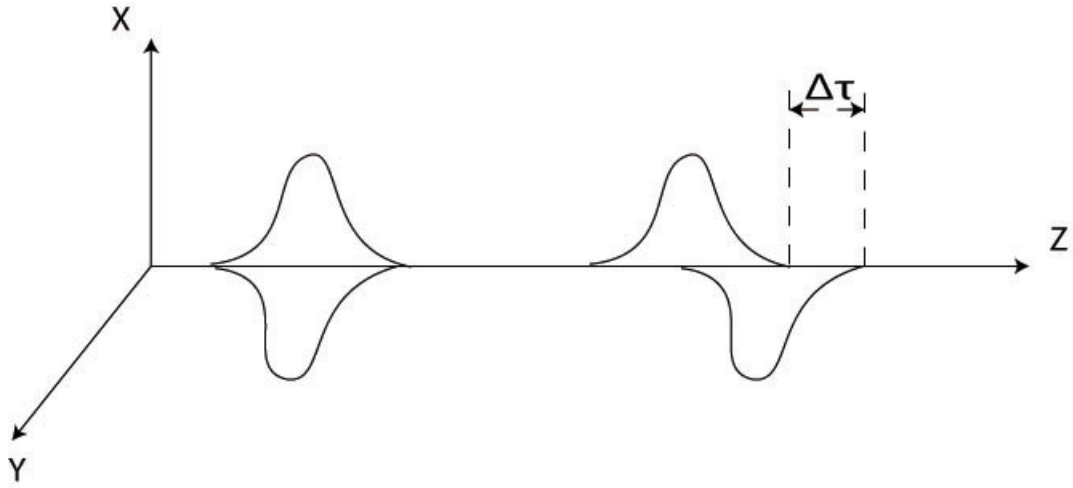

Figure 3-3: *Differential Group Delay (DGD) Effect [57].*

The DGD can be expressed as

$$\Delta\tau_{\mathrm{PMD}} = D_{\mathrm{PMD}}\sqrt{\mathrm{L}} \tag{3.8}$$

where L is the length of the fibre, D_{PMD} is the amount of PMD incurred in the fibre.

As the DGD of two orthogonal modes exist, the signal pulse will be distorted when the two modes are coupled, as shown in Fig. 3-4

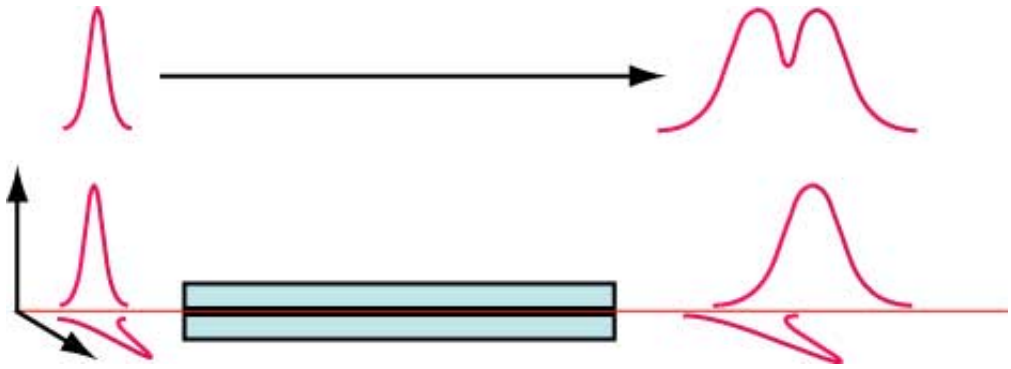

Figure 3-4: *Distorted pulse when the two orthogonal modes coupled.*

Loss of the circular symmetry gives rise to birefringence which means two orthogonal modes travel at different speeds because of the difference of their re-

fractive indices. Birefringence is defined as the difference between the propagation constants of the slow and fast modes [58]:

$$\beta_x - \beta_y = \omega(n_x - n_y)/c = \omega\Delta n/c \tag{3.9}$$

This birefringence is the source of PMD resulting in DGD between two orthogonal modes. As a result of DGD, the slow mode is retarded $\Delta\tau$ seconds with respect to the fast mode.

3.2.2 The Jones Matrix

In 1941 R. C. Jones invented a method of describing polarized light in optics. Polarized light is represented by the Jones vector, and linear optical elements are represented by Jones matrices. When light crosses an optical element the resulting polarization of the emerging light is found by taking the product of the Jones matrix of the optical element and the Jones vector of the incident light [59].

If the input and output states of polarization are stated by using Jones vectors $E_{in}(\omega)$ and $E_{out}(\omega)$, $J(\omega)$ represents the Jones transfer matrix, then the relationships between $E_{in}(\omega)$ and $E_{out}(\omega)$ is

$$E_{out}(\omega) = \boldsymbol{J}(\omega)E_{in}(\omega) \tag{3.10}$$

For ideal fibre with perfect circular symmetry, the transfer matrix $\boldsymbol{J}(\omega)$ is

$$\boldsymbol{J}(\omega) = \begin{pmatrix} e^{-j\beta L} & 0 \\ 0 & e^{-j\beta L} \end{pmatrix} \tag{3.11}$$

However, for real fibres, the Jones transfer matrix is different because the two orthogonal polarization modes have different propagation constants leading to DGD. The Jones transfer matrix for a birefringent fibre with the same length is given by:

$$J(\omega) = \begin{pmatrix} e^{-j\beta_x L} & 0 \\ 0 & e^{-j\beta_y L} \end{pmatrix} \tag{3.12}$$

where the DGD is given by

$$\Delta\tau = L\frac{d}{d\omega}(\beta_x - \beta_y) \tag{3.13}$$

As can be seen from Eq. (3.13), DGD for a short segment of fibre (fixed polarization axis) is directly proportional to the length of the fibre L. If long-haul optical links are taken into account where the length of the single-mode fibre can exceed 10 km, high data rate transmission would be impossible because of the accumulated PMD. Fortunately the situation is not the same for long fibres. This linear length dependence of DGD applies to fibres shorter than 100-1000 m. However, DGD does not accumulate along a long link of fibre in a linear fashion, as the slow axis and fast axis can switch the roles during propagation. The DGD can be self-mitigated during this process and it is totally random. While talking about long fibres, they can be modelled as the concatenation of many short fibre sections whose polarization axis are fixed over their lengths.

These small sections are all independent from each other and changing continuously (over time scales as small as milliseconds) to emphasize the statistical random nature of PMD. Because of random variations in the perturbations along the fibre, the DGD in one section may either add to or subtract from another section of the fibre. As a result of this, mean DGD in long fibre accumulates in a random-walk-like fashion leading to a square-root length dependence. PMD is a statistical process, it has an associated probability density function which is Maxwellian.

Since PMD modelling of long single-mode fibres is accomplished by concatenation of many short fibre sections, more than 100 fibre sections have been thought necessary to get realistic PMD statistics with Maxwellian distribution. The most popular mathematical description of PMD is the 2 x 2 frequency dependent Jones matrix. It indicates the equivalent baseband transmission properties of the channel PMD. With the given insight, PMD is mathematically modelled as a concatenation of M polarization-maintaining fibres with varying group delays and rotations of the principal axes. Fibre frequency response $U(\omega)$ is given by,

$$U(\omega) = \prod_{i=1}^{M} D_i(\omega)S_i \tag{3.14}$$

where

$$D_i(\omega) = \begin{pmatrix} e^{-j\omega\frac{\Delta\tau_i}{2}} & 0 \\ 0 & e^{-j\omega\frac{\Delta\tau_i}{2}} \end{pmatrix} \tag{3.15}$$

and

$$S_i(\omega) = \begin{pmatrix} \cos(\alpha_i)e^{j\phi_i} & \sin(\alpha_i)e^{j\phi_i} \\ -\sin(\alpha_i) & \cos(\alpha_i) \end{pmatrix} \tag{3.16}$$

Here, $\Delta\tau_i$ represents the group delay induced by the i^{th} section (each section has equal length). S_i is the scattering matrix and gives a frequency independent coordinate transformation of the principal axes. α_i and ϕ_i respectively denote the random polarization and phase angles, and are randomly generated with uniform distributions over $(0, 2\pi)$. Based on the scattering matrices used, $U(\omega)$ may be a general unitary matrix or a structured unitary matrix in the following form

$$U(\omega) = \begin{pmatrix} u_1(\omega) & u_2(\omega) \\ -u_2^*(\omega) & u_1^*(\omega) \end{pmatrix} \quad \omega \in [0, 2\pi) \tag{3.17}$$

satisfying the unitaryness constraint which can be defined as,

$$|u_1(\omega)|^2 + |u_2(\omega)|^2 = 1 \quad \text{for all } \omega \in [0, 2\pi) \tag{3.18}$$

As a result, it can be said that overall channel PMD transfer function is a paraunitary matrix [60, 61, 62, 63].

3.2.3 Polarization Dependent Loss

Definition Polarization dependent loss is the difference of the peak-to-trough power transmission of an optical component or system with respect to all possible states of polarization. It is defined as the ratio of the maximum and the minimum transmission intensity or output power of an optical device with respect to all polarization states [64], as shown in Eq. (3.19)

$$\mathrm{PDL_{dB}} = 10 \times \log\left(\frac{\mathrm{P_{Max}}}{\mathrm{P_{Min}}}\right) \tag{3.19}$$

Mueller Matrix In Stokes' space, a polarized light beam can be written in the form of Stokes' vector $\vec{S} = (S_0, S_1, S_2, S_3)^T$ [65], where

$$\begin{aligned} S_0 &= I_p \\ S_1 &= I_p \cos 2\psi \cos 2\chi \\ S_2 &= I_p \sin 2\psi \cos 2\chi \\ S_3 &= I_p \sin 2\chi \end{aligned}$$

Here I_p, 2ψ and 2χ are the spherical coordinates in Stokes space, so the Stokes' vector $\vec{S}$ can present any polarization state of the polarized light beam.

After passing through a device which changes the state of polarization, the Stokes vector of this light beam can be described as $\vec{S_{out}} = M\vec{S}$ where M is the Mueller Matrix used to describe the polarization device [66]

$$M = \begin{pmatrix} m_{11} & m_{12} & m_{13} & m_{14} \\ m_{21} & m_{22} & m_{23} & m_{24} \\ m_{31} & m_{32} & m_{33} & m_{34} \\ m_{41} & m_{42} & m_{43} & m_{44} \end{pmatrix}$$

The output power of this light beam

$$P_{out} = m_{11}S_0 + m_{12}S_1 + m_{13}S_2 + m_{14}S_3 \tag{3.20}$$

By the definition of Stokes vector, the following relationship holds

$$S_0^2 = S_1^2 + S_2^2 + S_3^2 = I_p^2 \tag{3.21}$$

Physically, the output power of the light beam reach its maximum or minimum value when the polarization components had the same or opposite state of polarization with the input polarized light, relatively. Therefore, P_{out} takes its maximum or minimum values when the condition $\frac{m_{12}}{S_1} = \frac{m_{13}}{S_2} = \frac{m_{14}}{S_3} = k$ holds. Maximum or minimum values are achieved respectively when k is positive or negative. Therefore, Eq. (3.20) can be rewritten as [67]

$$\mathrm{PDL_{dB}} = 10 \times \log \left(\frac{\mathrm{m_{11}} + \sqrt{\mathrm{m_{12}^2} + \mathrm{m_{13}^2} + \mathrm{m_{14}^2}}}{\mathrm{m_{11}} - \sqrt{\mathrm{m_{12}^2} + \mathrm{m_{13}^2} + \mathrm{m_{14}^2}}} \right) \tag{3.22}$$

By considering the systems which consist of multiple PDL components M_1, $M_2...M_n$ can be connected with each section of optical fibre F_1, $F_2...F_n$. It follows that the Stokes vector of the output light beam of a multi-section link can be described as

$$\vec{S_{out}} = F_n M_n ... F_2 M_2 F_1 M_1 \vec{S} \tag{3.23}$$

By assuming the states of polarization do not change within the relative short distance, the Mueller Matrix of each section of an optical fibre link can be written as

$$F_1 = \begin{pmatrix} \exp(-\alpha L_1) & 0 & 0 & 0 \\ 0 & \exp(-\alpha L_1) & 0 & 0 \\ 0 & 0 & \exp(-\alpha L_1) & 0 \\ 0 & 0 & 0 & \exp(-\alpha L_1) \end{pmatrix},$$

$$F_2 = \begin{pmatrix} \exp(-\alpha L_2) & 0 & 0 & 0 \\ 0 & \exp(-\alpha L_2) & 0 & 0 \\ 0 & 0 & \exp(-\alpha L_2) & 0 \\ 0 & 0 & 0 & \exp(-\alpha L_2) \end{pmatrix},$$

...

$$F_n = \begin{pmatrix} \exp(-\alpha L_n) & 0 & 0 & 0 \\ 0 & \exp(-\alpha L_n) & 0 & 0 \\ 0 & 0 & \exp(-\alpha L_n) & 0 \\ 0 & 0 & 0 & \exp(-\alpha L_n) \end{pmatrix}$$

where α is the loss parameter of the fibre and L_n is the length of fibre n.

The Mueller matrices for polarization controllers can be considered as four independent matrices for each paddle in four-paddle polarization controller. The Mueller matrix of one paddle is given by [68]

$$M_p ncn = \begin{pmatrix} 1 & cos(2\theta) & sin(2\theta) & 0 \\ cos(2\theta) & cos^2(2\theta) & sin(2\theta)cos(2\theta) & 0 \\ sin(2\theta) & sin(2\theta)cos(2\theta) & sin^2(2\theta) & 0 \\ 0 & 0 & 0 & 0 \end{pmatrix} \tag{3.24}$$

where θ is the rotated angle of the controller paddle.

Therefore, the final equation of the output Mueller Matrix is

$$\vec{S_{out}} = F_n M_{pnc4} M_{pnc3} M_{pnc2} M_{pnc1} ... \\ F_2 M_{p2c4} M_{p2c3} M_{p2c2} M_{p2c1} F_1 M_{p1c4} M_{p1c3} M_{p1c2} M_{p1c1} \vec{S} \quad (3.25)$$

3.2.4 The Statistics of PDL

As polarization is a time-dependent factor in optical transmission systems, PDL plays its role as a random attenuator. It generates irregularities in the power evolution along the link and may cause a significant degradation in the optical signal-to-noise ratio. Previous research showed that for a typical range of parameters the PDL of a communication system has a Maxwellian distribution when it is expressed in dB [69].

Theoretically, even though the distribution of PMD also obeys Maxwellian distribution, the distribution of PDL is independent of the system's PMD [70]. The dependence of the mean square PDL (in dB) on system length is linear in most cases, but it may become exponential in systems extending over trans-oceanic lengths.

The polarization dependent component of the power gain or loss of a generic optical element can be described as $1 + \vec{\Gamma} \cdot \vec{S_0}$, where $\vec{S_0}$ is a unit Stokes vector that corresponds to the polarization state of the incident optical field and $\vec{\Gamma}$ is a the vector that represents the PDL. Therefore, the highest and lowest gains are $1 \pm \Gamma$ with $\Gamma = |\vec{\Gamma}|$. The high gain is achieved when $\vec{S_0}$ is parallel to $\vec{\Gamma}$ in Stokes space, and the lowest gain is achieved when $\vec{S_0}$ is anti-parallel to $\vec{\Gamma}$. Based on the definition of PDL, it follows that it can be described as $\boldsymbol{PDL} \equiv 10 \log_{10}[(1+\Gamma)/(1-\Gamma)]$. In order to derive the PDL distribution, the following evolution equation of $\vec{\Gamma}$ obtained by Huttner [71] is considered:

$$\frac{\partial \vec{\Gamma}}{\partial z} = \vec{\beta} \times \vec{\Gamma} + \vec{\alpha} - \vec{\Gamma}(\vec{\alpha} \cdot \vec{\Gamma}). \quad (3.26)$$

The vector $\vec{\beta}(\omega, z)$ is the local birefringence and $\alpha(z)$ is the local vector of polarization dependent loss. ω is the optical frequency and z is the position along the fibre link.

By considering the transmission system as consisting of a large number of elements that contribute to PDL in a statistically independent way, it can be assumed that PDL vectors of the individual elements are Gaussian vectors in Stokes space so that their orientation is uniformly distributed. Therefore, the first term on the right hand side of Eq. (3.26) can be omitted. It is arbitrary to assume that the local PDL vectors have Gaussian distributed components. However, it becomes acceptable when the number of PDL elements in the system is large enough to provide sufficient coverage of true available polarization states [72]. Now the PDL vector can be described as an individual element by $\eta d\vec{W}$, where $d\vec{W}$ is an increment of a standard three-dimensional Brownian motion [73] and its most relevant property is $d\vec{W} \cdot d\vec{W} = dz$. Therefore, the mean-square value of the local PDL element is $\eta^2 dz$ where η is a constant. To simplify the notation, the position parameter z can be normalized such that $\eta^2 = 1$. The normalized z can be interpreted as the accumulated sum of mean-square PDL values from the system input (where $z = 0$) to any given point along the link. With these assumptions, Eq. (3.26) can be rewritten in a stochastic differential form

$$d\vec{\Gamma} = d\vec{W} - \vec{\Gamma}(d\vec{W} \cdot \vec{\Gamma}) - \frac{1}{3}\vec{\Gamma}(2 - \Gamma^2)dz \tag{3.27}$$

where the last term is the byproduct of translating a physical differential equation such as Eq. (3.26) into a stochastic differential equation. With the relation between $\vec{\Gamma}$ and ρ, the stochastic equation for ρ can be written as

$$d\rho = \frac{\gamma/3}{\tanh(\rho/\gamma)}dz + \frac{\gamma}{\sqrt{3}}dW \tag{3.28}$$

where $\gamma \equiv 20/\ln(10) \backsimeq 8.7$ and the scalar dW is an increment of a one-dimensional Brownian motion satisfying $dW^2 = dz$. A new vector process $\vec{\rho}(z)$ in Stokes space is introduced to obtain the distribution of ρ, such as

$$d\vec{\rho} = [\frac{\rho/\gamma}{\tanh(\rho/\gamma)} - 1]\frac{\vec{\rho}}{3\rho^2}\gamma^2 dz + \gamma d\vec{W} \tag{3.29}$$

and it has the relation $\rho = |\vec{\rho}|$. It shows the stochastic equation for $\sqrt{\vec{\rho} \cdot \vec{\rho}}$ is identical to Eq. (3.28). While $\vec{\rho}$ has no obvious physical interpretation, it is useful for deriving the distribution of ρ, because Eq. (3.29) can be approximated by performing a Taylor expansion of the first term on its right-hand side

$$d\vec{\rho} = [1 - \frac{1}{15\gamma^2}\rho^2 + \frac{2}{315\gamma^4}\rho^4 \cdots]\frac{1}{9}\vec{\rho}dz + \gamma d\vec{W} \tag{3.30}$$

If the first term in the square brackets in Eq. (3.30) is considered, a linear equation is obtained, the solution of which is a random vector with three independent Gaussian components of zero mean and variance $\sigma(z)^2 = 3\gamma^2/2(e^{2z/9} - 1)$. Therefore, the distribution of ρ is Maxwellian and it is given by

$$P_z(\rho) \approx \frac{4\rho^2}{\sqrt{\pi}[2\sigma^2(z)]^{3/2}} \exp[-\frac{\rho^2}{2\sigma^2(z)}] \tag{3.31}$$

The above approximation should be valid as long as the second term in the expansion is significantly smaller than the first (i.e., $\rho^2 \ll 15\gamma^2$), a condition that is well satisfied for values of $\rho \ll 34$ dB. The mean-square value of the PDL is

$$\langle \rho^2 \rangle = 3\sigma(z)^2 = \frac{9\gamma^2}{2}(e^{2z/9} - 1) \tag{3.32}$$

and the mean PDL is given by $\langle \rho \rangle = \sqrt{8\langle \rho^2 \rangle/(3\pi)}$, a relation that is defined by the Maxwellian distribution. Eq. (3.32) can be approximately written as $\langle \rho^2 \rangle \backsimeq \gamma^2 z$ when $2z/9 \ll 1$, where z is the accumulated local mean-square PDL of the system.

Eq. (3.32) shows that the mean PDL exponentially increases along the fibre for long distance transmission but it can be seen as approximately linear when the distance is small enough.

3.2.5 PDL Effects in Real Transmission Systems

The PDL factor in modern built single mode fibre is about less than 0.02 dB per metre or less than 0.05 dB per 10km at the wavelength of 1550 nm which is relatively small (standard attenuation in the same kind of single mode fibre is about 0.2 dB/km and its increase is linear). However, the mean value of PDL

increases nonlinearly with distance increasing in a ultra-long-distance system, for example, hundreds or thousands of kilometres.

PDL will affect ultra-long-distance systems in another way. It can cause a significant degradation in the optical signal-to-noise ratio because PDL is randomly changing with time. In order to compensate PDL, polarization dependent amplifiers (fibre-based Raman amplifiers) are applied along the systems. In order to achieve a better performance, the polarization dependent amplifiers (PDA) are expected to have the Maxwellian distribution related to the distribution of PDL in the system. Therefore, it is significant to understand the relationship between polarization components and communication fibres, not only the working parameters, but also the optimum positions of polarization components.

In practice, there is interaction between PMD and PDL that causes combined effects in real communication systems, when the PDL is significant. In the presence of both PMD and PDL, the two states of polarization are not orthogonal, which leads to interference producing anomalously large pulse spreading [17].

3.3 Nonlinear Schrödinger Equation

The nonlinear Schrödinger (NLS) equation is a nonlinear variation of the Schrödinger equation. It is a classical field equation with application to optical waves. It can include most of the factors which are relevant to lightwave propagation. By calculating its numerical solution, it can also be applied to build a simulation model.

3.3.1 Basic Format

Since the contribution of the third-order dispersion is quite small, it can be neglected in Eq. (2.88) and a simplified basic format NLS is then given by

$$j\frac{\partial A}{\partial z} + \frac{j\alpha}{2}A - \frac{\beta_2}{2}\frac{\partial^2 A}{\partial T^2} + \gamma|A|^2 A = 0 \tag{3.33}$$

where A is a typical plane wave defined as $A(z,t) = A(z)\exp(j\omega t)$, z is the direction of propagation, α is the loss parameter, β_2 is the second-order dispersion parameter, γ is the nonlinear parameter which is defined as $\gamma = \frac{2\pi n_2}{\alpha_0 A_{eff}}$ and $T = t - z/v_g$, where v_g is the group velocity.

In Eq. (3.33), $\frac{j\alpha}{2}A$ represents the effect of loss, $-\frac{\beta_2}{2}\frac{\partial^2 A}{\partial T^2}$ represents the effect of dispersion and $\gamma|A|^2A$ represents the effect of nonlinearity [74, 75]. Higher order dispersion and polarization mode dispersion are not included in this basic format.

3.3.2 Including Polarization Mode Dispersion

Assuming that the nonlinear effects do not affect the fibre mode significantly [34], the transverse dependence of E_x and E_y can be factored out using the following propagating envelope function

$$E(r,t) = F(x,y)A(z,t)\exp(j\beta_{0k}z) \tag{3.34}$$

where $F(x,y)$ is the spatial distribution of the single mode supported by the fibre, $A_k(z,t)$ is the slowly varying amplitude, and β_{0k} is the corresponding propagation constant ($k = x, y$). The dispersive effects can be included by expanding the frequency-dependent propagation constant. The slowly varying amplitudes, A_x and A_y, are found to satisfy the following set of two coupled-mode equations:

$$\frac{\partial A_x}{\partial z} + \beta_{1x}\frac{\partial A_x}{\partial t} + \frac{j\beta_2}{2}\frac{\partial^2 A_x}{\partial t^2} + \frac{\alpha}{2}A_x = j\gamma(|A_x|^2 + \frac{2}{3}|A_y|^2)A_x + \frac{j\gamma}{3}A_x^*A_y^2\exp(-2j\Delta\beta z) \tag{3.35}$$

$$\frac{\partial A_y}{\partial z} + \beta_{1y}\frac{\partial A_y}{\partial t} + \frac{j\beta_2}{2}\frac{\partial^2 A_y}{\partial t^2} + \frac{\alpha}{2}A_y = j\gamma(|A_y|^2 + \frac{2}{3}|A_x|^2)A_x + \frac{j\gamma}{3}A_y^*A_x^2\exp(-2j\Delta\beta z) \tag{3.36}$$

where

$$\Delta\beta = \beta_{0x} - \beta_{0y} = (2\pi/\alpha)B_m = 2\pi/L_B \tag{3.37}$$

is related to the modal birefringence of the fibre. The strength of the modal birefringence B_m is defined as

$$B_m = \frac{|\beta_x - \beta_y|}{k_0} = |n_x - n_y| \tag{3.38}$$

and beat length L_B is defined as

$$L_B = \frac{2\pi}{|\beta_x - \beta_y|} = \frac{\lambda}{B_m} \tag{3.39}$$

Modal birefringence also leads to different group velocities for the two polarization components because $\beta_{1x} \neq \beta_{1y}$ in general. In contrast, the parameters β_2 and γ are the same for both polarization components having the same wavelength λ.

The last term in Eq. (3.35) and Eq. (3.36) is due to coherent coupling between the two polarization components and leads to degenerate four-wave mixing [34]. If the fibre length $L \gg L_B$, the last term in Eq. (3.35) and Eq. (3.36) changes sign often and its contribution averages out to zero. In highly birefringent fibres ($L_B \sim 1$ cm typically), the four-wave mixing term can often be neglected for this reason. In contrast, this term should be included in weakly birefringent fibres, especially for short lengths.

The derivation of Eq. (3.35) and Eq. (3.36) assumes that the fibre is linearly birefringent, i.e. it has two principal axes along which already linearly polarized light remains linearly polarized in the absence of nonlinear effects. Although this is ideally the case for polarization-maintaining fibres, elliptically birefringent fibres can be made by twisting a fibre preforming it during the draw stage.

The coupled-mode equations are modified considerably for elliptically birefringent fibres. In this case, the slowly varying amplitudes A_x and A_y are found

to satisfy the following set of coupled-mode equations:

$$\begin{aligned}\frac{\partial A_x}{\partial z}+\beta_{1x}\frac{\partial A_x}{\partial t}+\frac{j\beta_2}{2}\frac{\partial^2 A_x}{\partial t^2}+\frac{\alpha}{2}A_x=\\ j\gamma[(|A_x|^2+B|A_y|^2)A_x+CA_x^*A_y^2e^{-2j\Delta\beta z}]\\ +j\gamma D[A_y^*A_x^2e^{i\Delta\beta z}+(|A_y|^2+2|A_x|^2)A_ye^{-j\Delta\beta z}]\end{aligned} \tag{3.40}$$

$$\begin{aligned}\frac{\partial A_y}{\partial z}+\beta_{1y}\frac{\partial A_y}{\partial t}+\frac{j\beta_2}{2}\frac{\partial^2 A_y}{\partial t^2}+\frac{\alpha}{2}A_y=\\ j\gamma[(|A_y|^2+B|A_x|^2)A_y+CA_y^*A_x^2e^{-2j\Delta\beta z}]\\ +j\gamma D[A_x^*A_y^2e^{i\Delta\beta z}+(|A_x|^2+2|A_y|^2)A_xe^{-j\Delta\beta z}]\end{aligned} \tag{3.41}$$

where B,C, and D are related to the ellipticity angle θ as

$$B=\frac{2+2\sin^2\theta}{2+\cos^2\theta},\quad C=\frac{\cos^2\theta}{2+\cos^2\theta},\quad D=\frac{\sin\theta\cos\theta}{2+\cos^2\theta} \tag{3.42}$$

For a linearly birefringent fibre ($\theta=0$), $B=\frac{2}{3}$, $C=\frac{1}{3}$, $D=0$, and Eq. (3.41) and Eq. (3.42) respectively reduce to Eq. (3.35) and Eq. (3.36).

For optical fibres with large birefringence, Eq. (3.40) and Eq. (3.41) can be simplified considerably. The beat length L_B is much smaller than typical propagation distances in these kinds of fibres. As a result, the exponential factors in the last three terms of Eq. (3.40) and Eq. (3.41) oscillate rapidly, contributing little to the pulse evolution process on average. If these terms are neglected, the propagation of optical pulses in an elliptically birefringent fibre is governed by the following set of coupled-mode equations:

$$\frac{\partial A_x}{\partial z}+\beta_{1x}\frac{\partial A_x}{\partial t}+\frac{j\beta_2}{2}\frac{\partial^2 A_x}{\partial t^2}+\frac{\alpha}{2}A_x\approx j\gamma[(|A_x|^2+B|A_y|^2)A_x \tag{3.43}$$

$$\frac{\partial A_y}{\partial z}+\beta_{1y}\frac{\partial A_y}{\partial t}+\frac{j\beta_2}{2}\frac{\partial^2 A_y}{\partial t^2}+\frac{\alpha}{2}A_y\approx j\gamma[(|A_y|^2+B|A_x|^2)A_y \tag{3.44}$$

These equations represent an extension of the scalar NLS equation, derived from Eq. (2.83), which does not include the polarization effects, to the vector case and are referred to as the coupled NLS equations. The coupling parameter B depends on the ellipticity angle θ and can vary from $\frac{2}{3}$ to 2 for values of θ in the range 0 to $\pi/2$. For a linearly birefringent fibre, $\theta=0$ and $B=\frac{2}{3}$. In contrast, $B=2$ for a circularly birefringent fibre ($\theta=\pi/2$). Also, $B=1$ when $\theta\approx 35^\circ$ [34, 76, 77].

3.4 Optical Phase Conjugation

Optical phase conjugation (OPC) is a laser-based technique developed since 1970s. Since it is feasible in many important applications, research into OPC has become one of the most active subjects in nonlinear optics.

Before the 1960s when the lasers were not practically realised, there were two impossibilities in conventional optics. One was that there was no method (including any optical imaging systems or specially designed devices) which could increase the brightness of any given light beam. This was solved by the invention of laser oscillators and amplifiers. The other was that the aberration influence from optical elements and propagating media made the perfectly reversible optical systems impossible to realise. This could be solved by the OPC technique.

Generally, a pair of optical waves are phase conjugated to each other by conjugating their complex amplitude functions with respect to their phase factors. Optical phase-conjugate waves can be generated through many nonlinear optical processes (such as four-wave mixing and three-wave mixing).

When the spectrum is inversed at the mid-point of a transmission system, the signal impairment caused by group velocity dispersion and nonlinear effects due to propagation before the mid-point will be compensated after the mid-point. Theoretically, the spectrum will be restored at the receiver in the ideal case [78, 79, 80, 81, 82].

3.5 Summary

This Chapter has introduced the background theory about the work described in this thesis, factors which affect the optical fibre communication systems notably. The background knowledge on polarization is a key part, both the polarization mode dispersion and polarization dependent loss are described.

CHAPTER 4

METHODOLOGY

The main work of this thesis is based on both emulation and simulation of polarization dependent effects in optical fibres. First, an emulator of polarization dependent loss (PDL) was built to be used to generate reliable, continuous PDL statistical measurement results for short fibre links. A simulation model was created with the same set of the emulator to ensure the statistical result matched the one from emulator and complied with theory. The simulation model can be extended to be able to simulate PDL statistics in optical fibre systems with ultra-long propagation lengths. The model can be used to study the signal attenuation as well.

4.1 PDL Emulation

The core of the PDL emulator is built with multiple polarization controllers and optical fibres. Polarization controllers are designed to be software-controlled by general purpose interface bus (GPIB) and the software to provide a continuous, fast-controlled change of the state of polarization of the lightwave propagating along single mode fibre.

4.1.1 Polarization Dependent Loss (PDL)

PDL refers to energy loss that is preferential to one polarization state. One axis suffers more loss than the other, and this differential loss changes the output polarization state and imparts a common loss to an unpolarized light beam. The complement of polarization dependent loss is polarization dependent gain (PDG), which is an effect that is related to preferential gain between signal and noise in optical amplifiers. PDL is defined as

$$PDL_{dB} = 10 \times \log(\frac{P_{Max}}{P_{Min}}) \tag{4.1}$$

where P_{Max} and P_{Min} are the maximum and minimum transmission intensities emitted from the system. Maximum transmission intensity occurs when the polarization state of a completely polarized probe beam is aligned to the maximum transmission axis of the PDL element. Minimum transmission occurs for the orthogonal polarization.

PDL is not confined to fibre, as there are many mechanisms that generate polarization-dependent loss along a fibre link. Micro-optic components generate PDL when there is preferential coupling through a focusing lens of one polarization-diversity path over another. Integrated optic filters generate PDL because the passband frequency locations are polarization dependent. Fused fibre couplers generate PDL due to polarization-dependent coupling ratios. Optical amplifiers generate PDG due to preferential gain of the signal polarization over the orthogonal noise polarization. Micro-bends in fibre will generate PDL. Materials themselves can generate PDL because of dichroism of the molecules, such as in polymer waveguides.

The combination of PDL and PMD creates effects which are quite complicated and which can impair a communication system more than either effect alone. For example, PDL is generally wavelength independent, while PMD is generally wavelength dependent. Addition of some PMD to PDL will generally result in wavelength-dependent PDL. The addition of some PDL to PMD can in some cases result in differential-group delay that exceeds what one would expect from the PMD alone.

4.1.2 Early PMD Emulator Design

I. T. Lima's Design of 2000

Before Lima's design, a fairly well-known technique of quasi-PMD emulation is to connect several short spans of polarization-maintaining fibre with some fixed angular offset between each section. However, the PMD characteristics of a real fibre could not be guaranteed by the multi-PM-section model, and it might lead to an unreliable measurement.

Lima designed a new emulator with 15 sections of polarization-maintaining fibre with randomly rotatable connections producing an almost ideal Maxwellian distribution of the differential group delay.

Different sections of PM fibre (Fibre Core, HiBi, Bow-tie) were connected by rotatable key FC connectors. By using rotatable connectors, The polarization axes of the two adjacent fibres can be rotated with respect to each other, and many realizations of concatenated PM fibres can be obtained. The average length of PM fibres has been chosen as 7 metres with a 20% Gaussian deviation. The beat length of the PM fibres is 1.2 mm at 633nm and scales for higher signal wavelengths. Therefore, by using 15 sections of PM fibres, 40 ps PMD is generated. The fibre lengths for the 15 sections are 5.1, 6.8, 8.6, 7.4, 6.3, 6.7, 10.0, 8.6, 5.4, 7.2, 6.9, 7.1, 6.1, 7.4, 4.6 metres. The total loss for the emulator is 6-10 dB, depending on the angles between the PM fibre sections. The PDL has been measured to be <0.2 dB and the DGD value measured using the Jones Matrix method [20].

The advantage of Lima's design is that it greatly improved the reproduction accuracy of PMD, compared with the earlier design. A much more reliable set of PMD statistics of Maxwellian distribution could be provided in a laboratory environment.

The disadvantage of this approach is that the lengths of the polarization-maintaining fibre it used were fixed to certain values, which was inadequate and inflexible for further adjustment.

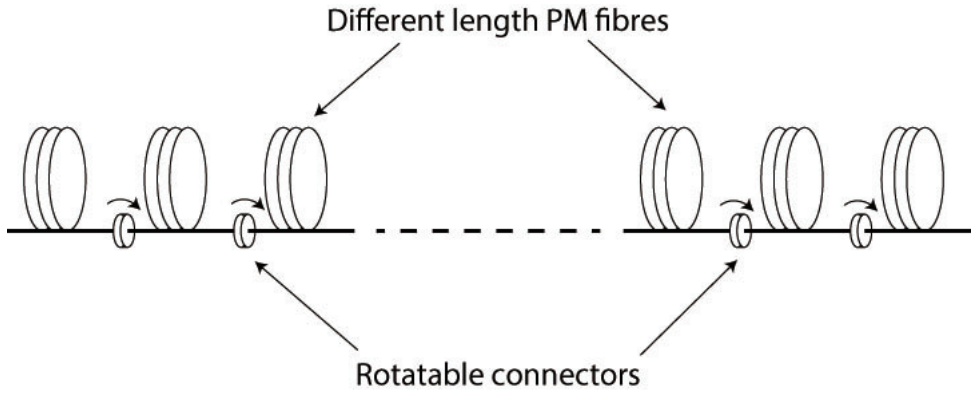

Figure 4-1: *Set up of I. T. Lima's emulator, with 15 polarization controllers [20].*

J. Damask's Early Design of 2000

J. Damask developed a programmable PMD emulator suitable for systematic testing of both optical and electronic PMD compensators under first and higher-order PMD conditions. Fig. 4-2 shows a diagram of the instrument. Twelve equal-length yttrium ortho-vanadate (YVO_4) birefringent crystals are mounted on twelve independent and motorized rotation stages placed in cascade at its core. Aspheric lenses couple light to and from the input and output fibres. The collimated beam between the input and output transits all crystals. The motors are controlled by computer and have motor encoders to relay their precise orientation. The high-accuracy motor control and stability of the birefringent crystals allows for accurate and repeatable PMD generation as well as real-time knowledge of the PMD state.

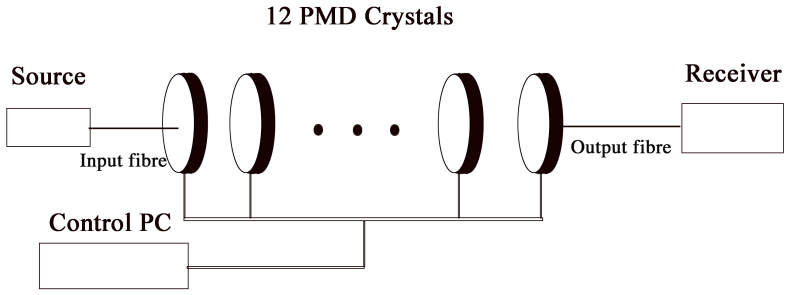

Figure 4-2: *Set up of J. Damask's emulator.*

The Damask's PMD emulator simplifies the complex models of statistic PMD by concentrating the DGD into twelve 10 ps blocks and confining the polarization rotations between adjacent sections to along the azimuth. Its stability is essential for systematic testing and real-time knowledge of the state of PMD.

The PMD emulator was used to generate two bit patterns at 10 Gb/s, one is only with the first order of PMD and the other is with higher order PMD. The bit patterns were generated with a $LiNbO_3$ modulator driven by a PRBS pattern generator and the input state of polarization was aligned to launch approximately equal power onto the axes of the first birefringent crystal [22].

M. Hauer's Design of 2004

The temperature sensitivity of polarization-maintaining (PM) fibres causes a change in the birefringent phase retardation between the two polarization eigenmodes according to the following equation

$$\frac{\Delta\phi}{\Delta T} = \frac{2\pi c}{\lambda}\left(\frac{\tau}{L}\right)\left(\frac{1}{B}\frac{\Delta B}{\Delta T} + \frac{1}{L}\frac{\Delta L}{\Delta T}\right) \tag{4.2}$$

where B is the modal birefringence, λ is the wavelength, c is the speed of light in vacuum, L is the fibre length and τ/L is the DGD per unit length of the PM fibre. The first term in the sum on the right hand side of the equation is the thermooptic coefficient $\sim 1.0 \times 10^{-3}$, which is responsible for the temperature-induced change in the birefringence. The second, which is much smaller term, is the thermal expansion coefficient, $\sim 5.5 \times 10^{-7}$, which accounts for the small

change in length.

The temperature sensitivity of PM fibres may be exploited to create electrically tunable waveplates by depositing short, thin layers of metal directly onto the glass surface of the fibre cladding. With an applied voltage, the fibre will be heated up by the resistance of the metallic film. The temperature is required to induce a 2π change in the birefringent phase retardation of the PM fibre, which will only depend on the length of the microheater and the sensitivity of the PM fibre. A more sensitive PM fibre or longer heater lengths will significantly reduce the temperature required to produce a full-waveplate change.

Hauer's design is shown in Fig.4-3. Thirty sections of Fibrecore HiBi polarization-maintaining fibre are fusion spliced together at 45 degree angle, as 45 degree leads to the most rapid frequency decorrelation of the PMD vector as the number of section increases. The beat length of the HiBi fibre at 1550 nm is 4.1 mm.

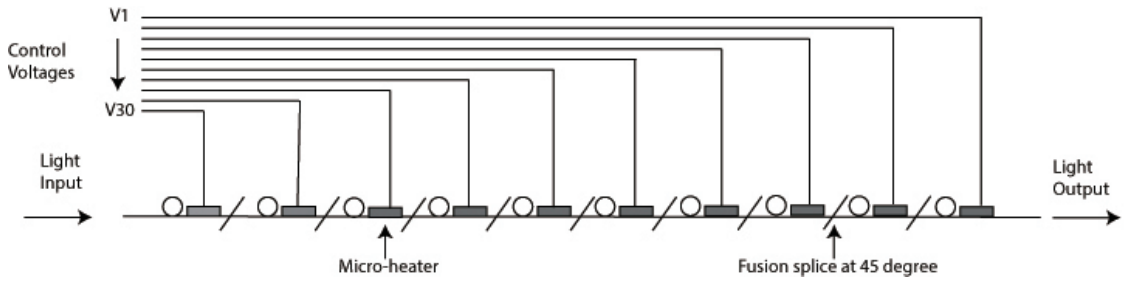

Figure 4-3: *Set up of M.Hauer's emulator. Schematic diagram of the PMD emulator using evaporated micro-heaters on PM fibre sections spliced together at 45 degree [23].*

The emulator was designed to have a mean DGD of 40 ps, which is a typical value for emulators that are used to test 10 Gb/s NRZ systems, for which severe outage probabilities will occur when the DGD is greater than or equal to a bit period (100 ps at 10 Gb/s). The mean DGD is chosen to be 30% to 40% of a bit period to ensure that several high-DGD points in the tail of the distribution will be encountered during a test of only 1000 or so samples.

Electron-beam evaporation was used to deposit 2.5 cm-long thin film heaters near the centre of each section. Each heater was comprised of a 15 nm titanium layer for good adhesion to the glass and a 120 nm gold layer for good electrical conductivity. To achieve a compact design, a 32-section silcon V-groove array with 1.25 mm spacing was used to mount the fibre heaters before the evaporation process. The 31st and 32nd sections were used to build test elements to characterize the temperature dependence of the DGD and output polarization state of single PM fibre sections [23].

Hauer's design focused on the PMD variance of temperature. Even though thermal crosstalk between macro heaters were introduced because of the 1.25 mm-spacing, the crosstalk did not adversely affect the statistical results of the emulator, thanks for the randomly chosen powers applied to the micro heaters.

The disadvantage of Hauer's design is that the angle of each section was fixed to 45 degree which limits the PMD variation on the other parts. Besides, temperature variance is not rapid enough to generate a reliable variance of the state of polarization.

L. Yan's Design of 2004

Yan's design is constructed from three variable DGD elements separated by two fibre-squeezer-based polarization controllers, as shown in Fig. 4-4. Each variable DGD element consists of several birefringent crystals. The lengths of these crystals increase in a binary series (such as 1, 2, 4, 8, ...) and are separated by electrically driven polarization switches. The elements are programmable to generate any DGD value from -45 ps to $+45$ ps with a tuning speed of < 1 ms and a resolution of 1.4 ps. This resolution is a consequence of the structure of the DGD of sections included in each variable DGD element. A computer is used to

control the emulator to randomly generate any desired DGD distribution for each element and to uniformly scatter the polarization between sections. To obtain a Maxwellian DGD distribution at the emulator output, the DGD values of each element are varied according to a Maxwellian distribution with the average DGD $\Delta\tau$. This yields an average DGD of $3^{1/2}\Delta\tau$ for the total emulator and an average second-order PMD distribution that has the correct shape but falls slightly short of that expected for a real fibre [24].

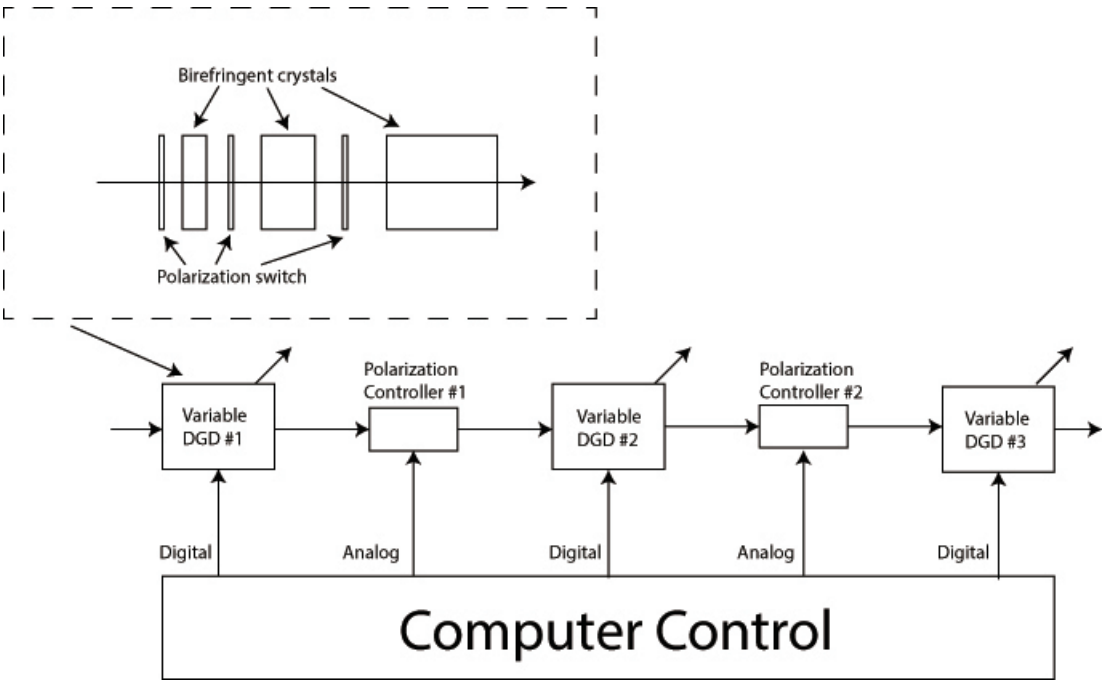

Figure 4-4: *Set up of L. Yan's emulator [24].*

J. Damask's Later Design of 2003

Figure 4-5 illustrates the four-stage enhanced coherent higher order (ECHO) PMD instrument built by J. Damask. The four stages are set with a fixed delay of 30 ps, and they are connected with intermediate polarization mode mixers, which are true zeroth-order half-wave waveplates, between each other. In order to drive the instrument into coherence, both of the second and third stage have an added birefringent phase shifter. Each delay stage is comprised of two birefringent crystals. The lengths of YVO4 and LiNbO3 crystals are 14.878 mm

and 2.262 mm, respectively. In comparison with polarization-maintaining fibre, birefringent crystal provides a completely stable source of DGD. The axes of all delay crystals are aligned to each other within an angle of ±0.5 degree. The phase shifters are operated with two true zeroth-order three-quarter waveplates. The rotation of the centre half-wave waveplate is equal to the shift of the birefringent phase of the section which the phase shifter is associated to. While the birefringent phase of each centre crystal pair is random, the phase shifters are calibrated during construction of the instrument to drive the sections to weak-sense coherence. All surfaces are antireflection coated and the two fibres with angle-polished terminations and collimating lenses couple light from one fibre to the other through the optical path of the ECHO instrument. The insertion loss is 1.8 dB and the polarization-dependent loss is less than 0.2 dB.

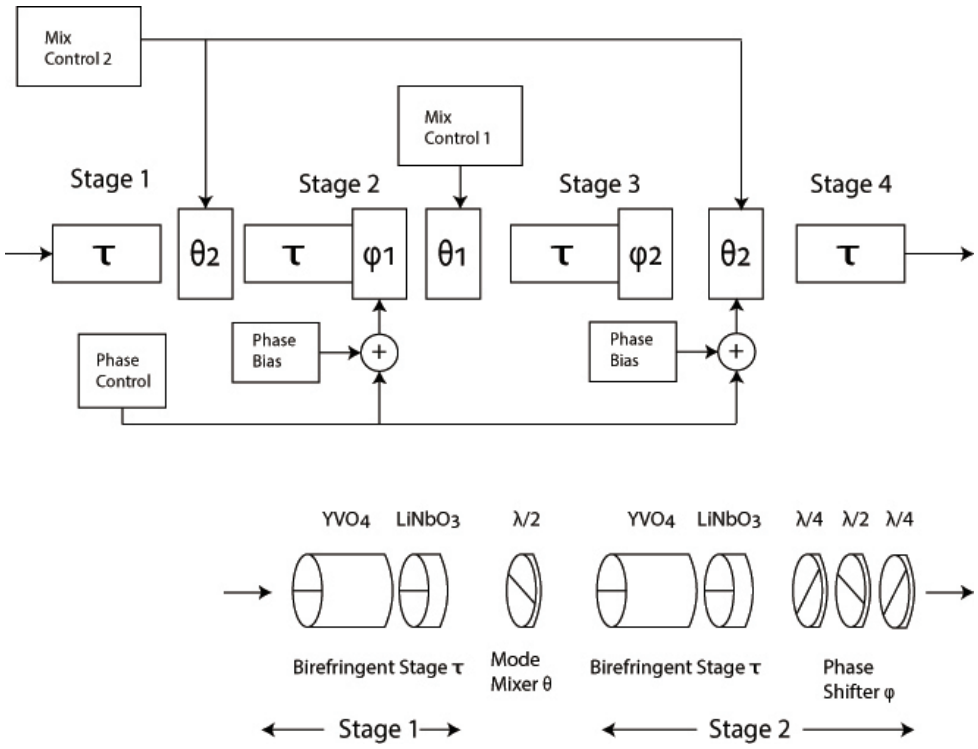

Figure 4-5: *Set up of J. Damask's emulator(2003) [25].*

Damask's design using coherent PMD technology can generate predictable PMD that includes DGD, SOPMD, and PDCD. The emphasis in this work on harmonic and coherent spectra serves two purposes. First, extreme higher order states require the constructive addition of the Fourier components. Without this,

states toward the centre of the Maxwellian will be generated in lieu of states on the tails. Second, coherence makes the programming of the instrument simple because there is a one-to-one correspondence between PMD state and motor angle.

4.1.3 Emulator Design in this Thesis

The PDL emulator has been built with computer-driven polarization controllers and sections of single mode fibre to provide a continuous statistical result known to obey a Maxwellian distribution, as shown in Fig. 4-6. A stable laser source is used to provide continuous lightwave at the wavelength of 1550 nm. A power splitter is deployed between the laser source and the system. 10% of the source power is sent to one channel of the multimeter as reference, and the other 90% goes into the emulator. Initially sections of 15m of single mode fibre (SMF) were used to connect each polarization controller. All of the polarization controllers were changing their paddle positions rapidly and randomly to maximize the system randomization.

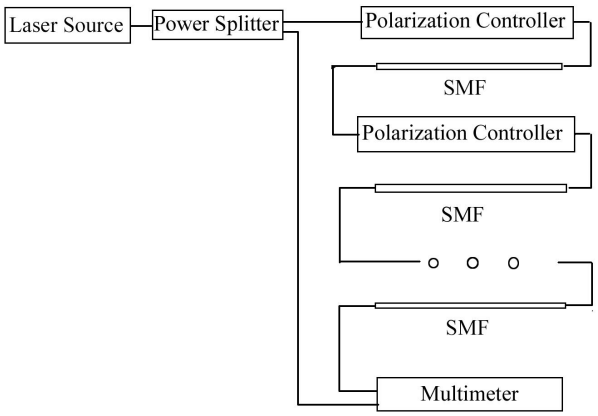

Figure 4-6: *Emulator design.*

The degree of randomness achieved is determined by the number of polarization controllers applied. By changing this number, it can be compared how PDL components in the transmission system affect the statistical results of the output PDL at the receiver. By changing the number of sections of optical fibre, it will

give different results corresponding to the different transmission distance. Another variable in the emulator system is the positions of polarization controllers within the fibre link. By changing this, it can be helpful to find out the effect of PDL component position changing and the relationship of PDL component position and the transmission distance.

4.1.4 Emulator's Hardware

Agilent 83433A Lightwave Transmitter The Agilent 83433A is a stable laser source which is based on a lithium niobate modulator driven by an internal continuous wave (CW) DFB 1552.52 nm laser. It can produce a polarised lightwave signal at a fixed but adjustable wavelength. It can produce an internal continuous wave at a nominal optical power of 10 dBm which is adjustable within a range 8.5 dBm to 11.5 dBm and at wavelength of 1552.5 nm nominal, which is adjustable within a range 1552.42 nm to 1552.62 nm. It is compatible with external polarization controlled turnable laser source (TLS) at wavelengths from 1530 nm to 1565 nm [83].

Figure 4-7: *Agilent 83433A Lightwave Transmitter [83].*

Agilent 11896A Polarization Controller The Agilent 11896A polarization controller can convert a transmitted state of polarization (SOP) of a light wave signal into a defined or random SOP. This device is suitable for laboratory pur-

poses and it can be used manually or automatically to change the SOP of a lightwave signal over a range of wavelength from 1250 nm to 1640 nm. Any SOP can be created with a very small variation in optical insertion loss (±0.002 dB) [84]. This polarization controller is classified as multiple waveplates with fixed retardation but variable orientation in an all fibre configuration. It consists of four fibre loop assemblies with each loop configured to represent a quarter-wave retarder response over a specified wavelength. Each fibre coil loop can be adjusted over an angular range of 180° in 1000 steps, where each step equivalent to an angular value of 0.18°. Adjusting the paddles can be achieved manually, or automatically over a GPIB network using instrument commands [84].

Figure 4-8: *Agilent 11896A Polarization Controller [84].*

Glan-Thompson Prism and XYZ Nano Positioning System A Glan-Thompson prism and XYZ-nano positioning system are needed in the polarization calibration experiment in order to split the polarized light into identifiable TM or TE linearly polarized status. The Glan-Thompson prism is a polarization beam splitter which is used to separate the two orthogonal SOP of a polarized light wave signal. The prism can be set to produce a TM or TE wave as required. High precision and minimal power losses from the transmission of a light beam from the polarization controller through the Glan-Thompson prism and back into an optical fibre are important. The XYZ-nano positioning systems were used to align and produce a collimated beam of light from an optical fibre from the polarization controller through the Glan-Thompson prism and back into another

receiving optical fibre.

Hewlett-Packard (HP) 8153A Lightwave Multimeter The Hewlett-Packard (HP) 8153A Lightwave Multimeter can accurately measure transmitted optical power and as a data acquisition device during the experiments described in this report. It can accurately measure power over wavelengths range of 450 nm to 1700 nm and can be automatically adjusted to measure power over a range of +27 dBm to -110 dBm. This multimeter can be automatically controlled and programmed over a GPIB network using instrument specific commands from the device manual [85].

Figure 4-9: *HP 8153A Lightwave Multimeter [85].*

National Instruments GPIB-USB-HS interface The emulator requires fast and efficient computer automated control of hardware. Easy and direct connection between the GPIB instruments and computer was achieved using the National Instruments GPIB-USB-HS interface. This GPIB interface is compatible with the IEEE 488.2 standard which made it possible to connect to multiple instruments by looping the connection with standard IEEE 488 GPIB cables.

Power Splitter A power splitter is a device used to split the output power from a source into two or more different sections of fibre. One of the sections of fibre took 90% power of the source to be launched to the emulator. The other one took 10% power and will be received by the lightwave multimeter directly

in order to monitor the optical power input to the emulator. Both of these two sections will be measured simultaneously to calibrate out the power fluctuation of the power source.

Thorlabs' Single Mode 1550BHP fibre Thorlabs' Single Mode 1550BHP fibre's operating wavelength is from 1460 nm to 1620 nm. The numerical aperture is 0.13, and the attenuation is 0.5 dB/km at 1550 nm. The minimum bend radius is 6mm for momentary and 13mm for long term.

4.1.5 Emulator's Software

LabVIEW is sophisticated graphical programming software developed by National Instruments. It consists of tools which can be used to perform automated instrument control, data acquisition and data analysis. LabVIEW was used to control the devices in these experiments because of the flexibility of its applications which allows programming of various instruments to perform various functions at once. LabVIEW consists of two graphical window interfaces which are the block diagram and the front panel. The block diagram is where the LabVIEW program code is written while the front panel is the interface which is used to manage and control the LabVIEW program. LabVIEW programs are called Virtual Instruments (VIs) and subprograms are called subVIs.

4.2 Polarization Simulation

4.2.1 Overview of Polarization Simulation

Polarization simulation in this thesis consists of two independent simulation models. One was built with the same mechanism as the PDL emulator, referred to as PDL power simulator in this thesis. The other one was built to simulate the signal attenuation and distortion caused by multiple factors, which can be added into the system independently to research their solo effects and combined effects.

The PDL power simulator was built for two purposes: first, to generate a

set of results as a comparison group to the PDL emulator to confirm that the experimental results from the PDL emulator are reliable; second, to simulate the impact of power for long distance systems which are beyond the emulator's capability.

The polarization signal attenuation simulator was built to study how signals were attenuated and distorted by the polarization effects in transmission systems. It will mainly focus on the impact to the signal-to-noise ratio and combined effects of PMD and other factors. Meanwhile, it will work on possible solutions.

4.2.2 PDL Power Simulator Implementation

The algorithm of PDL power simulator is based on the Mueller matrix calculation described in Chapter 3. The randomness is adjustable by controlling the range and frequency of the matrix M changing, which represents the polarization components. The propagation distance and fibre type can be adjusted by changing the matrix L, which represents the communication fibre.

On the other hand, the simulation of signal attenuation and distortion requires different approaches. The algorithms include Monte Carlo method and split-step Fourier method. The former is to provide a set of differential group delays which obeys Maxwellian distribution and the latter provides an approach to get a numerical solution of the nonlinear Schrödinger equation.

4.2.3 Monte Carlo Method

To test the effect of PMD in this simulation model, a set of PMD values must be able to be generated using a reliable method. Since the first order PMD, which is DGD, obeys Maxwellian distribution [86, 87], the probability density function of it is [88]

$$\mathrm{PDF}(\Delta\tau) = 3\sqrt{\frac{6}{\pi}}\frac{\Delta\tau^2}{\mathrm{PMD}^3}\exp\left(-\frac{3}{2}\frac{\Delta\tau^2}{\mathrm{PMD}^2}\right) \qquad \text{where} \qquad \mathrm{PMD} = <\Delta\tau^2>^{1/2} \tag{4.3}$$

The Monte Carlo method would be a proper method to generate a set of PMD values. The reliability will increase as the number of samples increases.

Monte Carlo methods are a broad class of computational algorithms that rely on repeated random sampling to obtain numerical results. The precision of results increases as the numbers of random sampling increases. Monte Carlo methods have been applied in wide range of experiments as it is the most simple way to achieve a numerical solution with computer [89, 90].

The basic idea of applying Monte Carlo method to achieve a set of data which obeys Maxwellian distribution is to select a random point in the area (Fig. 4-10). If the point is in the black area, or mathematically, $y < pdf(x)$, then this set of data obeys Maxwellian distribution.

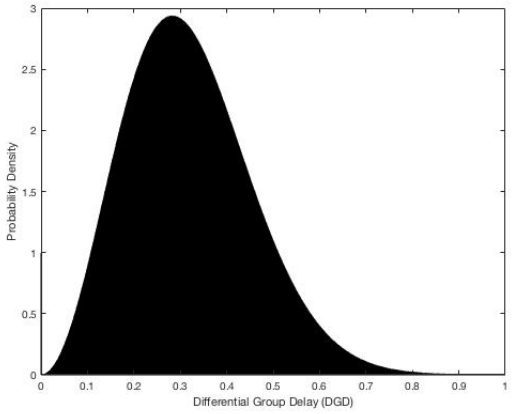

Figure 4-10: *PDF of Maxwellian Distribution.*

As the pdf function of Maxwellian distribution is a complicated function, it is necessary to transfer it to a different form to build a data generator. If a probability density function is like $f(x) = H(x)f_1(x)$, where $H(x)$ is a non-negative function and $f_1(x)$ is an arbitrary probability density function, then let M=sup($H(x)$), and the approach of sampling is

$$X_f = X_{f_1} \tag{4.4}$$

If the precondition

$$\xi \leq \frac{\mathrm{H}(X_{f_1})}{\mathrm{M}} \tag{4.5}$$

is true, where ξ is a pseudo-random number sequence.

So the probability density function of DGD in Eq. (4.3) can be transformed to

$$\mathrm{PDF}(x) = \frac{4}{\sqrt{\pi}}\beta^{\frac{3}{2}}\, x \exp(-\beta x) \tag{4.6}$$

by replacing $\Delta\tau^2$ with x and $\frac{3}{2\mathrm{PMD}^2}$ with β.

Let $f_1(x) = \frac{2}{3}\beta e^{-\frac{2}{3}\beta x}$, then $X_{f_1} = -\frac{3}{2\beta}\ln\xi_2$. $H(x) = \frac{6}{\sqrt{\pi}}\beta^{\frac{1}{2}} x e^{-\frac{1}{3}\beta x}$, so $M = sup(H(x)) = \frac{18}{e\sqrt{\pi\beta}}$. Then we have

$$X_f = X_{f_1} = -\frac{3}{2\beta}\ln\xi_2 \tag{4.7}$$

if

$$\xi_1 \leq \frac{\mathrm{H}(X_{f_1})}{\mathrm{M}} = \frac{e}{2}\sqrt{\xi_2}\ln\xi_2 \tag{4.8}$$

is true [91].

With the algorithm above, a reliable set of DGD values can be generated. Fig. 4-11 gives the distribution of one set of DGD values produced by this algorithm, which has an approximately Maxwellian distribution. By enlarging the amount of samples, this distribution approaches a Maxwellian distribution.

4.2.4 Split-step Fourier Method

The simplified Nonlinear Schrödinger Equation Eq. (3.33) [34] is a nonlinear partial differential equation that does not generally lend itself to analytic solutions except for some specific cases in which the inverse scattering method can be employed. Therefore, a numerical approach is often necessary for understand-

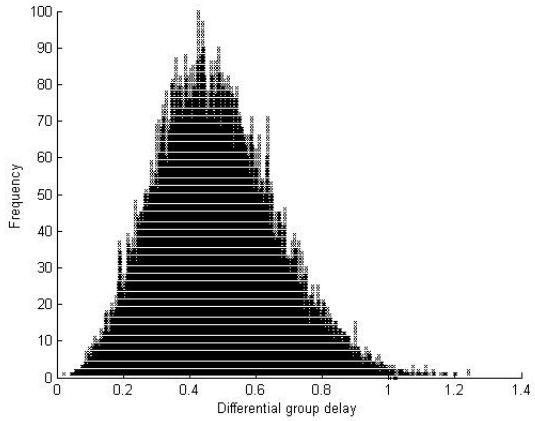

Figure 4-11: *DGD(first order PMD) distribution generated with the algorithm in Section 4.2.3*

ing the nonlinear effects in optical fibres. Many numerical methods have been proposed for this purpose [92, 93, 94], which can be classified into two broad categories known as (i) the finite-difference methods and (ii) the pseudospectral methods. Pseudospectral methods are faster by up to an order of magnitude to achieve the same accuracy [95]. The one method that has been used to solve the pulse-propagation problem in nonlinear dispersive media is the split-step Fourier method [96]. The relative speed of this method compared with most finite-difference schemes can be attributed in part to the use of the Fast-Fourier-transform (FFT) algorithm [97].

The basic process of getting the numerical approach of Nonlinear Schrödinger Equation with split-step Fourier method starts with writing Eq. (3.33) in the form of

$$\frac{\partial A}{\partial z} = (\widehat{D} + \widehat{N})A \tag{4.9}$$

where $\widehat{D}$ is a differential operator that accounts for dispersion and absorption in a linear medium and $\widehat{N}$ is a nonlinear operator that governs the effect of fibre nonlinearities on pulse propagation. These operators are give by

$$\widehat{D} = -\frac{j\beta_2}{2}\frac{\partial^2}{\partial T^2} - \frac{\alpha}{2} \tag{4.10}$$

$$\widehat{N} = j\gamma|A|^2 \tag{4.11}$$

In general, dispersion and nonlinearity act together along the length of the fibre. The split-step Fourier method obtains an approximate solution by assuming that

in propagating the optical field over a small distance h, the dispersive and nonlinear effects can be assumed to act independently. More specifically, propagation from z to $z+h$ is carried out in two steps. First, the nonlinearity acts alone, and $\widehat{D} = 0$. Mathematically,

$$A(z+h,T) \approx exp(h\widehat{D})exp(h\widehat{N})A(z,T) \tag{4.12}$$

The exponential operator $exp(h\widehat{D})$ can be evaluated in the Fourier domain using the formula

$$exp(h\widehat{D})B(z,T) = F_T^{-1}exp[h\widehat{D}(j\omega)]F_T B(z,T) \tag{4.13}$$

where F_T denotes the Fourier transform operation, $\widehat{D}(j\omega)$ is obtained from Eq. (4.10) by replacing the differential operator $\partial/\partial T$ by $j\omega$, and ω is the frequency in the Fourier domain. As $\widehat{D}(j\omega)$ is just a number in the Fourier space, the evaluation of Eq. (4.13) is straightforward. The use of the FFT algorithm makes numerical evaluation of Eq. (4.13) relatively fast. It is for this reason that the split-step Fourier method can be faster by up to two orders of magnitude compared with most finite-difference schemes.

The accuracy of split-step Fourier method can be improved by replacing Eq. (4.12) by

$$A(z+h,T) \approx exp(\frac{h}{2}\widehat{D})exp(\int_z^{z+h}\widehat{N}(z')dz')exp(\frac{h}{2}\widehat{D})A(z,T) \tag{4.14}$$

The main difference is that the effect of nonlinearity is included in the middle of the segment rather than at the segment boundary [98]. When the step length h is small enough, $exp(\int_z^{z+h}\widehat{N}(z')dz')$ can be approximated by $exp(h\widehat{N})$.

By applying Eq. (4.14) in a continuous M segments, 4.14 can be developed to

$$A(L,T) \approx e^{-\frac{1}{2}h\widehat{D}}(\prod_{m=1}^{M} e^{h\widehat{D}}e^{h\widehat{N}})e^{\frac{1}{2}h\widehat{D}}A(0,T) \tag{4.15}$$

where $L = Mh$ is the total length of optical fibre. Therefore, all the middle steps of the calculation can be implemented on all the segments of h, except the first and last steps where dispersion needs to be counted in. This feature reduces the calculation of FFT by half, so the calculation speed is approximately doubled. It

is also acceptable by exchanging $\widehat{D}$ and $\widehat{N}$, which gives another algorithm

$$A(L,T) \approx e^{-\frac{1}{2}h\widehat{N}}(\prod_{m=1}^{M} e^{h\widehat{N}}e^{h\widehat{D}})e^{\frac{1}{2}h\widehat{N}}A(0,T) \tag{4.16}$$

It has the same accuracy as Eq. (4.15), and it is much more easy to implement. Therefore, this algorithm is applied in the simulation model described in this report.

In this simulation model, the main goal is to observe how PMD affects the system performance, so the part of fibre loss is removed from Eq. (3.33), which gives

$$j\frac{\partial A}{\partial z} - \frac{\beta_2}{2}\frac{\partial^2 A}{\partial T^2} + \gamma|A|^2A = 0 \tag{4.17}$$

It is helpful to normalize Eq. (4.17) by introducing three dimensionless variables

$$U = \frac{A}{\sqrt{P_0}}, \qquad \xi = \frac{z}{L_D}, \qquad \tau = \frac{T}{T_0} \tag{4.18}$$

and write in the form of

$$j\frac{\partial U}{\partial \xi} = sgn(\beta_2)\frac{1}{2}\frac{\partial^2 U}{\partial \tau^2} - N^2|U|^2U \tag{4.19}$$

where P_0 is the peak power, T_0 is the width of the incident pulse, and the parameter N is introduced as

$$N^2 = \frac{L_D}{L_{NL}} = \frac{\gamma P_0 T_0^2}{|\beta_2|} \tag{4.20}$$

The dispersion length L_D and the nonlinear length L_{NL} are defined as

$$L_D = \frac{T_0^2}{|\beta_2|}, \qquad L_{NL} = \frac{1}{\gamma P_0} \tag{4.21}$$

where T_0 has the relationship of

$$\tau = \frac{T}{T_0} = \frac{t - z/v_g}{T_0} \tag{4.22}$$

By introducing

$$u = NU = \sqrt{\gamma L_D}A \tag{4.23}$$

to Eq. (4.19) the parameter N can be eliminated. So the new normalized NLS equation is

$$j\frac{\partial u}{\partial \xi} + \frac{1}{2}\frac{\partial^2 u}{\partial \tau^2} + |u|^2 u = 0 \tag{4.24}$$

With the numerical solution of Eq. (4.24), the basic simulation model is built as shown in Fig. 4-12. In this basic model PMD is not included and fibre loss is ignored in the original settings, so the pulse broadening and amplitude attenuation are caused by chromatic dispersion.

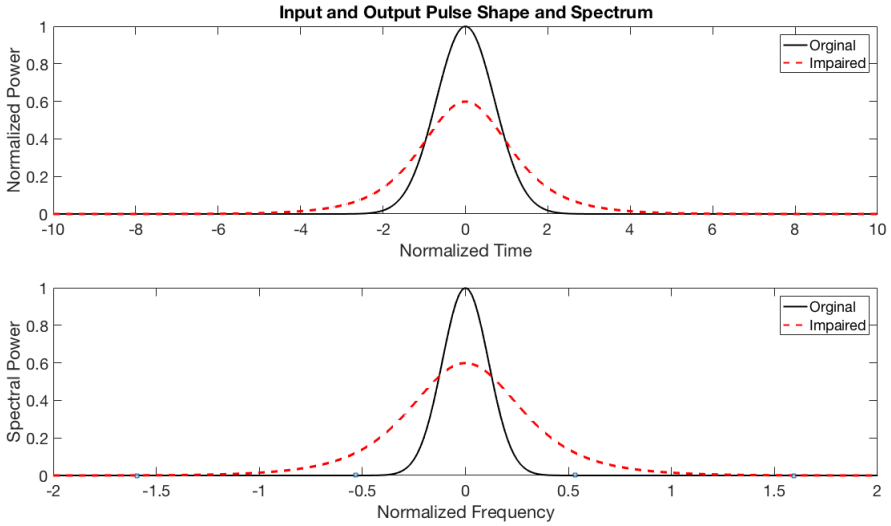

Figure 4-12: *Simulation results of launched pulse transmitted for 10km. Fibre loss and PMD are not included.*

4.3 Summary

This chapter described the basic of both emulation and simulation. That includes the hardware and software used for emulation, the design of emulation and the approach used for simulation.

CHAPTER 5

EMULATION EXPERIMENTS

Polarization dependent loss (PDL) can be considered as a time-related and distance-related random attenuation in optical fibre communication systems. It can be accumulated positively or negatively over time and distance. It is impossible and uneconomical to build an emulator with the fibre of thousands kilometres as in real systems, so the idea is to build one with shorter fibre link and polarization-changing elements to emulate the statistical result and evaluate the effects in real communication systems.

As PMD is considered to be the major polarization effect in fibre communication, many PMD emulators have been developed in previous research. A fairly well-know early design of PMD emulator is constructed with a series of polarization controllers (PC), connected by sections of polarization maintain fibres (PMF), see Fig. 5-1. Further designs reduced the cost by replacing some of the polarization controllers with more polarization-maintaining fibres, with random but fixed angles between each span of PMFs.

Figure 5-1: *Early design of polarization emulator*

Early configurations include twisted fibre sections [20] and motor-driven rotatable crystals [22], and recent designs include a micro-heater and PMF based emulator [23], a tunable emulator using variable DGD elements [24] and a coherent programmable PMD source [25].

To be compared with PMD, PDL is less important so it has received very limited research interest. Few PDL emulator designs have been developed. However, as PDL is introduced to the system by the same mechanism as PMD, a PMD emulator can be used as a PDL emulator as well.

5.1 Polarization Controller Calibration

The aim of this polarization controller calibration experiment is to determine the paddle positions of the polarization controllers which produce maximum optical power. The laser produces polarized light which propagates through a single mode fibre into the polarization controller. The XYZ positioning systems are manually controlled to align the optical fibre between the polarization controller, Glan-Thompson prism and the lightwave multimeter. Fig. 5-2 shows the block diagram of polarization controller calibration experiment. All of the five available polarization controllers were calibrated by this method. The Glan-Thompson prism can be set to filter out TM or TE. Either TM or TE can be used to determine position of the paddles of polarization controller that transmit maximum optical power. Fig. 5-3 shows the working principle of the Glan-Thompson prism.

The whole set of this calibration experiment was controlled by LabVIEW. The first paddle of the calibrating polarization controller was automatically scanned

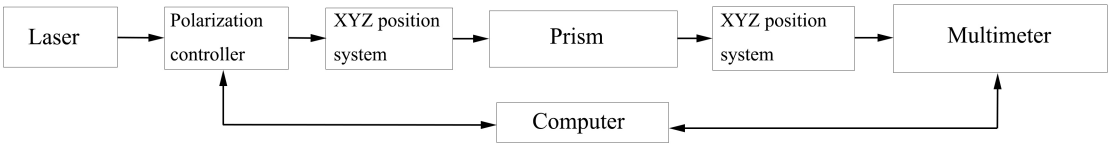

Figure 5-2: *Block diagram of polarization controller calibration experiment.*

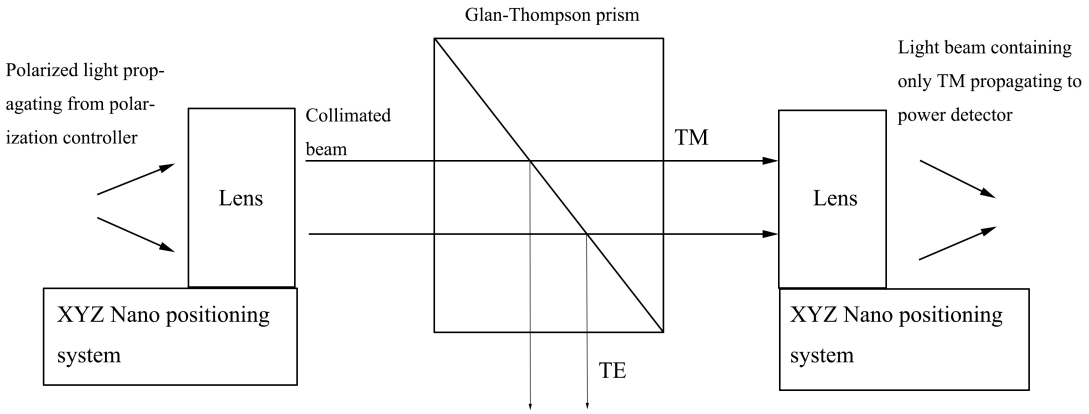

Figure 5-3: *Working principle of Glan-Thompson prism.*

from position 000 to 999 with a 1 second interval between each setting while the other 3 paddles were kept in position 000. The readings from multimeter were recorded and mapped onto computer synchronously and the positions which produce maximum and minimum power would be highlighted and recorded at the end of this loop. The loop ran 3 times to confirm the consistency.

After the calibration of the first paddle, it is set to the optimum position, which produces the maximum power, and the following three paddle positions calibrated with the same procedure. This calibration experiment operated on all of the five polarization controllers. The results are shown in Table 5.1.

Polarization Controller 1				
	Paddle 1	Paddle 2	Paddle 3	Paddle 4
MAX	896	539	110	512
MIN	167	126	453	808
Polarization Controller 2				
	Paddle 1	Paddle 2	Paddle 3	Paddle 4
MAX	340	000	375	073
MIN	745	654	675	693
Polarization Controller 3				
	Paddle 1	Paddle 2	Paddle 3	Paddle 4
MAX	711	217	003	312
MIN	215	595	662	691
Polarization Controller 4				
	Paddle 1	Paddle 2	Paddle 3	Paddle 4
MAX	070	674	021	012
MIN	820	353	737	663
Polarization Controller 5				
	Paddle 1	Paddle 2	Paddle 3	Paddle 4
MAX	709	154	008	011
MIN	022	764	542	706

Table 5.1: *Results of polarization controller calibration experiment.*

5.2 Link Emulator

The link PDL emulator developed in this thesis takes a different approach from those reviewed in section 4.1.2. It exploits the capability of computer-controlled polarization controllers to introduce variations in the polarization state of a given optical element. Moreover, the four-paddle design of the polarization controllers used allows freedom for introducing random changes in the state of polarization.

The basic block diagram of the link emulator is shown in Fig. 5-4. The laser source was connected with one section of single mode fibre to the input of polarization controller 1. Then the output of polarization controller 1 was connected with the input of polarization controller 2 directly. Polarization controller 2 and 3 were connected the same way. In the end, the output of polarization controller 3 was connected to the multimeter.

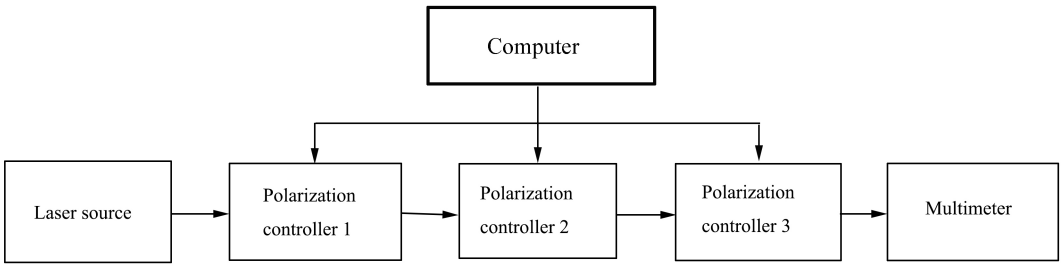

Figure 5-4: *Block diagram of link emulator experiment*

5.2.1 Laser Source Fluctuation Evaluation

Evaluation of the power output fluctuations of the laser source is very important to help understand the cause of changes in the received signal power. The experimental set-up is a little different from the basic set-up of the link emulator (see Fig.5-5). Instead of the section of single mode fibre, the splitter was applied to split the power before the signal went into the first polarization controller. 10% of the source power was sent directly to the second channel the dual-input lightwave of the multimeter for measuring and recording. 90% was sent as normal to the emulator. Both of the channels output were recorded on the computer.

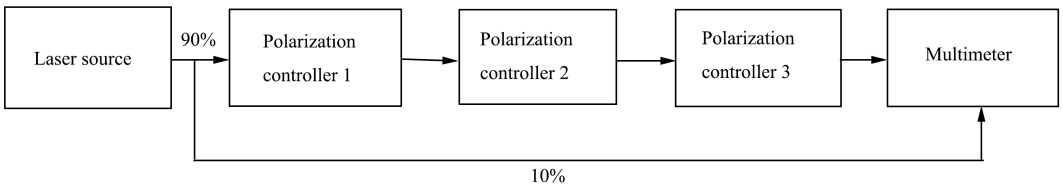

Figure 5-5: *Block diagram of link emulator with power spitter*

The laser source fluctuation evaluation experiment lasted for 24 hours. The correlation index of these two channel readings was calculated for evaluation. This experiment was operated for 3 times and the average correlation index is 0.237. It indicated the fluctuations of laser source and final output from emulator were

largely uncorrelated. As a consequence the fluctuations in the received power of the light transmitted via the polarization controllers were too large to be the damage induced by power source, but induced by variations in the settings of the polarization controllers.

5.2.2 Experiments over Short Term (10 minutes)

First, the emulator ran for 10 minutes to examine the basic performance. All of the paddles of polarization controller 1 and 3 were fixed to the optimum positions. Paddles of polarization controller 2 were fixed to the positions which produce the minimum output power. The output power was then recorded every second. The results are shown in Fig.5-6. In this experiment, the polarization controllers were set to fixed so the power dropping at the end of the experiment was confirmed from the power fluctuation from the source.

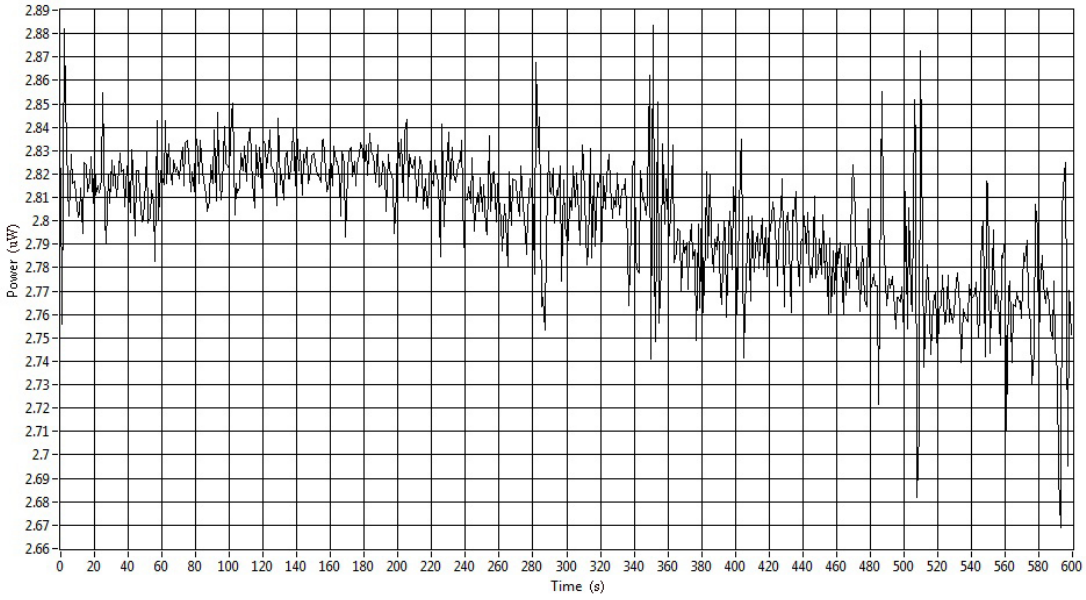

Figure 5-6: *10 minutes experiment. Polarization controller 1 and 3 were in maximum position and polarization controller 2 was in minimum position.*

For comparison, another experiment was run with some adjustments. Polarization controller 1 and 3 kept the same setting. The paddles of polarization controller 2 varied every second in a range of ±20 from their minimum positions.

Output power was recorded every second. The results are shown in Fig.5-7.

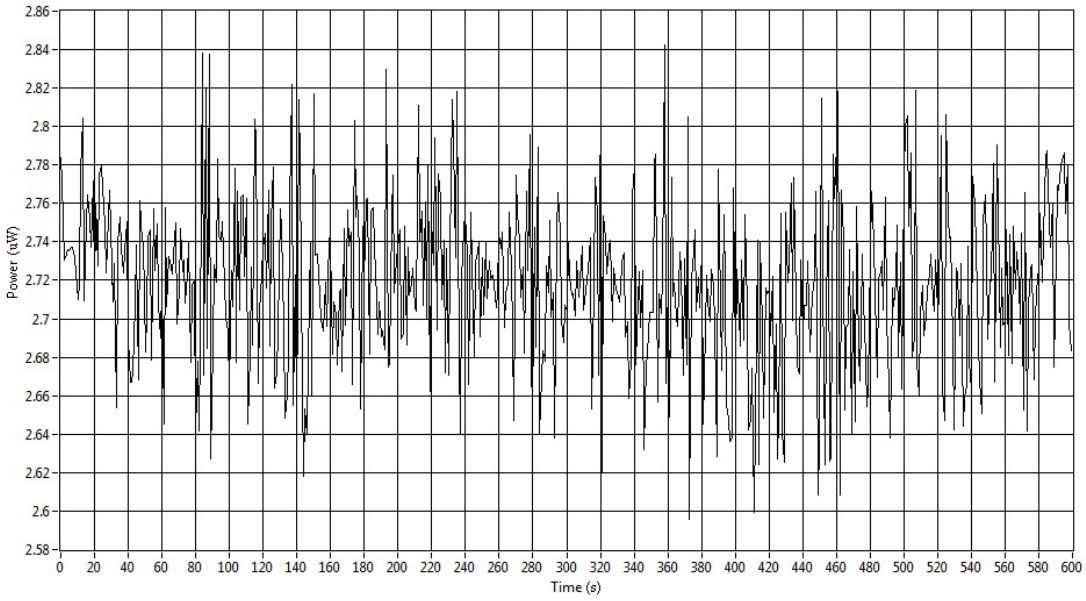

Figure 5-7: *10 minutes comparison experiment. Polarization controller 1 and 3 were in optimum position and polarization controller 2 varied around minimum position.*

By varying the paddles of polarization controller 2, the fluctuation of output power was slightly enlarged but the overall curve is more stable, not decreased as in the first experiment.

5.2.3 Experiments with Medium Term (24 hours)

Single Polarization Controller Variation Experiments

After testing the performance of the emulator with 10 minute duration experiments, the experiment time was increased to 24 hours. The results are shown in Fig. 5-8. The emulator experiments ran for two times with different settings.

In the first run (Case 1, black dot curve in Fig. 5-8), the paddles of polarization controller 1 and 3 were fixed to the optimum positions and paddles of polarization controller 2 varied every second in a range of ± 20 around the minimum positions. Readings on the multimeter were recorded every second at this

point. The curve was mapped with the average value of every minute from the recorded data, because the density of data points was too large to make a clear graph if all data were plotted in this figure.

In the second run (Case 2, blue solid curve in Fig. 5-8), the paddles of polarization controller 1 were fixed to the optimum positions and paddles for polarization controller 2 were fixed to the minimum positions. The paddles of polarization controller 3 then varied randomly every second in a range of ±20 around the optimum positions. Readings on the multimeter were recorded every second, and the curve was mapped with the average value of every minute as well.

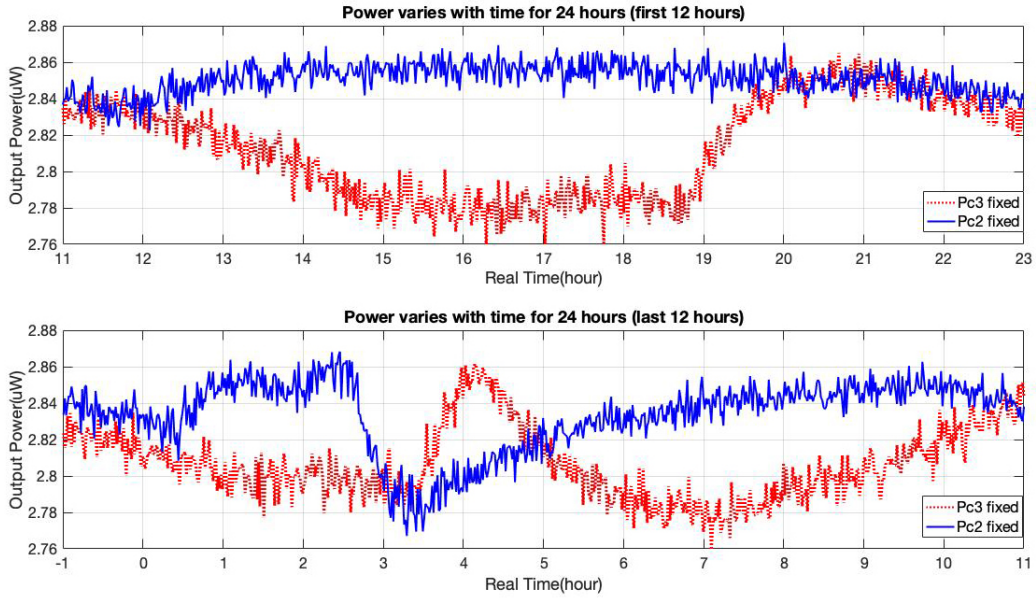

Figure 5-8: *Results of 24 hours experiments.*

Three things are indicated in Fig. 5-8. The first is that these two curves roughly had the same fluctuation within the short term, which means this kind of fluctuations are relevant to the range of paddle position variation (±20), but not which polarization controller was varying. The second is that both of these two curves showed some big fluctuations at certain times, mostly in the early morning from 2 am to 6 am. There are multiple reasons for that kind of fluctuations, such as variation of temperature and vibrations (securities entering the lab). The third is that the big fluctuations mentioned in the second point hap-

pened at different times in these two curves. Considering these two experiments were performed on two different days, this could be caused by different environmental conditions.

Temperature Checking

Considering the big fluctuations in the results, temperature variation is the first probable reason. Based on this assumption, an experiment with measuring output power and temperature synchronously was performed. The results are shown in Fig. 5-9. Whilst the output powers and temperature vary by $\sim 5-6\%$ over a 24 hour period, there is no obvious correlation, as these occur at different times. Therefore, temperature changes are unlikely to be the cause of the large, $\sim 6\%$ swings in output power.

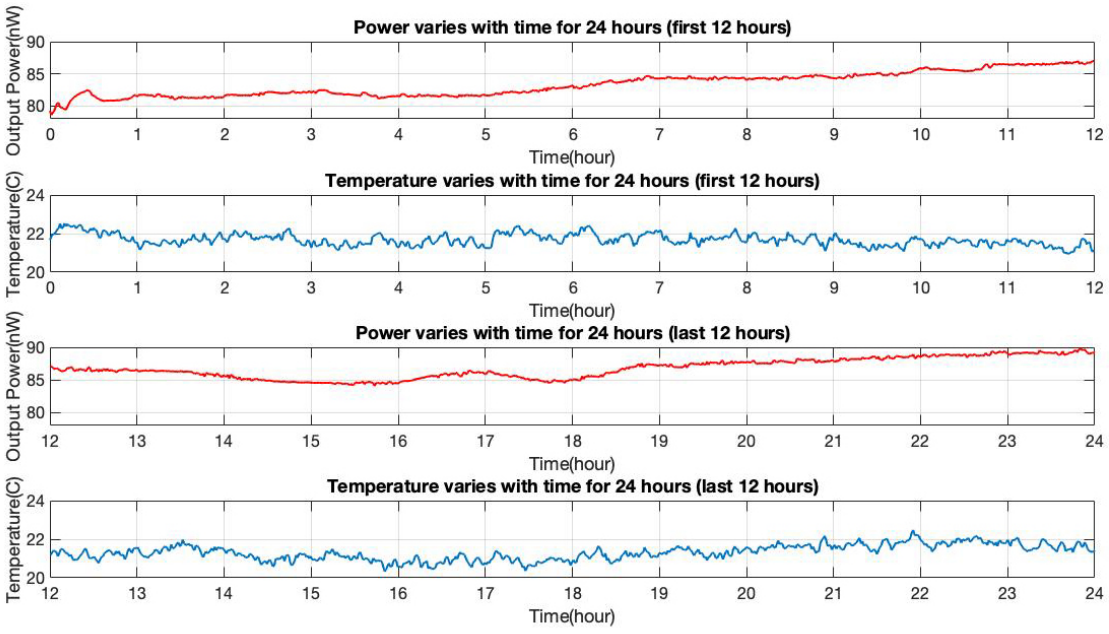

Figure 5-9: *Comparison of variations of output power and temperature*

In Fig. 5-9, the output power shows the big fluctuations in certain times. However, the fluctuations of temperature are very limited and irrelevant with these big fluctuations in output power. Therefore, the reason of power fluctuation may be vibrations.

Multiple Polarization Controller Variation Experiment

By varying all of the paddles of the three polarization controller randomly, it brought more variation into the emulator, which should be able to generate a set of PDL which is more similar to real fibre link. In the new setting of the experiment, all paddles of all polarization controllers varied randomly in a range from 000 to 999, which is in a range of 180 degrees, and the time intervals between variations were random as well. Readings from the multimeter were recorded every second. The experiment duration was 24 hours.

Figure 5-10 shows the result of the first 10 minutes output power. From the figure, it shows that the random variation of paddle positions affected both the fluctuations in short term and the average output power. To prove this result is closer to real fibre link, the statistics of output power of this 24 hours experiment were calculated. The result is shown in Fig. 5-11. The result shows that with the statistics result, Gaussian fit is better than Maxwellian fit which means this emulator needs to be given more independent random factors, such as setting the paddles varying position independently, to generate a set of data close to a real fibre link.

5.3 PDL Emulator

The PDL emulator shown in Fig. 5-12 has been built with computer-driven polarization controllers and sections of single mode fibre (SMF) to provide a continuous statistical result which obeys the Maxwellian distribution. A stable laser source is used to provide continuous lightwave at the wavelength of 1550 nm. A power splitter is deployed between the laser source and the system. 10% of the source power is sent to one channel of the multimeter as a reference, and the other 90% goes into the emulator. The sections of SMF which are used to connect each

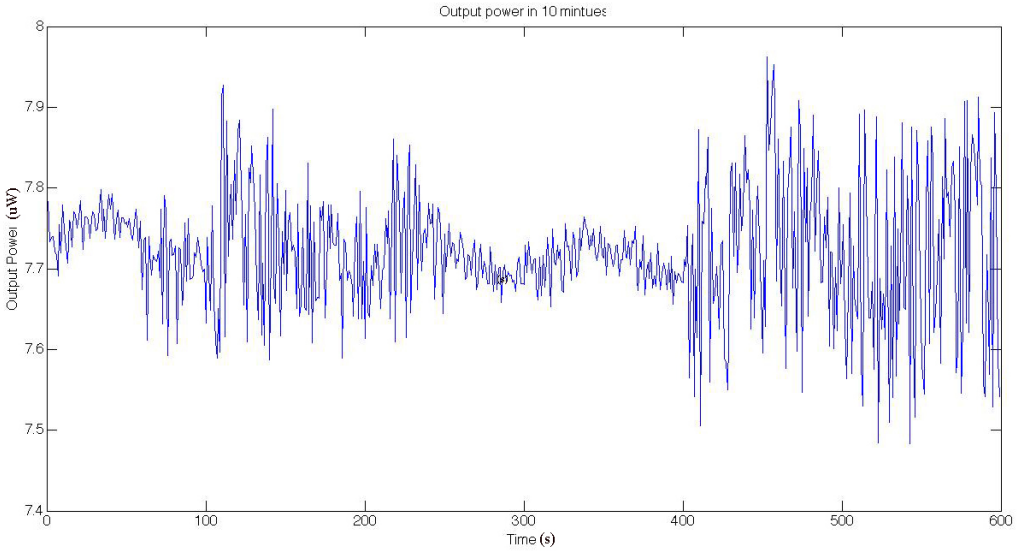

Figure 5-10: *Output power of 3 random varied polarization controllers in 10 mintues.*

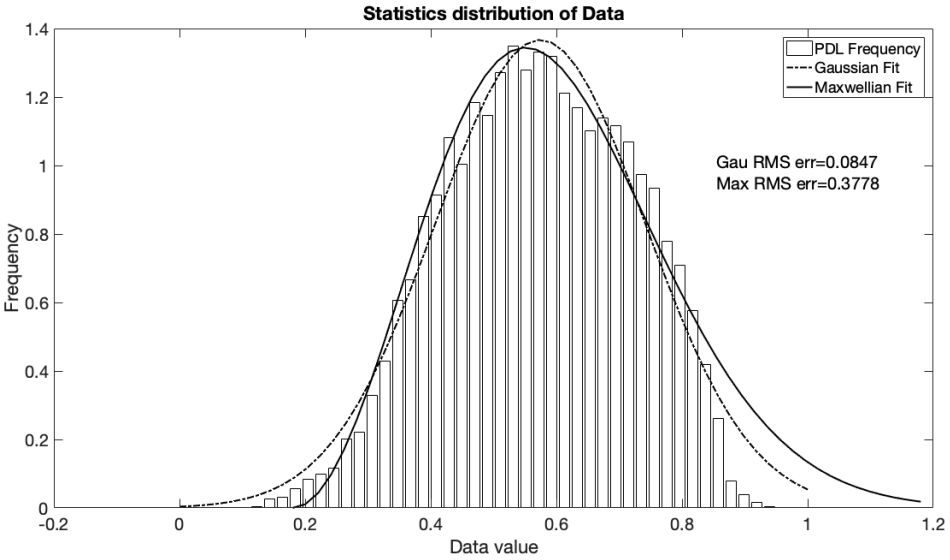

Figure 5-11: *Statistics of output power in 24 hours experiment.*

polarization controller are 15 metres long. All of the polarization controllers are changing their paddle positions rapidly and randomly to maximize the system randomization.

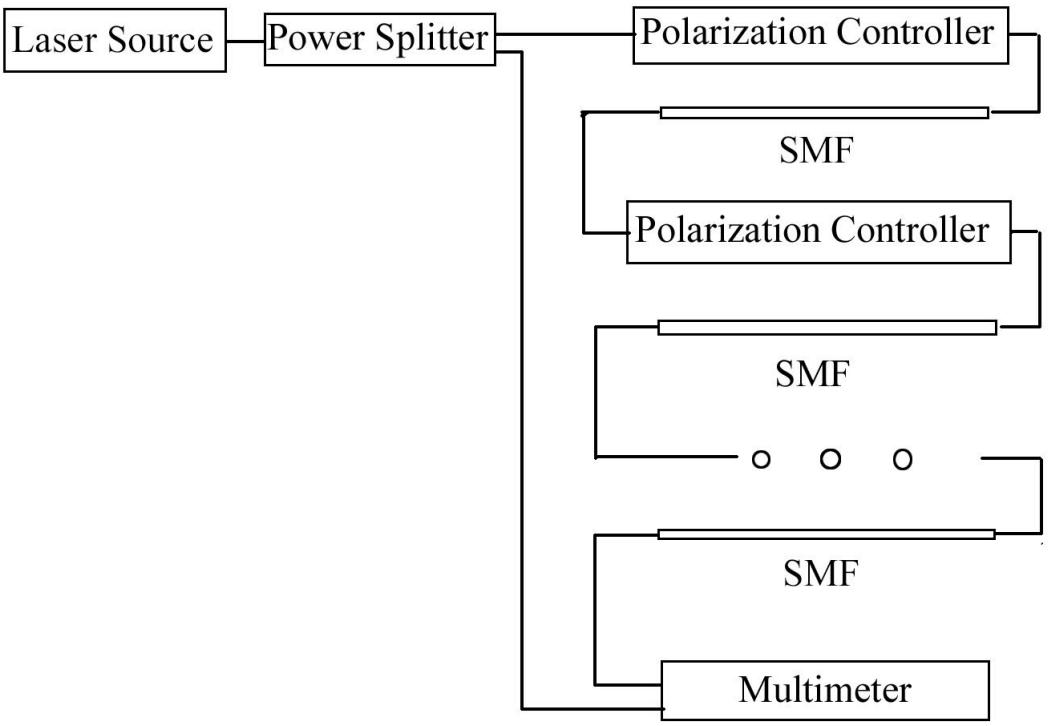

Figure 5-12: *The design of PDL emulator.*

5.3.1 The Effect of Random Temporal Variations in the Paddles of the Polarization Controllers

To set up a comparison group, the paddles of each controller are set to vary their positions randomly and simultaneously at the same time interval of between 30 seconds to 5 minutes.

Figure 5-13 shows the statistical distribution that resulted from changing the paddles of just one polarization controller followed by 1 section of SMF (15 metres). The x-axis shows the normalized PDL value and the y-axis shows the frequency with which each PDL value occurred. The peak in pdf shifts to the right of the centre slightly, compared with a true Maxwellian distribution, which makes it a reversed Maxwellian distribution.

As there is only one controller set in this experiment and its paddle positions vary at the same time interval, the randomness it can provide is limited. That is the reason why the result shows a reversed Maxwellian distribution. This

should be improved by increasing the number of polarization controllers and by setting the paddles to vary their position at independently random time interval.

By increasing the fibre length to 45 metres, the new statistical distribution is shown in Fig. 5-14. The statistics is more like a Gaussian distribution in this case.

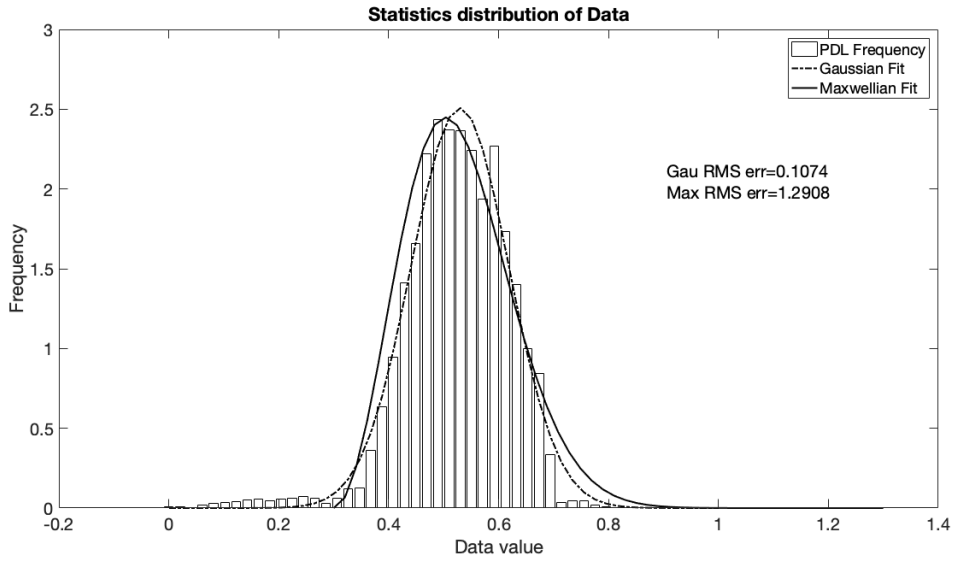

Figure 5-13: *Statistics of PDL in 24 hours experiment (1 controller followed by 15 metre SMF).*

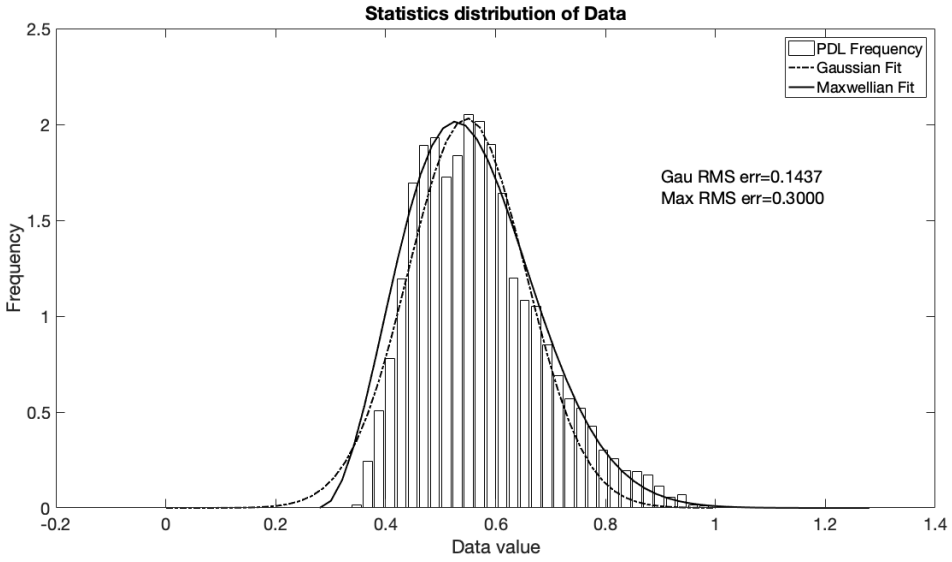

Figure 5-14: *Statistics of PDL in 24 hours experiment (1 controller followed by 45 metre SMF).*

To enhance the randomness, a second polarization controller is introduced into the system. The four paddles of the second polarization controller are set to randomly vary their position at the same time interval (from 30 seconds to 5 minutes.), but independent from the time interval of the first polarization controller. The second controller is directly connected to the first controller via the first 15m section of SMF.

Figure 5-15, 5-16, 5-17 and 5-18 respectively show the statistical distribution of this experiment with the length of the SMF at 15 metres, 45 metres, 75 metres and 105 metres. As they show, the pdf peak shifts to the left of the centre slightly which makes the statistics more Maxwellian than the results of the experiment with one polarization controller.

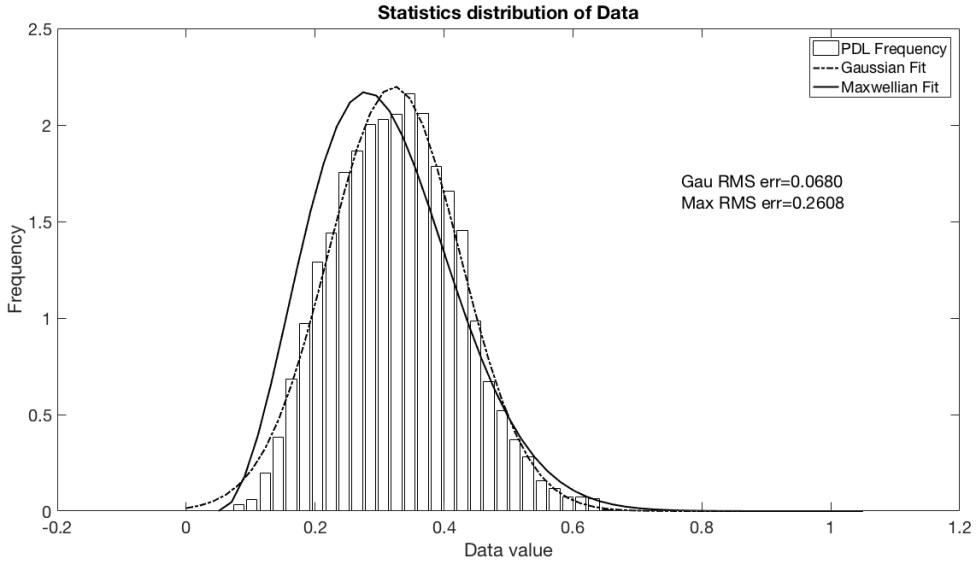

Figure 5-15: *Statistics of PDL in 24 hours experiment (2 controllers followed by 15 metre SMF).*

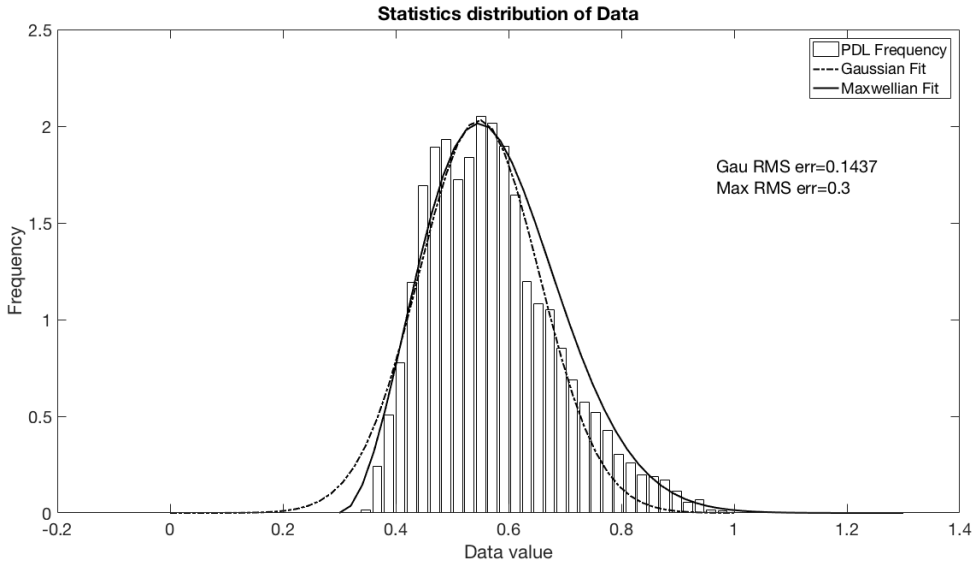

Figure 5-16: *Statistics of PDL in 24 hours experiment (2 controllers followed by 45 metre SMF).*

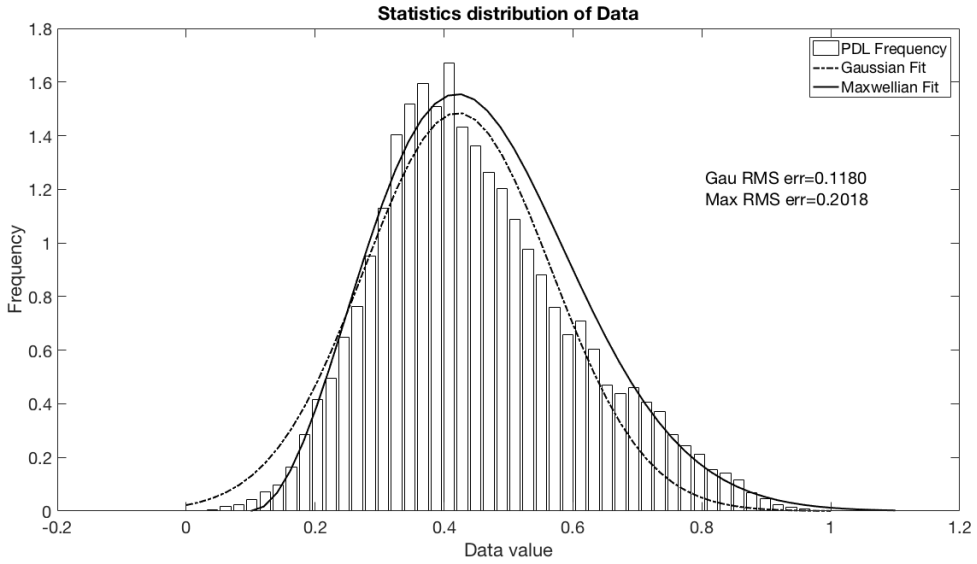

Figure 5-17: *Statistics of PDL in 24 hours experiment (2 controllers followed by 75 metre SMF).*

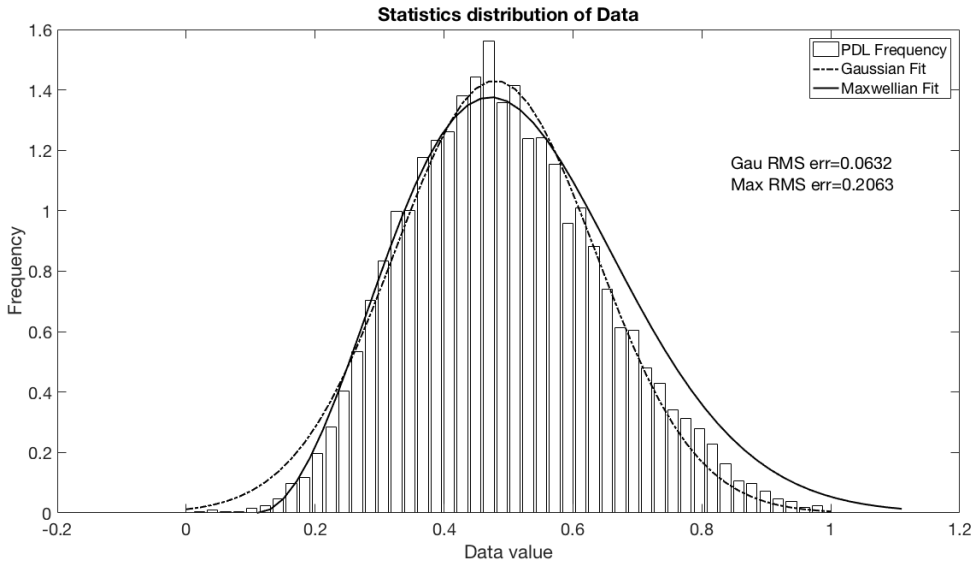

Figure 5-18: *Statistics of PDL in 24 hours experiment (2 controllers followed by 105 metre SMF).*

5.3.2 Two Polarization Controllers Connected with Single Mode Fibre

Random Initial State of Polarization

To test the effect of the length of SMF between the two polarization controllers, the paddles of both controllers are set to vary positions independently from each other at individual time intervals (30 seconds to 5 minutes). But now all of the 7 sections of SMF (105 metres) are connected into the systems, the difference being the length between the first and the second controllers generating different setups of this experiment. Assuming the fibre length between the first and the second controllers is L metres, the fibre length between the second controller and the multimeter is 105-L metres. All the setups are shown in Table 5.2.

Table 5.2: *Case list of the different sets of emulator. PC1 and PC2 indicate polarization controller 1 and polarization controller 2 respectively, SMF indicates single mode fibre.*

Case 1 (L=0)	PC 1⟶ PC 2⟶7 sections of SMF
Case 2 (L=15)	PC 1⟶ 1 section of SMF⟶PC 2⟶6 sections of SMF
Case 3 (L=30)	PC 1⟶ 2 sections of SMF⟶PC 2⟶5 sections of SMF
Case 4 (L=45)	PC 1⟶ 3 sections of SMF⟶PC 2⟶4 sections of SMF
Case 5 (L=60)	PC 1⟶ 4 sections of SMF⟶PC 2⟶3 sections of SMF
Case 6 (L=75)	PC 1⟶ 5 sections of SMF⟶PC 2⟶2 sections of SMF
Case 7 (L=90)	PC 1⟶ 6 sections of SMF⟶PC 2⟶1 section of SMF

Figure 5-19, 5-20, 5-21, 5-22, 5-23, 5-24 and 5-25 respectively show the statistical distribution of this experiment with the length of SMF between polarization controller 1 and polarization controller 2 being L= 0, 15 metres, 30 metres, 45 metres, 60 metres, 75 metres and 90 metres. As the graphs show, the statistics still fit Gaussian better than the Maxwellian distribution, but the differences decreased.

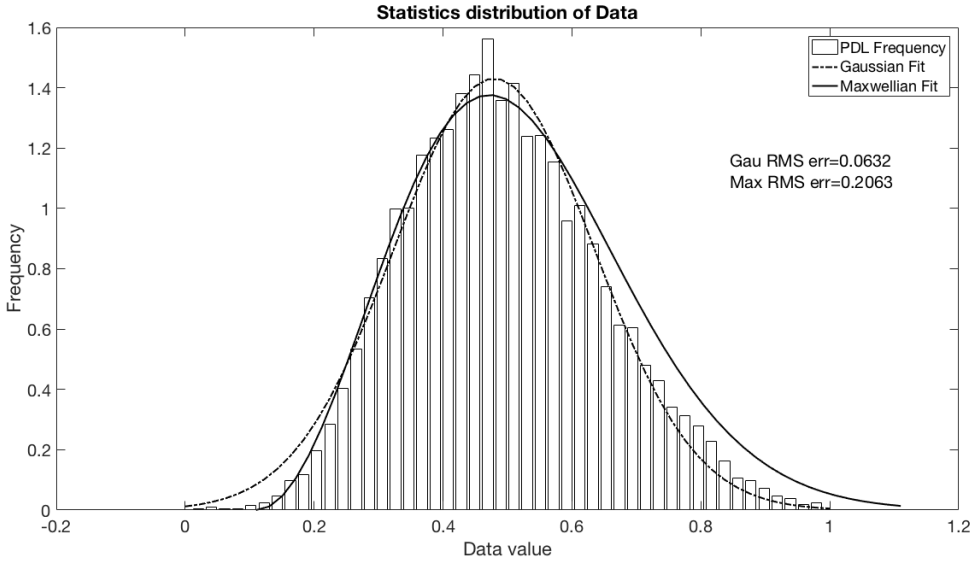

Figure 5-19: *Statistics of PDL in Case 1 (2 controllers).*

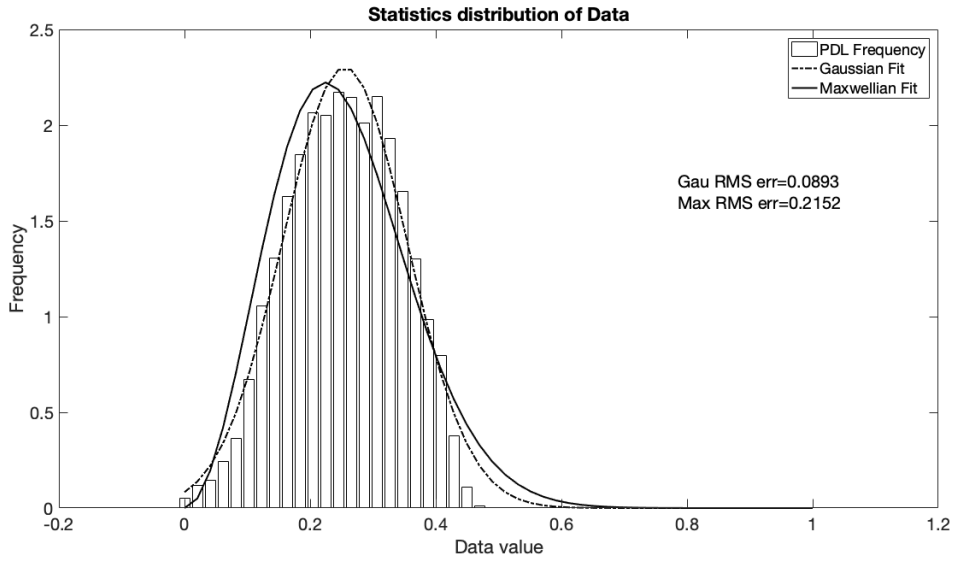

Figure 5-20: *Statistics of PDL in Case 2 (2 controllers).*

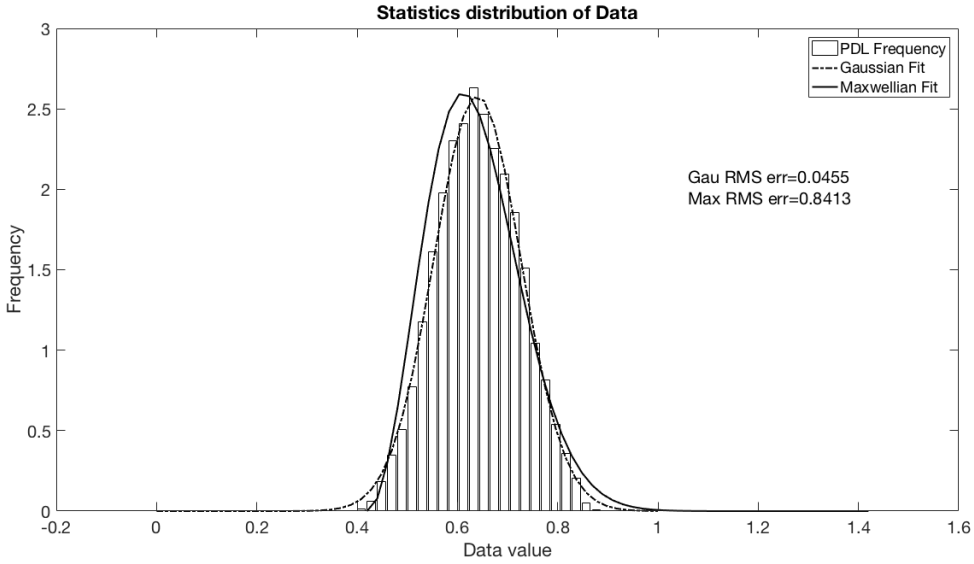

Figure 5-21: *Statistics of PDL in Case 3 (2 controllers).*

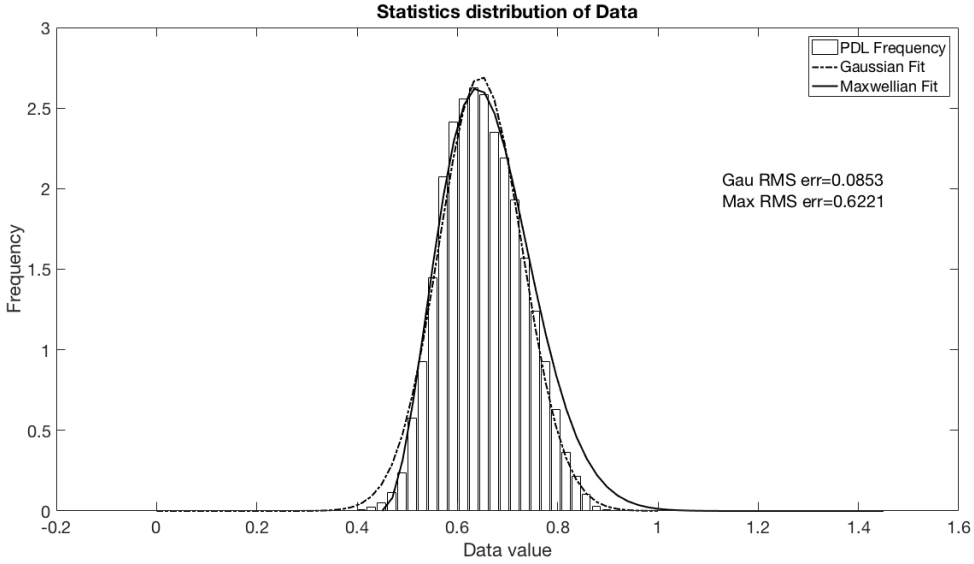

Figure 5-22: *Statistics of PDL in Case 4 (2 controllers).*

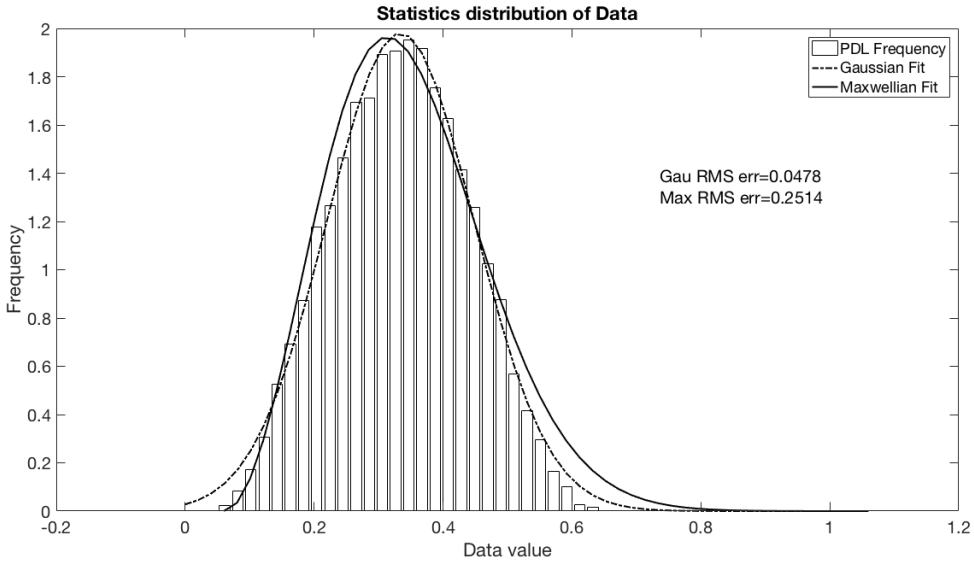

Figure 5-23: *Statistics of PDL in Case 5 (2 controllers).*

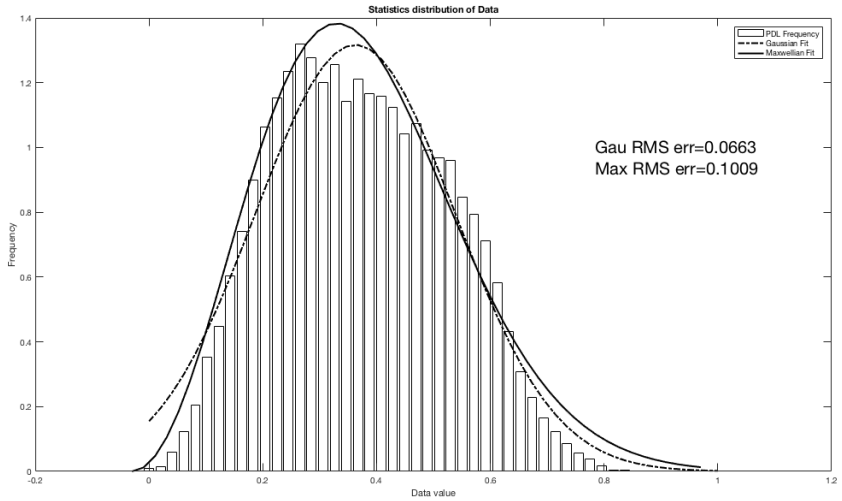

Figure 5-24: *Statistics of PDL in Case 6 (2 controllers).*

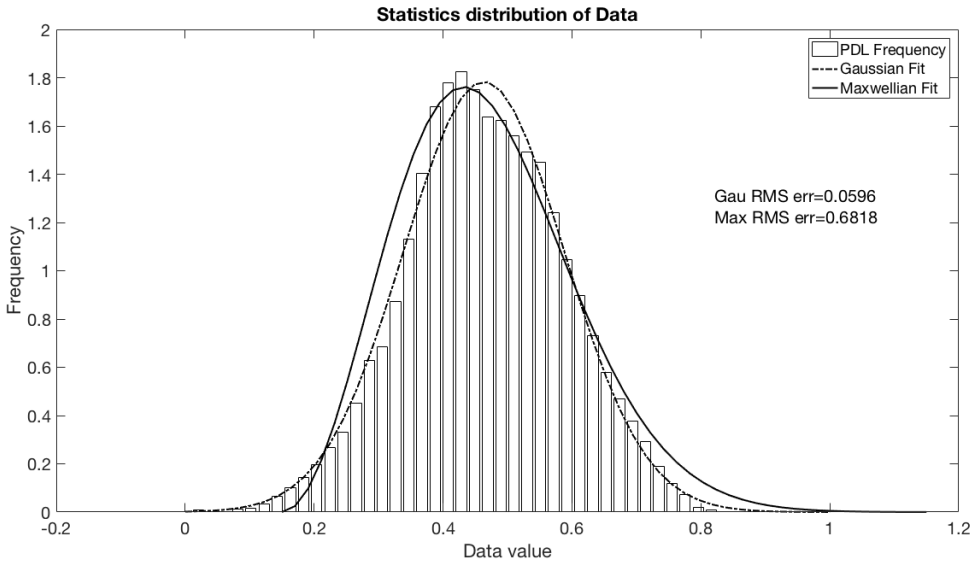

Figure 5-25: *Statistics of PDL in Case 7 (2 controllers).*

With the measured data, the mean value and the variance of the PDL in the 7 cases are calculated and presented in Table 5.3. The first point to make is that the variance is minimum for case 1 and 7 (as shown in Fig. 5-27) where the total length of fibre is a maximum, either between the two polarization controllers or after the second polarization controller. The reason for this is unclear, but it could be that the power reflection from the fibre connectors interfered the output reading.

Table 5.3: *Mean value and Variance of PDL in different cases.*

Case No.	Mean value of PDL (in dB)	Variance of PDL
Case 1	0.2424	0.0025
Case 2	0.2522	0.0032
Case 3	0.5665	0.0031
Case 4	0.5831	0.0044
Case 5	0.5568	0.0033
Case 6	0.5639	0.0038
Case 7	0.3139	0.0026

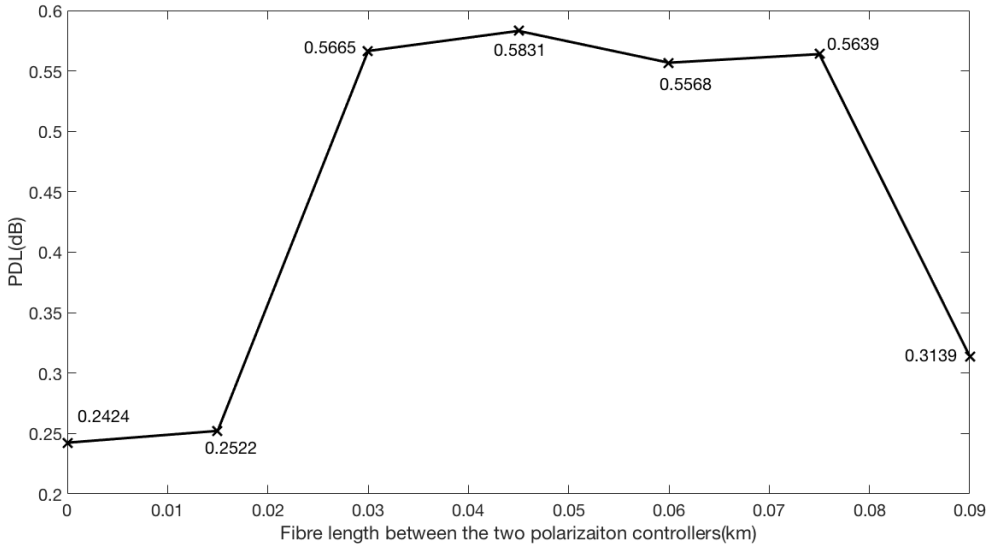

Figure 5-26: *PDL mean value from Case 1 to Case 7 (2 controllers).*

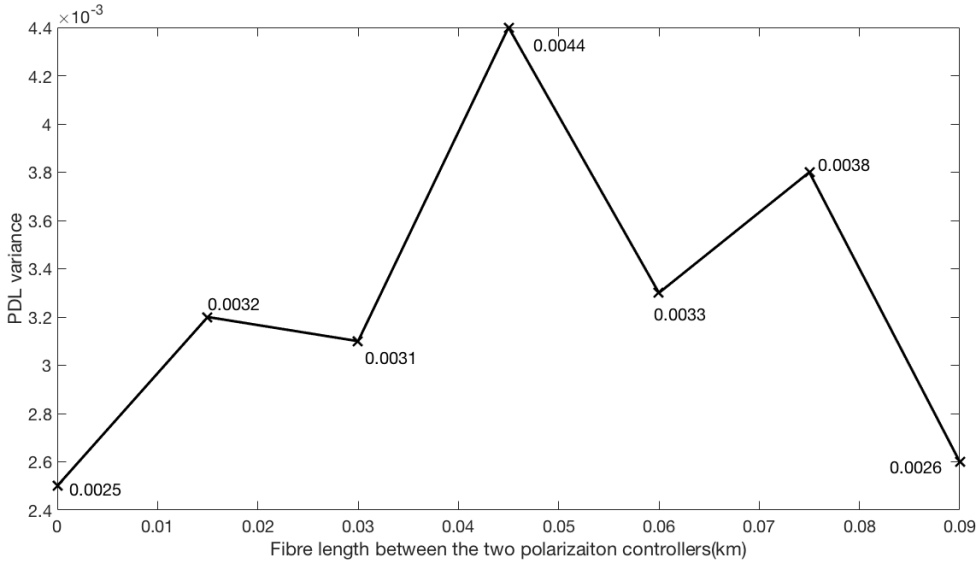

Figure 5-27: *PDL variance from Case 1 to Case 7 (2 controllers).*

Based on Eq. 3.29, the mean-square value of the PDL ρ^2 exponentially increases as the communication length increases. However, even if the communication distance is fixed to a constant, the statistical results in the system varies. In this experiment, the communication fibre is a constant length, so the main factor which varies the statistical results is the position of the two controllers, which have been used to emulate the PDL components in real systems. This effect is now investigated.

The PDL components statistically vary the results in two ways. Their random patterns change as their working environment changes in time. On the other hand, the positions where the PDL components were deployed in the systems can lead to different results as the combination of PDL component and the fibre length is changed.

As shown in Fig. 5-26, when the fibre length is fixed and the initial state of polarization is random, a continuous fibre link without any change of state of polarization can generate a smaller mean value of PDL in statistics, such as Case 1,2 and 7. Inserting PDL components at different points can significantly increase the mean value of PDL, even though the total length and total number of PDL components remains the same.

Fixed Initial State of Polarization

By manually setting the paddles of the first controller to their position of maximum light through-put (see Table 5.1), and repeating the experiment can be used to estimate the PDL mean value variation with a fixed initial state of polarization. Case 1 (L=0) is no longer needed in Table 5.2 so there are 6 sets of data required, see Table 5.4.

The mean values of Case 1 to Case 6 are presented in Table 5.5 and the trend is shown in Fig. 5-28. Comparing Fig. 5-28 with Fig. 5-26, reveals that the trend of PDL value with a fixed initial state of polarization is different from the one with a random initial state of polarization. With a fixed initial state of polarization, the PDL mean value decreases to a minimum value and then increases as the fibre length L between the two controllers increases. The physical mechanism behind this phenomenon may be that when the fibre lengths between

polarization components were equal or close to each other, there was bigger chance that the PDL could be self-compensated during signal transmission, as the effects of change of state of polarization were more likely to be compensated when the propagation distances were similar.

Table 5.4: *Case list of the different setting of the emulator. PC1 and PC2 indicate polarization controller 1 and polarization controller 2 respectively, SMF indicates single mode fibre.*

Case 1 (L=15)	PC 1⟶ 1 section of SMF⟶PC 2⟶6 sections of SMF
Case 2 (L=30)	PC 1⟶ 2 sections of SMF⟶PC 2⟶5 sections of SMF
Case 3 (L=45)	PC 1⟶ 3 sections of SMF⟶PC 2⟶4 sections of SMF
Case 4 (L=60)	PC 1⟶ 4 sections of SMF⟶PC 2⟶3 sections of SMF
Case 5 (L=75)	PC 1⟶ 5 sections of SMF⟶PC 2⟶2 sections of SMF
Case 6 (L=90)	PC 1⟶ 6 sections of SMF⟶PC 2⟶1 section of SMF

Table 5.5: *Mean value of PDL in different cases.*

Case No.	Mean value of PDL (in dB)
Case 1	0.4525
Case 2	0.3030
Case 3	0.2852
Case 4	0.2373
Case 5	0.2605
Case 6	0.2830

5.3.3 Three Polarization Controllers Connected with Single Mode Fibre

To further enhance the randomness, a third polarization controller is introduced into the system. With the third controller, the experiment has more complicated setups. Assuming the fibre length between the first and the second controllers is L1 metres, the fibre length between the second and the third controllers is L2 metres, the fibre length between the third controller and the lightwave multimeter is 105-L1-L2 metres. The paddles of the first controller are manually set to their maximum position (see Table 5.1) to create a fixed initial state of polarization. The paddles of the second and the third controllers are set to vary position independently at individual time intervals (from 30 seconds to 5 minutes). All

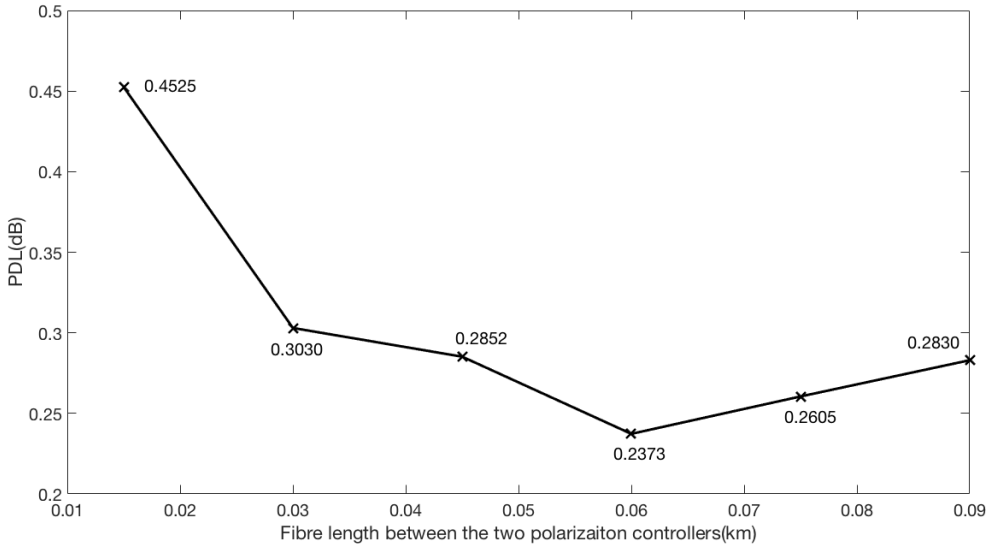

Figure 5-28: *PDL mean value from Case 1 to Case 6 (2 controllers).*

the setups with three controllers are shown in Table 5.6.

Figure 5-29 - 5-40 respectively show the statistical distribution of this experiment with the setup in Table 5.6. As they show, the statistics obeys Maxwellian distribution.

Table 5.6: *Fibre lengths in different cases*

	Between 1st and 2nd controllers (L1)	Between 2nd and 3rd controllers (L2)	Between 3rd controllers and receiver (105-L1-L2)
Case 1	15m	15m	75m
Case 2	15m	30m	60m
Case 3	15m	45m	45m
Case 4	15m	60m	30m
Case 5	15m	75m	15m
Case 6	30m	15m	60m
Case 7	30m	30m	45m
Case 8	30m	45m	30m
Case 9	30m	60m	15m
Case 10	45m	15m	45m
Case 11	45m	30m	30m
Case 12	45m	45m	15m

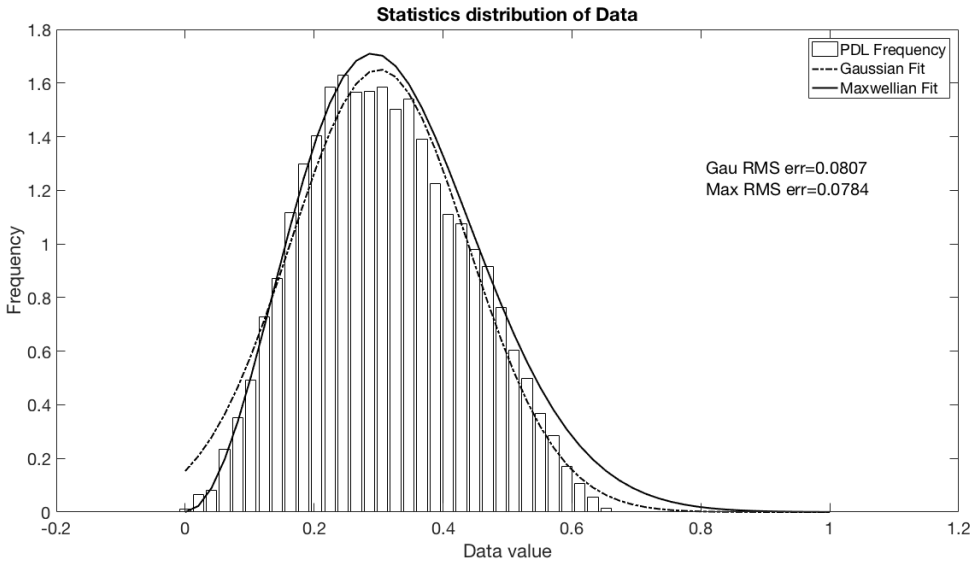

Figure 5-29: *Statistics of PDL in Case 1 (3 controllers).*

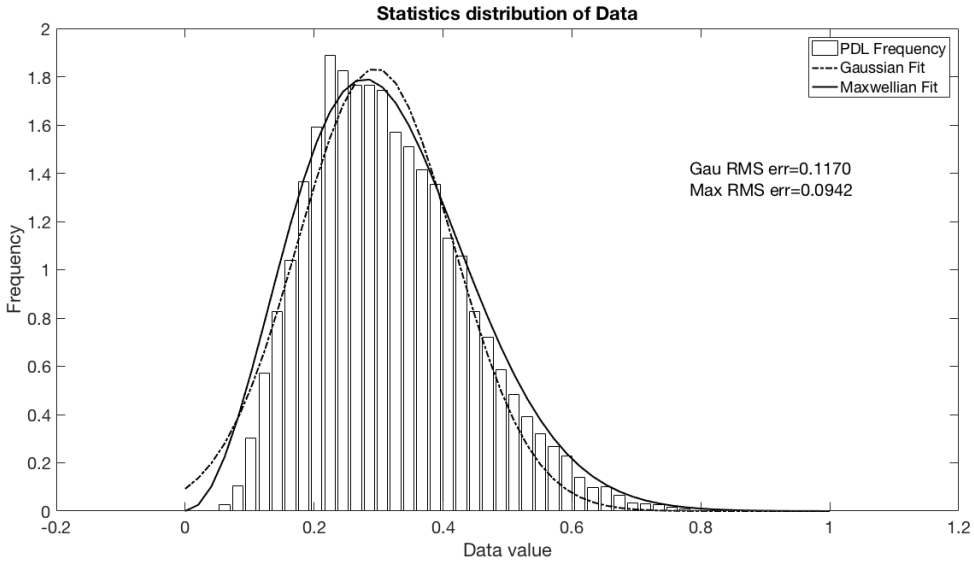

Figure 5-30: *Statistics of PDL in Case 2 (3 controllers).*

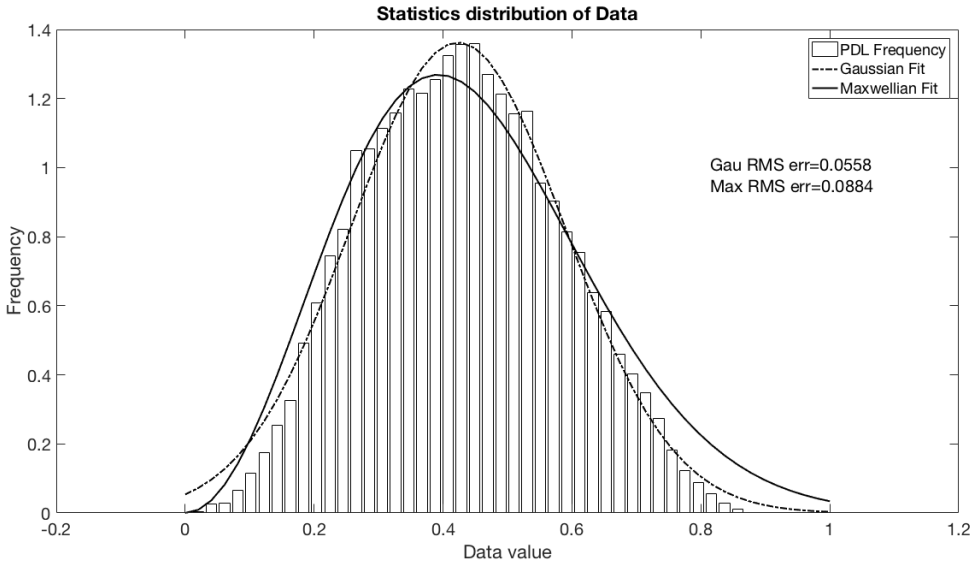

Figure 5-31: *Statistics of PDL in Case 3 (3 controllers).*

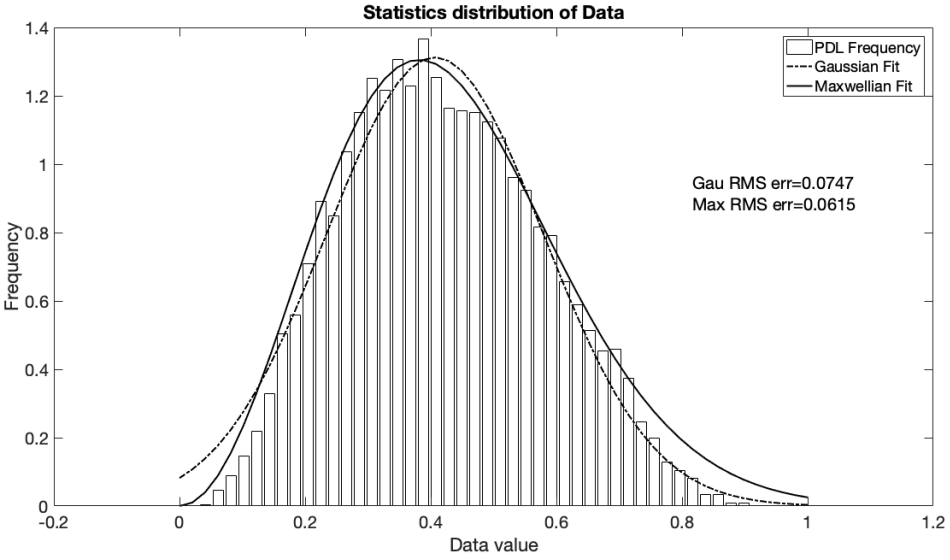

Figure 5-32: *Statistics of PDL in Case 4 (3 controllers).*

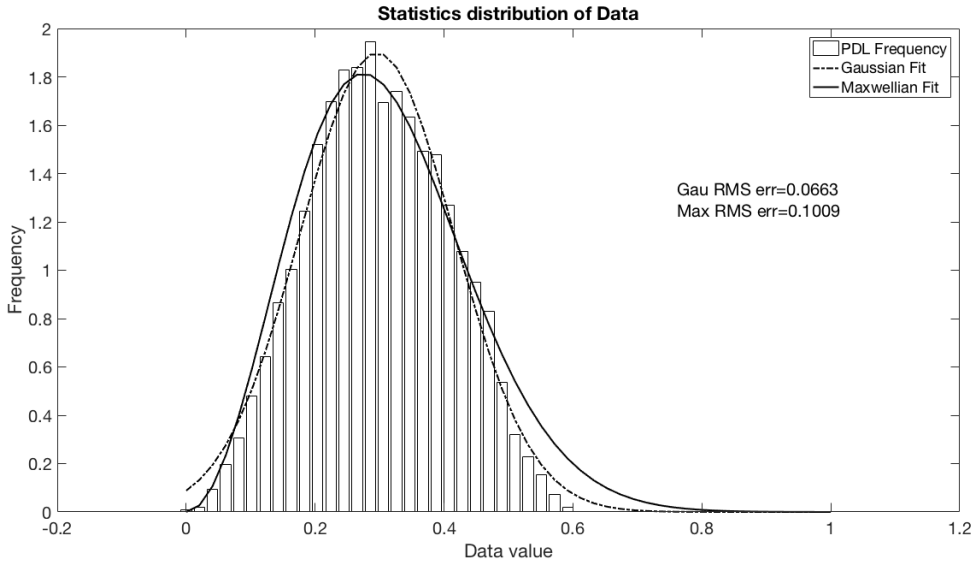

Figure 5-33: *Statistics of PDL in Case 5 (3 controllers).*

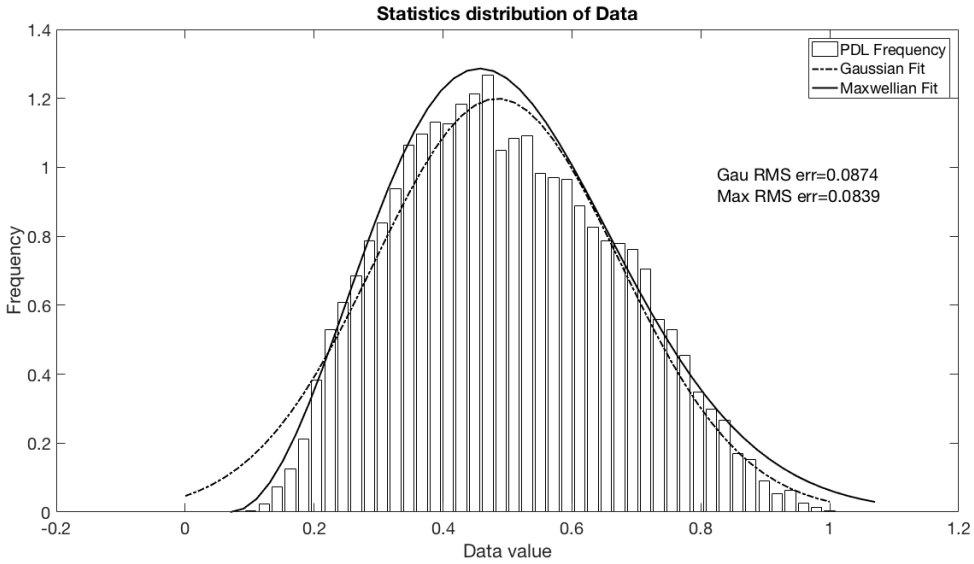

Figure 5-34: *Statistics of PDL in Case 6 (3 controllers).*

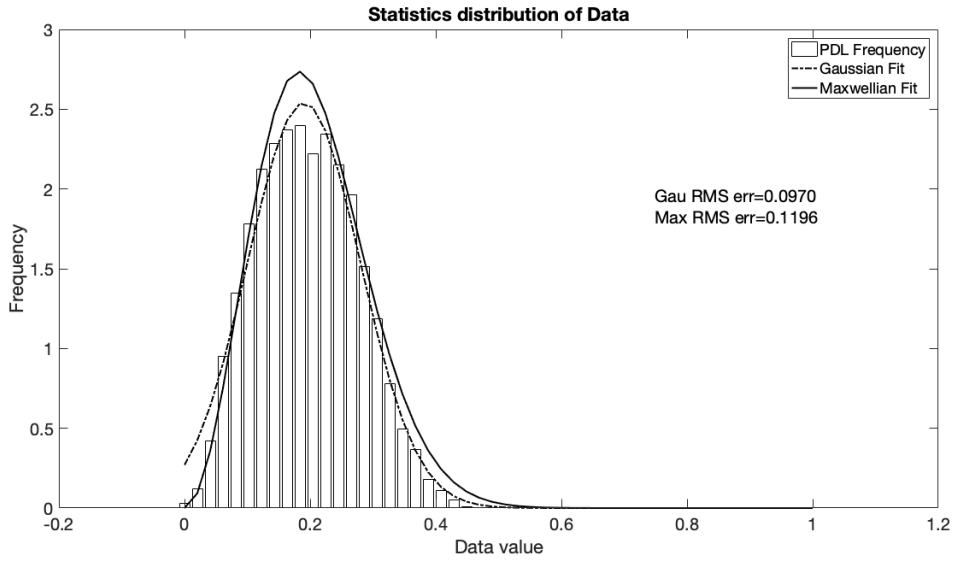

Figure 5-35: *Statistics of PDL in Case 7 (3 controllers).*

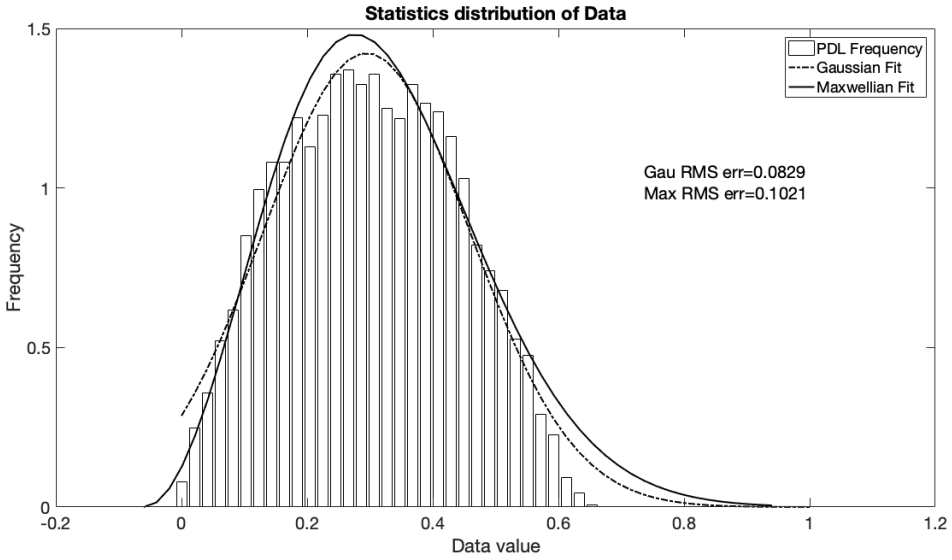

Figure 5-36: *Statistics of PDL in Case 8 (3 controllers).*

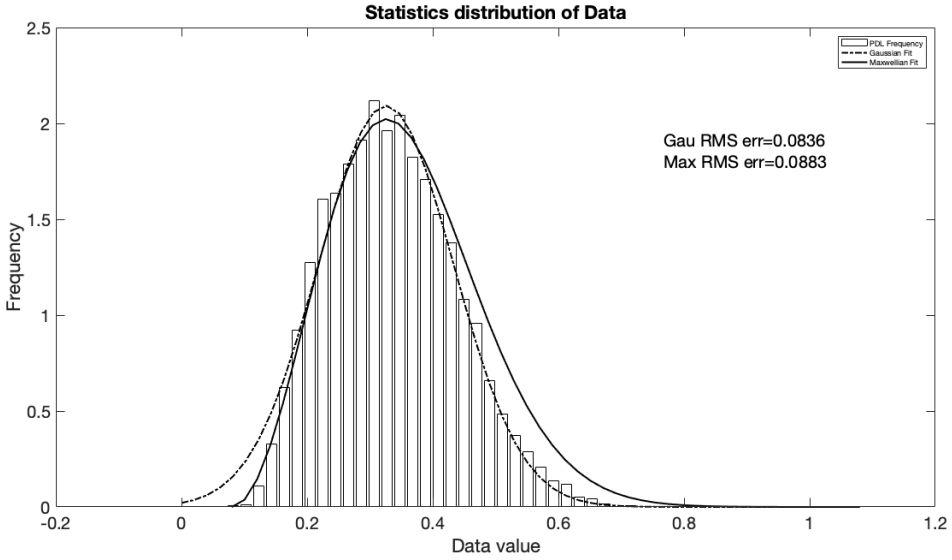

Figure 5-37: *Statistics of PDL in Case 9 (3 controllers).*

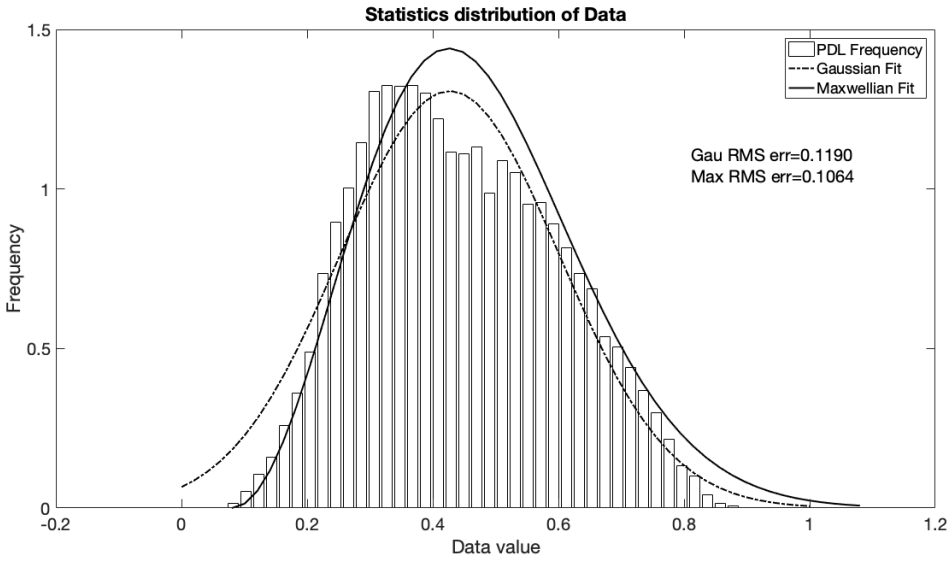

Figure 5-38: *Statistics of PDL in Case 10 (3 controllers).*

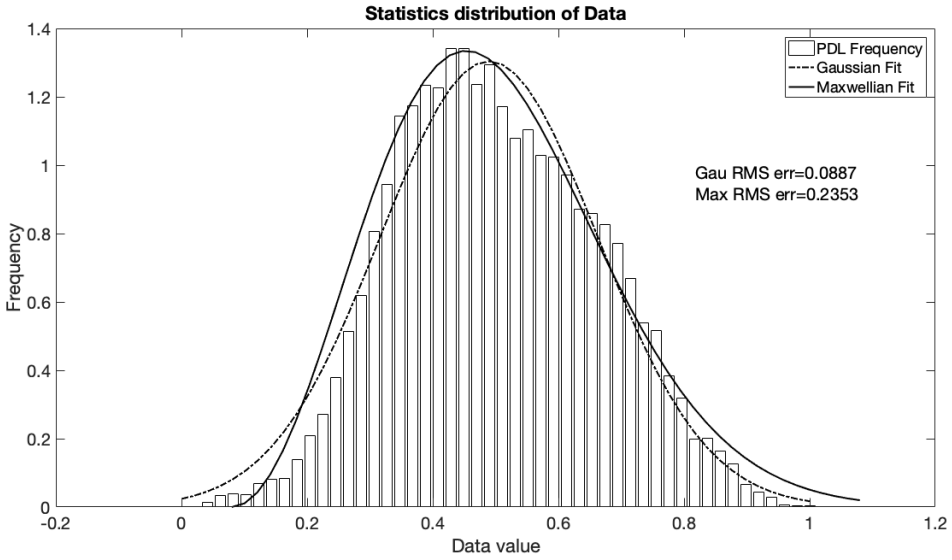

Figure 5-39: *Statistics of PDL in Case 11 (3 controllers).*

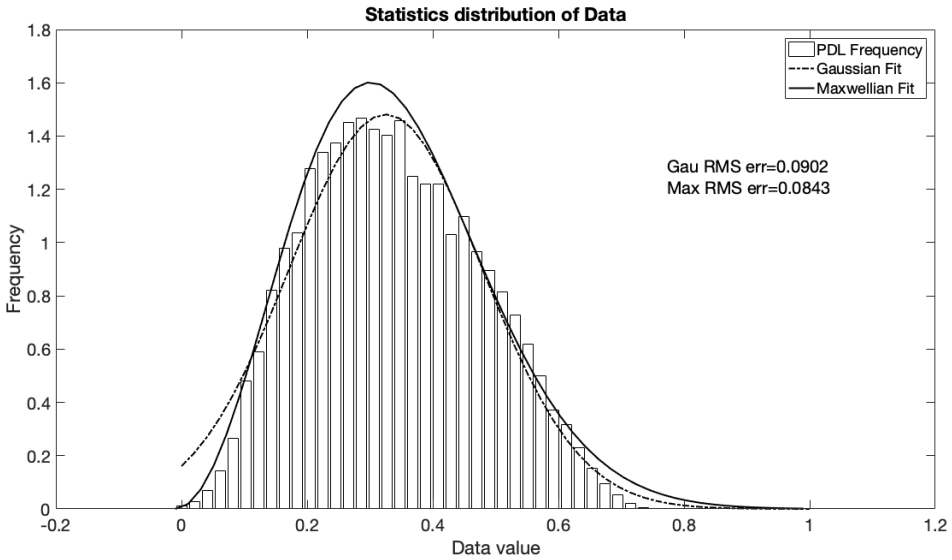

Figure 5-40: *Statistics of PDL in Case 12 (3 controllers).*

Figure 5-41, 5-42 and 5-43 respectively show the trends of PDL mean value when L1=15, 30 and 45 metres. All of the 3 figures indicates that when L2 increases, the PDL mean value decreases to the minimum and increases after that. The minimum PDL mean value appears when the fibre length of the second and the third fibre link are equal or close.

Figure 5-41, 5-42 and 5-43 also show that the variance of PDL value decreases when the first fibre link increases from 15 metres to 45 metres, as shown in Table 5.7. It shows that the PDL variance decreases when each of the fibre lengths are approximately equal.

Table 5.7: *PDL variances in Fig. 5-41, 5-42 and 5-43.*

	PDL variance
Fig. 5-41	0.0037
Fig. 5-42	0.0035
Fig. 5-43	0.0012

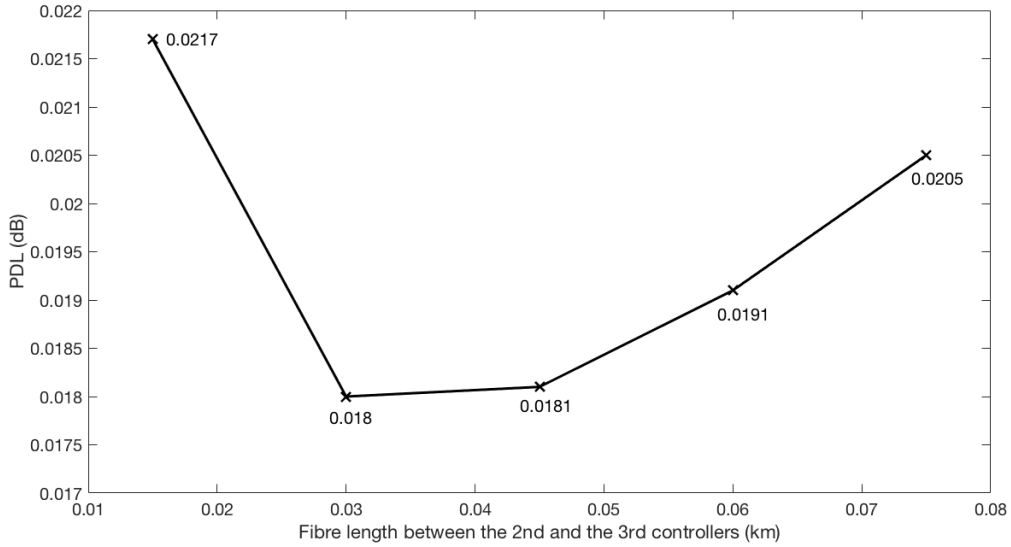

Figure 5-41: *Mean PDL value when L1=15 metres (3 controllers).*

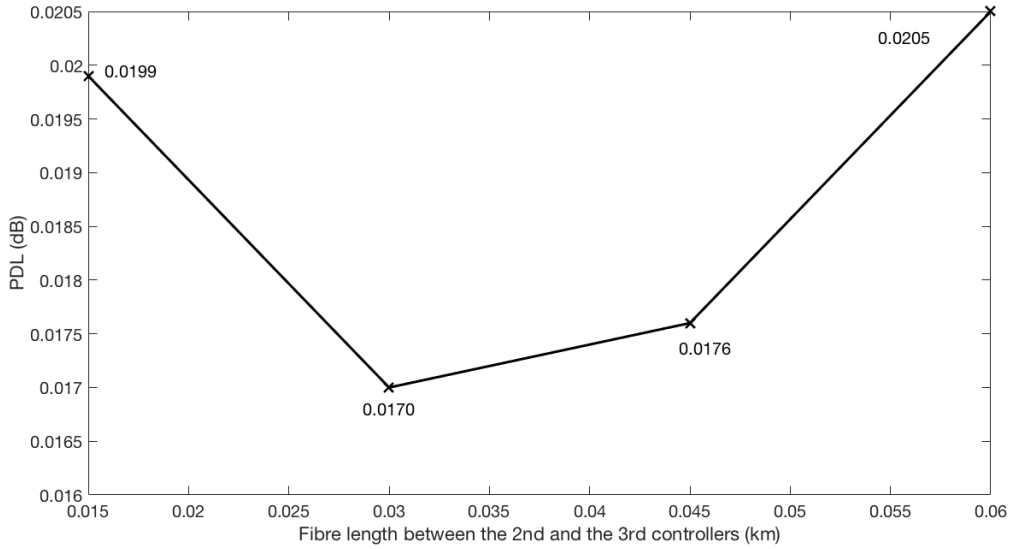

Figure 5-42: *Mean PDL value when L1=30 metres (3 controllers).*

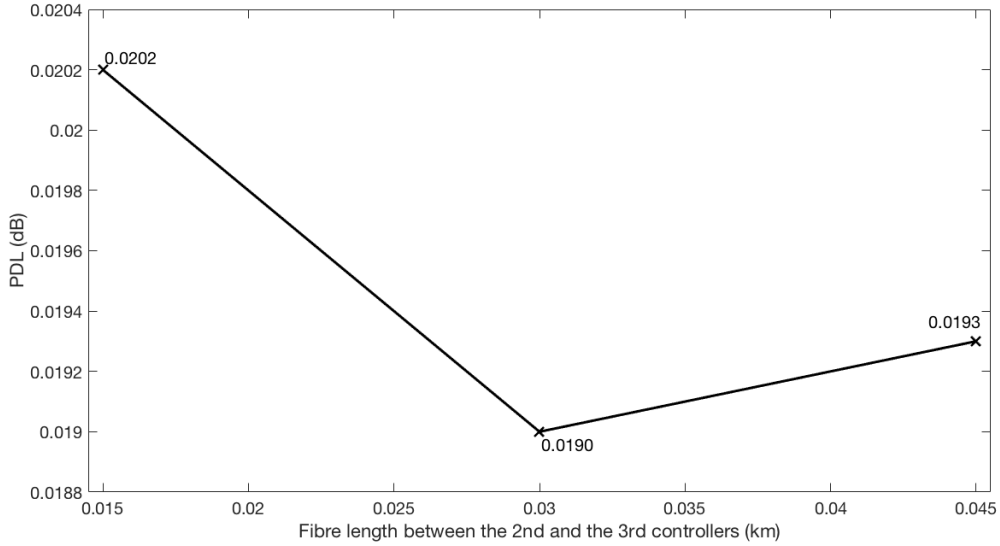

Figure 5-43: *Mean PDL value when L1=45 metres (3 controllers).*

5.3.4 Discussion

Comparing with two polarization controllers, it is obvious that the statistics results of PDL in three polarization controller emulation have increased Maxwellian fits. They are now very close to Gaussian fits, or even better than Gaussian fits. This is because the extra four paddles from the third polarization controller introduced more randomness into the system which made the results were more close to real systems.

With a fixed state of polarization, PDL mean value reaches minimum when the lengths of SMF sections between polarization controllers are equal or close. One possible reason of this is that when the lightwave with a fixed state of polarization propagated through the first section of SMF, it experienced PDL caused by the difference of loss factors on the two axes. When it reaches the polarization controller and the state of polarization was changed, the lightwave experienced a new PDL figure caused by the difference of loss factors on the two axes, which potentially compensates the loss it experienced in the first section of fibre. If the two sections of fibre are equal or close on lengths, it can reach a maximum compensation so a minimum PDL is achieved.

More results will be discussed in the next chapter, comparing with the simulation results.

5.4 Summary

In this chapter, the demand of PDL emulator has been discussed at the beginning of the chapter, as well as the earlier designs of polarization emulators. The emulator design and the parameter setup has been discussed after that, then the experiments and results are represented.

With the experiments, it has been found out that the emulator can meet the requirements of a proper PDL emulator, and the positioning of the polarization components can affect the PDL statistics even though the number of polarization components and fibre length are fixed.

CHAPTER 6

SIMULATION EXPERIMENTS

6.1 Simulation of the Designed Emulator

As PDL emulation is limited by the transmission distance and the number of PDL components in the laboratory environment, it is important to extend the technique to simulation models, which is able to cover a longer-distance system with dozens of PDL components.

As discussed in Chapter 2, based on the theory of Mueller, any PDL component can be described as [66]

$$M = \begin{pmatrix} m_{11} & m_{12} & m_{13} & m_{14} \\ m_{21} & m_{22} & m_{23} & m_{24} \\ m_{31} & m_{32} & m_{33} & m_{34} \\ m_{41} & m_{42} & m_{43} & m_{44} \end{pmatrix}$$

and the state of polarization is defined as $\vec{S} = (S_0, S_1, S_2, S_3)^T$, then the output power can be calculated by

$$P_{out} = m_{11}S_0 + m_{12}S_1 + m_{13}S_2 + m_{14}S_3 \tag{6.1}$$

. The PDL can be calculated using [67]

$$PDL_{dB} = 10 \times log(\frac{m_{11} + \sqrt{m_{12}^2 + m_{13}^2 + m_{14}^2}}{m_{11} - \sqrt{m_{12}^2 + m_{13}^2 + m_{14}^2}}) \tag{6.2}$$

In this case, by considering each paddle of polarization controller as an individual PDL component, its Mueller matrix can be rewritten as [68]

$$M_{paddle} = \begin{pmatrix} 1 & cos(2\theta) & sin(2\theta) & 0 \\ cos(2\theta) & cos^2(2\theta) & sin(2\theta)cos(2\theta) & 0 \\ sin(2\theta) & sin(2\theta)cos(2\theta) & sin^2(2\theta) & 0 \\ 0 & 0 & 0 & 0 \end{pmatrix}$$

where θ is the angle the paddle turned. Therefore, the Mueller matrix of the polarization controller is

$$M_{controller} = M_{paddle1} M_{paddle2} M_{paddle3} M_{paddle4} \tag{6.3}$$

By assuming the states of polarization do not change within the relative short distance, the Mueller matrix of one section of single mode fibre can be written as

$$F_{fibre} = \begin{pmatrix} exp(-\alpha L) & 0 & 0 & 0 \\ 0 & exp(-\alpha L) & 0 & 0 \\ 0 & 0 & exp(-\alpha L) & 0 \\ 0 & 0 & 0 & exp(-\alpha L) \end{pmatrix}$$

where α is the fibre loss figure and L is the length of the fibre. Therefore, the change of the state of polarization after one polarization controller and one section of single mode fibre with arbitary length can be calculated by

$$\vec{S_{out}} = F_{fibre} M_{controller} \vec{S_{in}} \tag{6.4}$$

. With this approach, it is possible to simulate the process of the emulation.

6.1.1 Measured and Estimated PDL Values from Previous Research

In order to simulate the impact of PDL on the optical communication systems, it is important to finish the simulation program with a set of proper PDL values. Previous researchers have performed measurements and estimations of PDL values in real transmission systems.

Based on the information from the user manual of Agilent Technologies, the typical PDL values for common lightwave components are shown below.

Table 6.1: *Typical PDL values for common lightwave components. [99]*

Components	PDL value
Single mode fibre (1m)	<0.02 dB
Single mode fibre (10km)	<0.05 dB
Optical connector (straight)	<0.05 dB
Optical connector (angled)	<0.1 dB
Open beam launch	<0.3 dB
Isolator	<0.3 dB
Coupler	<0.1 dB
Polarizer	>30 dB
EDFA	<0.4 dB

M. G. Taylor's Research in 1993 [100] Taylor's research reported a study into the effects of PDL on the signal and amplified spontaneous emission (ASE) levels in a 3100 km amplified system, containing 69 amplifier sections with 45 km repeater spacing. In the experiment, a passive PDL value of ±0.65 dB was measured, as well as a fixed offset from the active PDL, which was 0.07 dB per amplified section, this under the assumption that active PDL increases linearly with the number of elements.

Y. Sun's Research in 2001 [101] Sun's research used a recirculating loop of 107 km, which was configured with a dispersion map with 100 km of fibre ($D = -1ps/nm \cdot km$) followed by a section of 7 km fibre ($D = 17ps/nm \cdot km$). Four erbium-doped fibre amplifiers (EDFAs) are equally spaced to compensate for fibre loss and another EDFA was used to overcome the loss of the loop switch and coupler. The isolators in these EDFAs were the primary source of the PDL in the loop.

The researcher bypassed the loop switch and coupler to study the PDL of the link itself. The measured result showed the PDL value was about 0.35 dB and the PDG per EDFA was about 0.05 dB.

H. F. Hannstein's Research in 2001 [102] Hannstein's emulation was a concatenation of 6 groups of polarization components. Each group was a concatenation of 10 sections of polarization-maintaining fibre, followed by a PDL component (shown in Fig. 6-1).

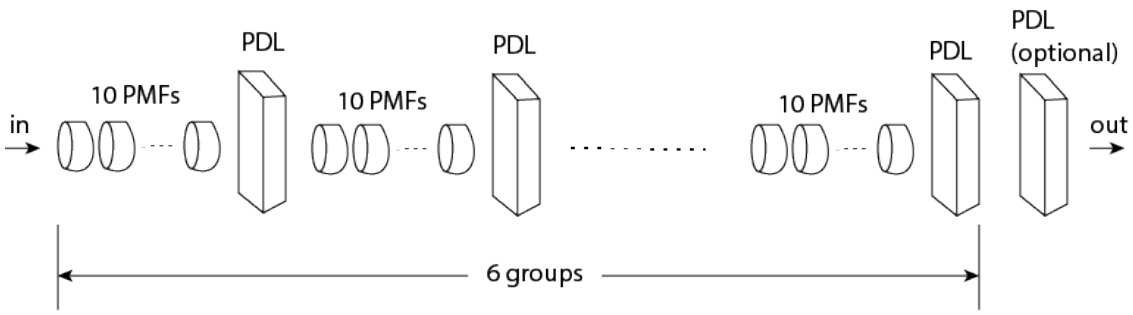

Figure 6-1: *Hannstein's research in 2003.*

The simulation value of PDL in the research was 6 dB in total. The researcher used 2 cases. In the first case, each group was set to 1 dB, which led to a sum of 6 dB in total. In the second case, each group was set to 0.5 dB, followed by another PDL component (3 dB) at the end of the link, which contributed 6 dB PDL in total as well.

S. L. Jansen's Research in 2006 [103] Jansen's research model is a dense wavelength division multiplexing (DWDM) system with 16 × 42.7 Gb/s NRZ transmitting over an 800-km straight link of standard single mode fibre (SSMF). The 16 100-GHz-spaced CW channels with wavelengths ranging from 1548.5 nm to 1560.6 nm are multiplexed in an AWG multiplexer and modulated at 42.7 Gb/s with a $2^{31} - 1$ pseudorandom binary sequence (PRBS). After the modulator, 510 ps/nm dispersion pre-compensation is applied, optimized to obtain the highest Q-factor after transmission. The PDL value measured from the system is less than 0.5 dB.

J. Jiang's Research in 2009 [104] Jiang's research was based on one segment of submarine fibre-optic system runs from Manasquan, NJ, USA, to Blaabjerg, Denmark, a path approximately 7500 km long, with 147 EDFAs. A chirped RZ modulation format was used in the DWDM transmitters, and intra-bit polarization scrambling was used to suppress the effects of polarization-hole burning and other nonlinear waveform distortions such as four-wave mixing and cross-phase modulation. The system's PDL value was found as approximately 2.6 dB.

L. E. Nelson's Research in 2011 [105] Nelson's Research were conducted over a portion of AT&T's ultra-long-haul network between Florida and Louisiana, US. An existing 900 km link optimized for 10 Gb/s and 40 Gb/s transmission on a 50 Ghz space grid was looped back to form an 1800 km optical link. The 900 km link consists of 12 spans of SSMF with EDFAs and fibre-based dispersion compensating modules (DCF) at each EDFA's mid-stage to compensate $\sim 96\%$ of the dispersion of each span. The average span length was 78 km and the average loss was 16.5 dB. The average PMD of the transmission fibre was 0.03 $ps/km^{1/2}$, and each of the DCFs had an average PMD of 0.35 ps. The system was loaded with 12 WDM channels.

The mean PDL over all measurements of all 12 channels was 1.50 dB. The maximum PDL values were measured for the 1540 nm channels (1.70 dB at 194.45 THz and 1.66 dB at 194.55 THz). The minimum PDL values were measured for the 1550 nm channels (1.37 dB at 193.00 THz and 1.29 dB at 192.90 THz).

In addition, the PDL values of another 2 channels near 1530 nm (196.00 THz and 195.95 THz) were also measured. The mean values of PDL were about 3.5 dB, which were significantly higher than the estimated value of 1.9 dB. The researcher attributed the large PDL near 1530 nm to polarization hole burning (PHB) in the EDFAs, which was not significant for the other 12 measurement channels.

L. E. Nelson's research in 2012 [106] Nelson's later research used a 100 Gb/s system with 40 WDM channels at 50 GHz spacing. The test-channel wavelength was chosen to be 1552.52 nm, which was approximately at the centre of the wavelength band. The signals were transmitted through 10 spans of 100 km of SSMF, with an average loss of 20.5 dB, and no optical compensation for chromatic dispersion (CD) or PMD was used in the link. A two-stage EDFA was used after each span. The measured PDL value of this system was less than 0.8 dB.

6.1.2 Two Polarization Controllers Connected with Single Mode Fibre

With the approach of the Mueller matrix, with two polarization controllers and 105 metres SMF, Eq. (6.4) can be developed to

$$\vec{S_{out}} = F_2 M_{controller2} F_1 M_{controller1} \vec{S_{in}} \tag{6.5}$$

where F_1 is the matrix of the fibre between the two controllers (length is L metres) and F_2 is the matrix of the fibre between the second controller and the multimeter (length is 105-L metres). The comparisons of the simulation and emulation results are shown in Fig. 6-2 and 6-3. The dotted line, which represents the simulation result, basically matches the result from emulation measured with the emulator mentioned previously. Error bars are included with the results from multiple repeating experiments. It confirms that despite the short fibre link the

emulator is still able to provide reliable results. Rather with reference to Fig. 6-2 the maximum difference between the results of emulation and simulation is only ∼0.05dB, whilst the variation in PDL with the length of fibre between the two polarization controller is accurately reproduced, when the initial state of polarization of the input light takes a randomly selected value.

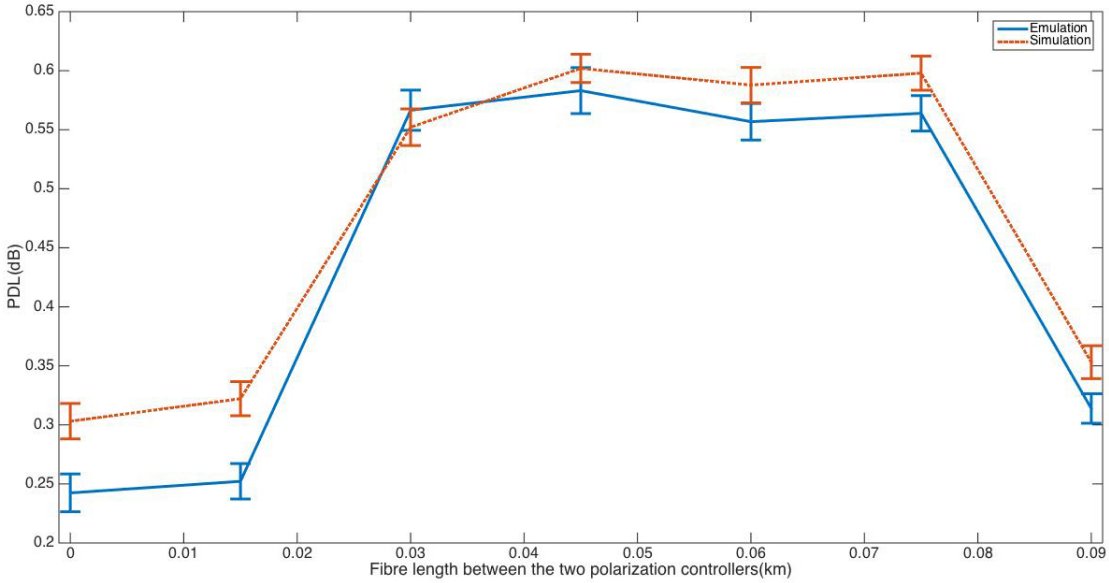

Figure 6-2: *The comparison of PDL emulation and simulation with random initial state of polarization.*

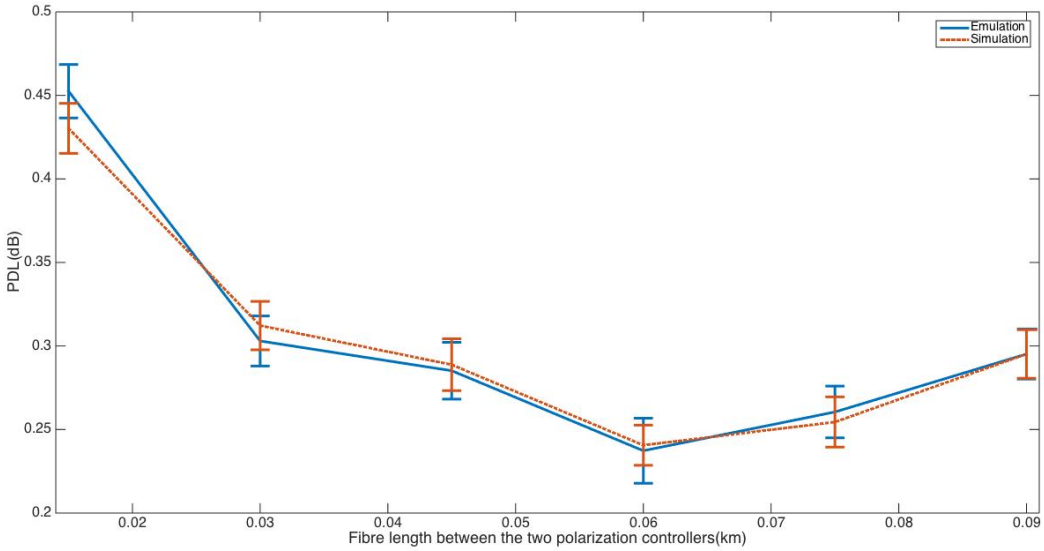

Figure 6-3: *The comparison of PDL emulation and simulation with fixed initial state of polarization.*

Further, Fig. 6-3 shows that the agreement between the simulated and emulated PDL is virtually identical as the length of the fibre connecting the two polarization controllers is varied when the polarization state of the input light is fixed.

As discussed in Chapter 5, by switching the first polarization controller from the case of random (automatically controlled by computer to provide random initial state of polarization) to the case of fixed (manually set all paddles to maximum position to provide fixed initial state of polarization), the PDL statistics show different trends when the fibre length between the two controllers increases. Fig. 6-2 and 6-3 also confirm that the simulation results obey the trend as well.

6.1.3 Three Polarization Controllers Connected with Single Mode Fibre

With 3 polarization controllers the setup is more complicated than 2 controllers, as discussed in Chapter 4. Eq. (6.4) becomes

$$\vec{S_{out}} = F_3 M_{controller3} F_2 M_{controller2} F_1 M_{controller1} \vec{S_{in}} \tag{6.6}$$

where F_1 is the matrix of the fibre between the first and second controllers (length L1), F_2 is the matrix of the fibre between the second and the third controllers (length L2) and F_3 is the matrix of the fibre between the third controller and the multimeter (length 105m-L1-L2). Fig. 6-4, 6-5 and 6-6 respectively indicate the comparisons when the fibre length between the first two controllers L=15 metre, 30 metre and 45 metre.

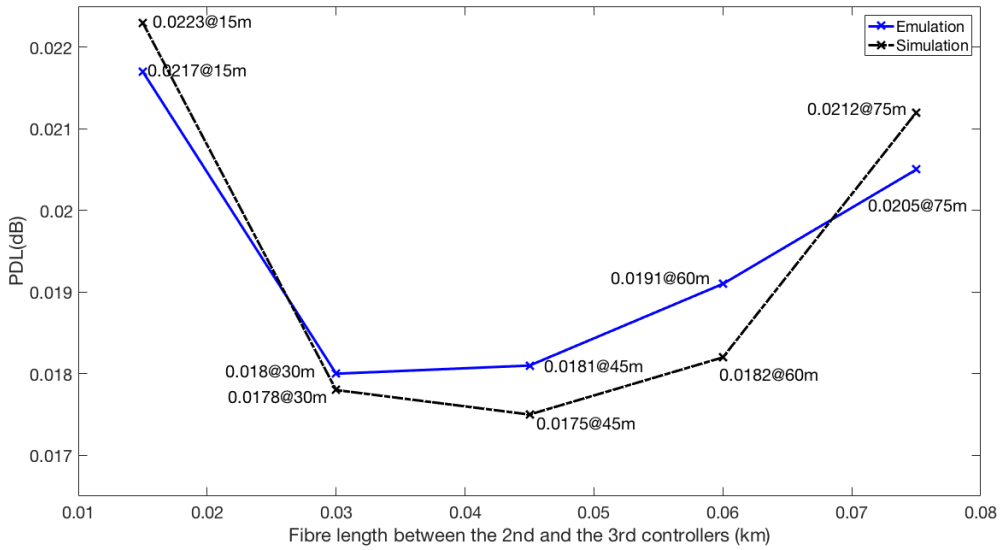

Figure 6-4: *The comparison of PDL emulation and simulation with 3 controllers (L=15m) .*

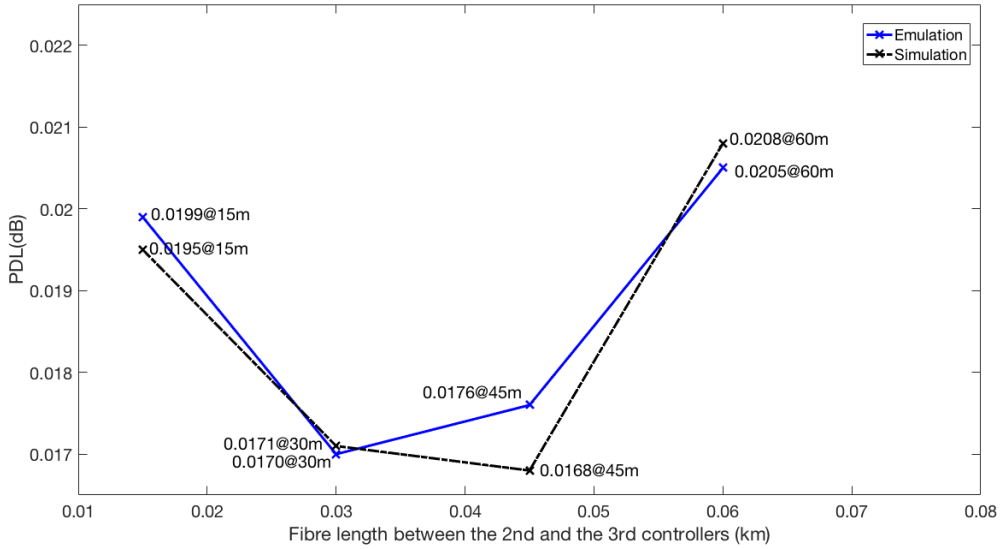

Figure 6-5: *The comparison of PDL emulation and simulation with 3 controllers (L=30m) .*

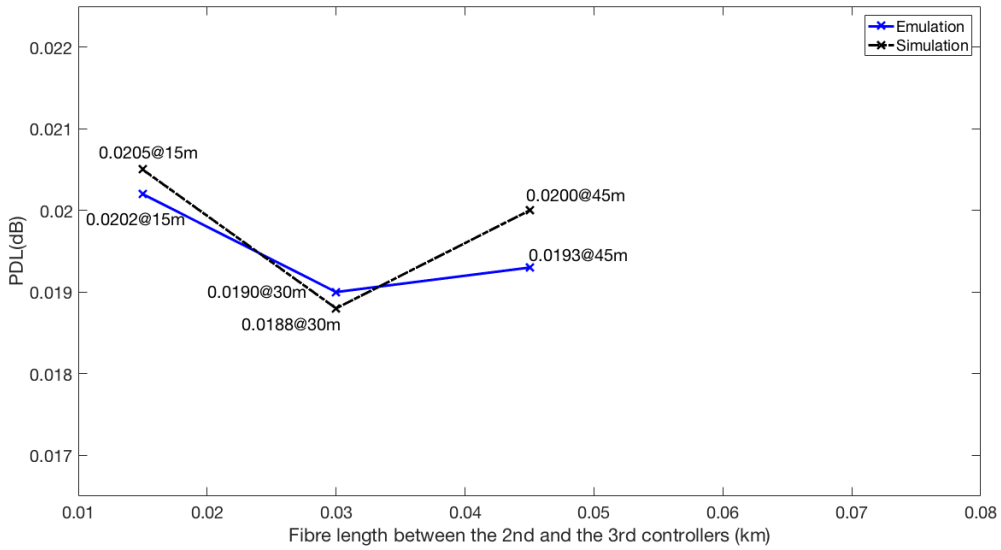

Figure 6-6: *The comparison of PDL emulation and simulation with 3 controllers (L=45m) .*

Figure 6-4, 6-5 and 6-6 also confirm that the result from the simulation model matches the result from the emulation work. The trends of simulation results also confirm the conclusion that with fixed initial state of polarization, the PDL statistics reaches the optimum (minimum PDL mean value) when the fibre length between each PDL components are equal or close. That makes it possible to extend the simulation model to a system with longer transmission distance.

6.2 Simulation with the Scenario of Long-distance Transmission Systems

Single mode fibre (SMF) cannot be considered as a PDL-free component when it is deployed in real system, as it can be affected by external environment variation, such as temperature, fibre twist and bending. Typically, the PDL is less than 0.05dB in 10km SMF [107]. In the simulation model, every 10km SMF is considered as one section of PDL-free fibre combined with one PDL component.

The erbium-doped optical fibre amplifier (EDFA) is used to compensate the regular fibre loss in this simulation model. Typically, EDFA is deployed every 80 to 100 kilometres in real communication system. In this simulation model, it is applied after every 100km SMF.

Although the EDFA is essentially a polarization independent amplifier, a small proportion of the dopant ions interact preferentially with certain polarizations and a small dependence on the polarization of the input signal may occur, which is less than 0.5dB typically. This is as known as polarization dependent gain (PDG).

6.2.1 PDL Simulation for 10km Fibre link

In the simulation of the 10km fibre link, the EDFA is not applied. The fibre is considered as a PDL component. Therefore, the output Stoke's vector can be calculated by

$$\vec{S_{out}} = FM_{Fibre}\vec{S_{in}} \tag{6.7}$$

. The simulation is run 10 times and one statistical result of the 10 experiments is shown in Fig. 6-7. Based on the root mean square (RMS) error figure, the distribution is more close to Maxwellian than Gaussian and based on the bar chart, a tail emerged at the right side of the chart, while 0.35 of 1 of normalized PDL value appeared to be the most frequent PDL value, slightly left to the middle value of 0.5.

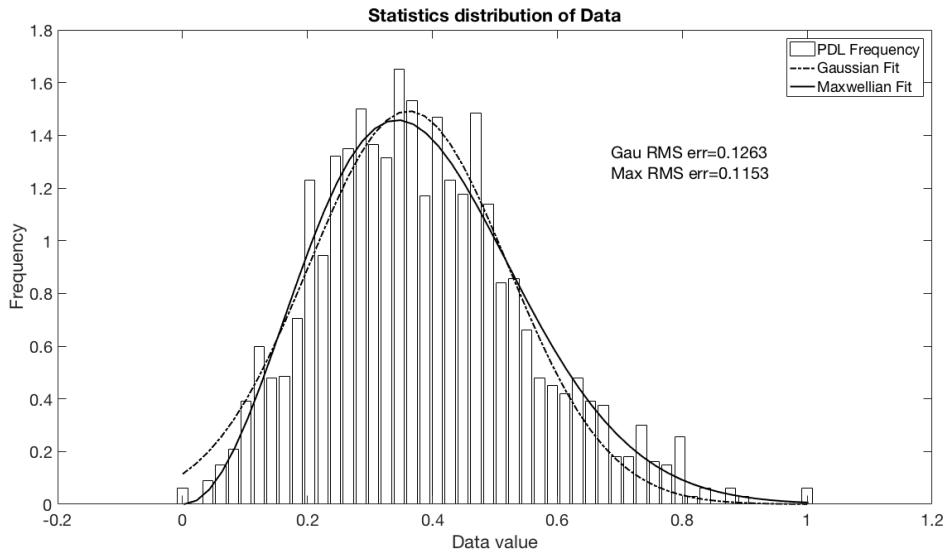

Figure 6-7: *The statistics of PDL simulation in 10km fibre link .*

The results of the 10 experiments are shown in Table 6.2.

Table 6.2: *PDL mean values in 10 km simulation.*

Simulation No.	PDL mean value
1	0.0370
2	0.0354
3	0.0331
4	0.0365
5	0.0345
6	0.0358
7	0.0360
8	0.0352
9	0.0358
10	0.0355
average	0.0355
variance	1.1707e-06

6.2.2 PDL Simulation for 100km Fibre link

In the simulation of 100 km fibre link, one EDFA is applied after the fibre link. The 100km fibre link is considered as a combination of 10 × 10km SMF. Therefore, the output Stoke's vector can be calculated by

$$\vec{S_{out}} = M_{DFA} T \vec{S_{in}} \tag{6.8}$$

where $T = F_{10}M_{10} \cdots F_1 M_1$. The statistical result is shown in Fig. 6-8. The RMS errors of Gaussian and Maxwellian are close but the tail on the right is observable and the peak frequency appears at about 0.36 of 1 of normalized PDL value.

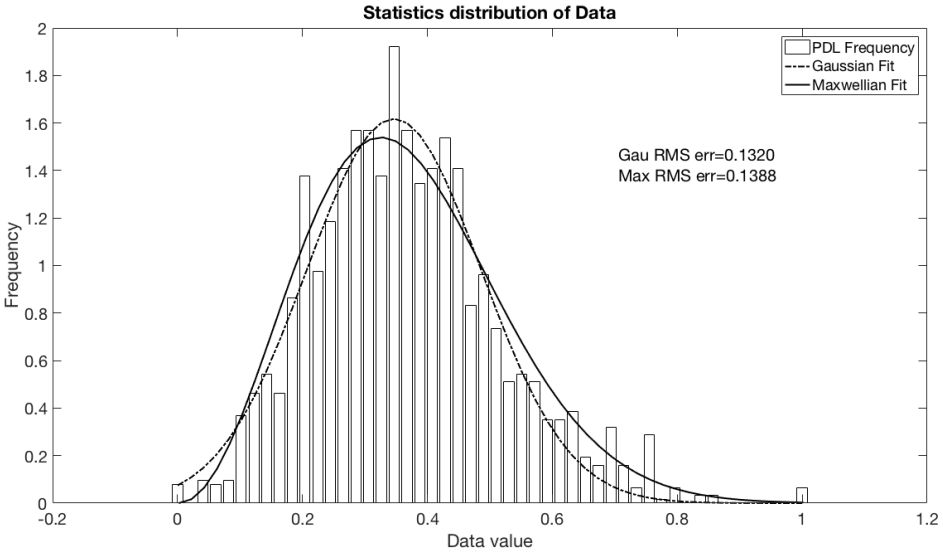

Figure 6-8: *The statistics of PDL simulation in 100km fibre link .*

The simulation is run 10 times and results are shown in Table 6.3.

Table 6.3: *PDL mean values in 100 km simulation.*

Simulation No.	PDL mean value
1	0.320
2	0.307
3	0.323
4	0.294
5	0.299
6	0.307
7	0.308
8	0.317
9	0.310
10	0.304
average	0.309
variance	8.2322e-05

6.2.3 PDL Simulation for 1000 km Fibre link

In the simulation of 1000 km fibre link, 10 EDFAs are applied after each 100 km fibre link. Each 100 km fibre link is considered as a combination of 10 × 10km SMF. Therefore, the output Stoke's vector can be

$$\vec{S_{out}} = M_{DFA10}T_{10}\cdots M_{DFA1}T_1\vec{S_{in}} \tag{6.9}$$

where $T = F_{10}M_{10}\cdots F_1M_1$. The statistical result is shown in Fig. 6-9. The RMS errors of Gaussian and Maxwellian are close but the tail on the right is much more observable and the peak frequency appears at about 0.3 of 1 of normalized PDL value (the spike at 0.46 is ignored).

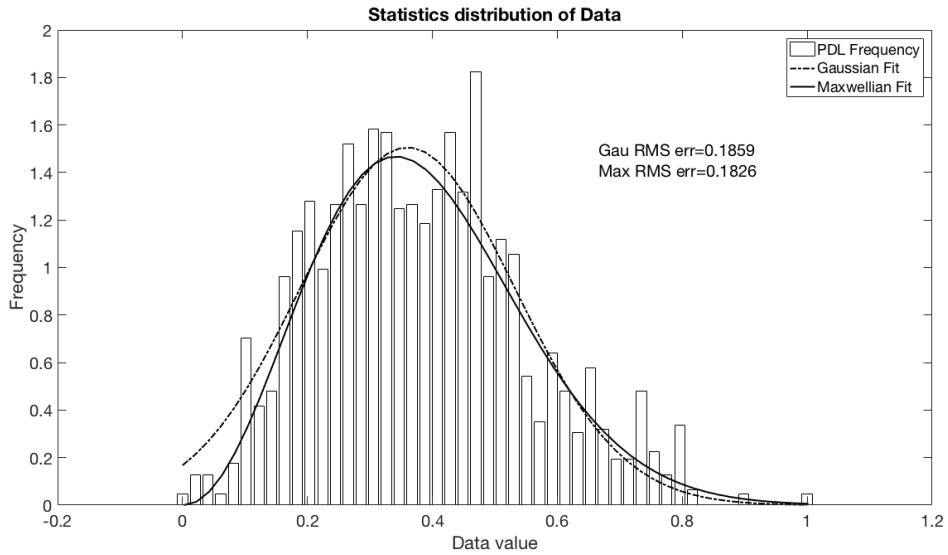

Figure 6-9: *The statistics of PDL simulation in 1000 km fibre link .*

The simulation is run 10 times and results are shown in Table 6.4.

Table 6.4: *PDL mean values in 1000 km simulation.*

Simulation No.	PDL mean value
1	0.802
2	0.798
3	0.803
4	0.799
5	0.804
6	0.782
7	0.783
8	0.792
9	0.805
10	0.809
average	0.798
variance	8.4900e-05

In early research [106], the measured PDL is less than 0.8 dB. Table 6.4 shows the simulation basically matches this result.

6.2.4 PDL Simulation for 7500 km Fibre link

In the simulation of 7500 km fibre link, 75 EDFAs are applied after each 100 km fibre link. Each 100 km fibre link is considered as a combination of 10 × 10 km SMF. Therefore, the output Stoke's vector can be

$$\vec{S_{out}} = M_{DFA80}T_{80}\cdots M_{DFA1}T_1\vec{S_{in}} \tag{6.10}$$

where $T = F_{10}M_{10}\cdots F_1M_1$. The statistical result is shown in Fig. 6-10. The RMS errors of Gaussian and Maxwellian are close. The tail on the right is observable and the peak frequency appears at about 0.36 of 1 of normalized PDL value.

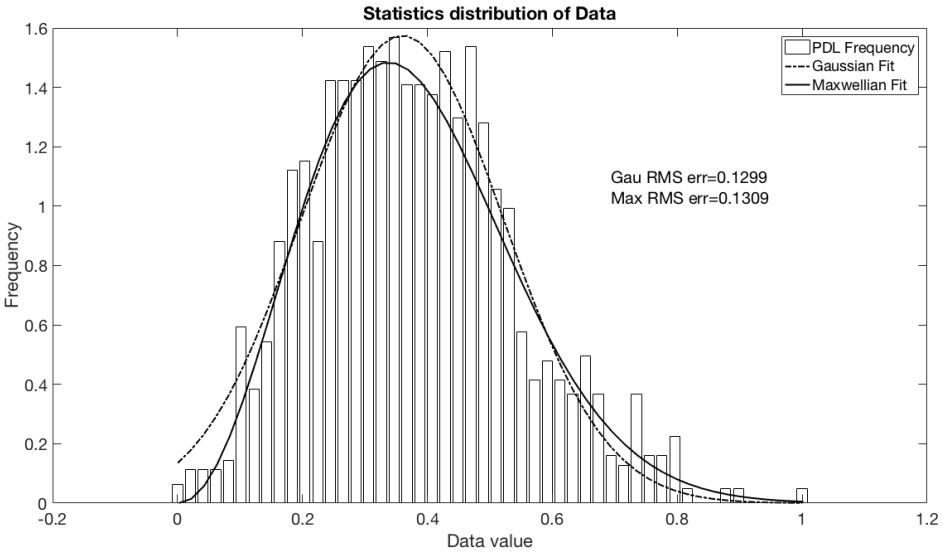

Figure 6-10: *The statistics of PDL simulation in 7500km fibre link .*

The simulation is run ten times and results are shown in Table 6.5.

Table 6.5: *PDL mean values in 7500 km simulation.*

Simulation No.	PDL mean value
1	2.795
2	2.747
3	2.722
4	2.701
5	2.832
6	2.782
7	2.756
8	2.812
9	2.828
10	2.744
average	2.772
variance	0.0020

Previous research [104] showed the measured PDL is about 2.6 dB in 7500 km system. The average PDL for the ten runs is 2.829, which compares well with this result.

In the simulations, PDL does not linearly increase with a linear increase of transmission distance. That means the polarization dependent gain (PDG, provided by EDFAs) partly compensates the PDL in the system. Via the comparison with previous research, it is concluded that the simulation model is able to generate results that match the results in real systems.

6.3 Simulation of Pulse Transmission in Long-distance Transmission Systems

Pulse transmission can be simulated with the solution of Nonlinear Schrödinger equation (NLS). As NLS is a nonlinear partial differential equation that does not generally lend itself to analytic solutions, the only way to achieve the simulation is to find its numerical solution. There are several methods [108, 109, 110, 111] able to calculate the numerical solution of the NLS. In this thesis, the method of split-step Fourier is applied, as discussed in Chapter 4.

6.3.1 Pulse Transmission with Only Dispersion and Nonlinear Effects

By ignoring all factors apart from chromatic dispersion and nonlinear effect, the basic solution of NLS can be found. Fig. 6-11 shows the result when a hyperbolic secant shaped pulse is launched as an initial pulse. $\beta_2 = -10ps/(nm * km)$ and the propagation distance is 4 km.

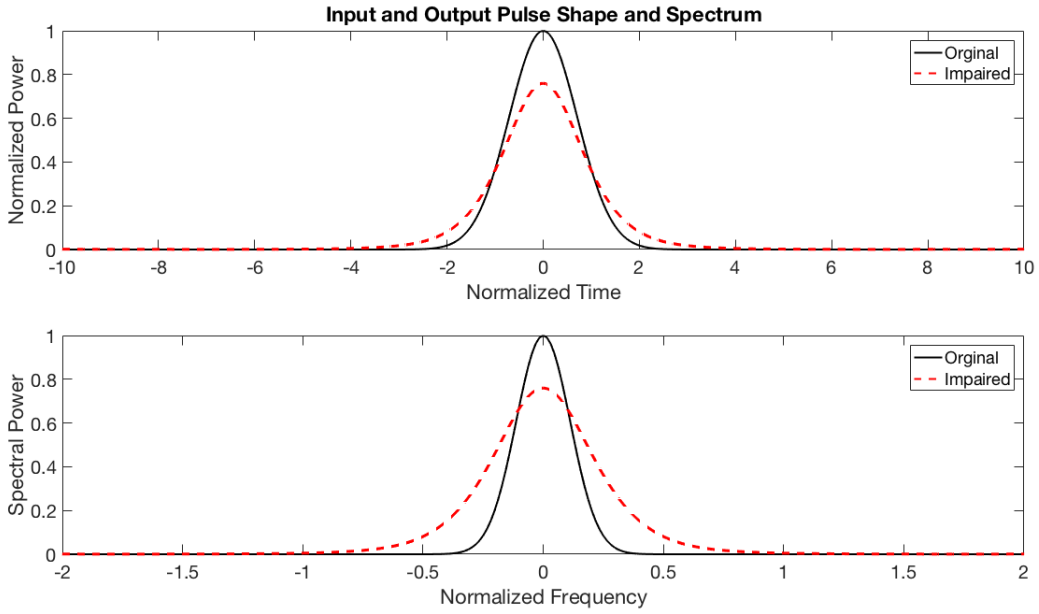

Figure 6-11: *Pulse transmission over 4 km ($\beta_2 = -10ps/(nm * km)$).*

The effect of increasing the propagation distance to 100 km is shown in Fig. 6-12. Comparing with Fig. 6-11, it can be seen that the shape of the pulse does not noticeable change with distance; its full width half maximum merely increases and its peak height reduces pro rata to conserve energy.

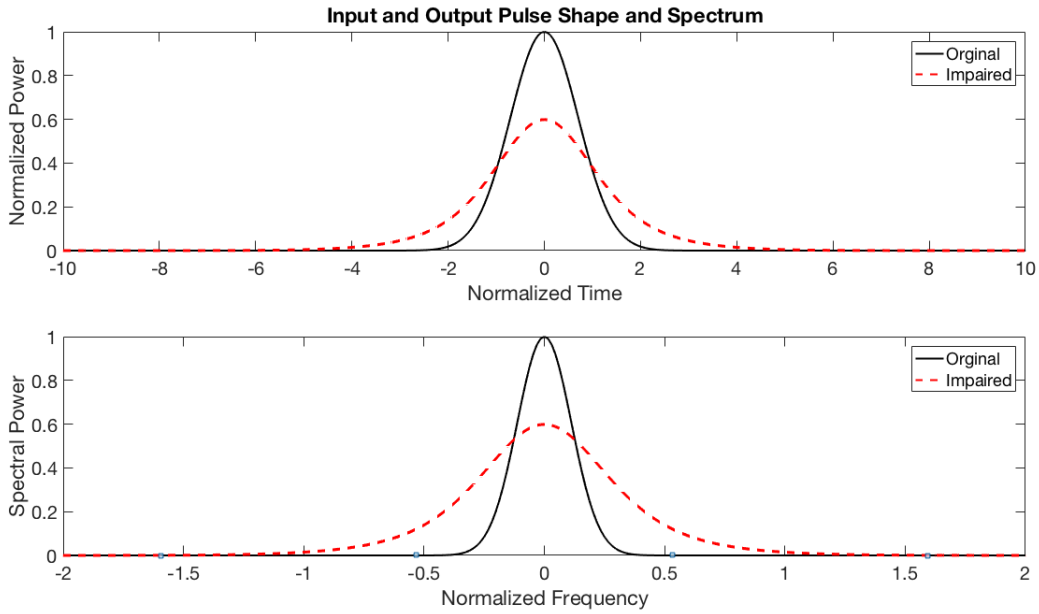

Figure 6-12: *Pulse transmission over 100 km ($\beta_2 = -10ps/(nm * km)$).*

Repeating these simulations with a dispersion parameter of $\beta_2 = -20ps/(nm * km)$ broadens the pulse more quickly, as shown in Fig. 6-13, although for a distance of 100 km the pulse breaks up into a series of ripples (Fig. 6-14).

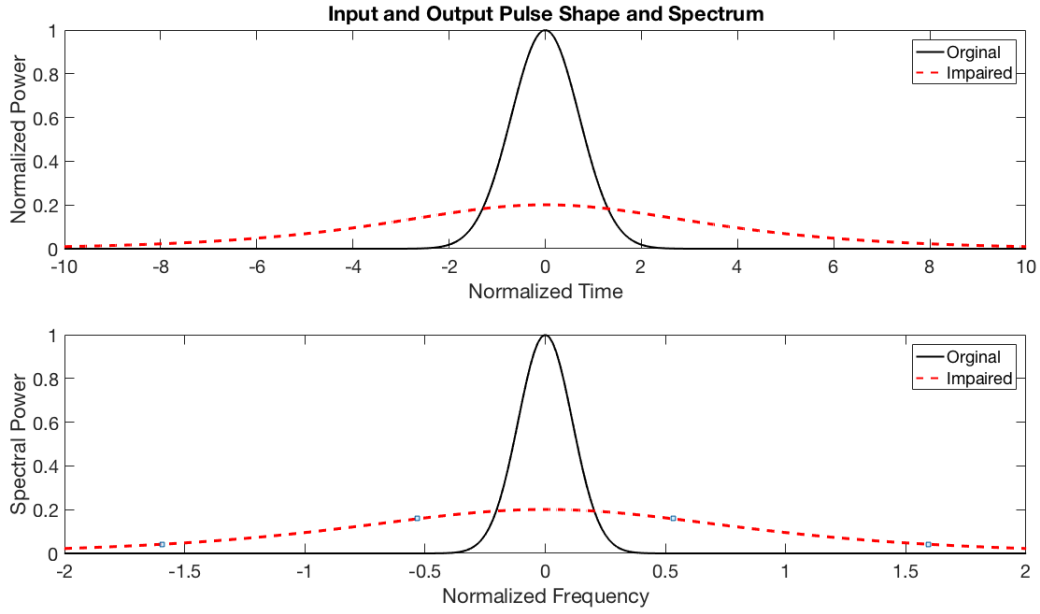

Figure 6-13: *Pulse transmission over 4 km ($\beta_2 = -20ps/(nm * km)$).*

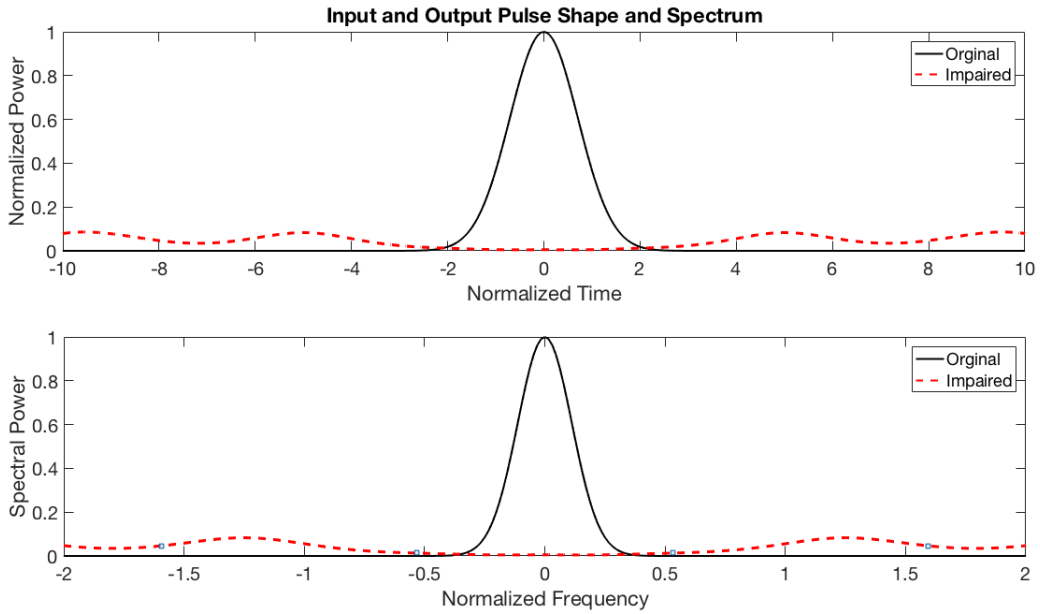

Figure 6-14: *Pulse transmission over 100 km ($\beta_2 = -20ps/(nm * km)$).*

As discussed in Chapter 3, optical phase conjugation is able to recover the signal attenuation from chromatic dispersion and nonlinear effects. This is shown in the simulations for results $\beta_2 = -20ps/(nm * km)$ in Fig. 6-15 and Fig. 6-16 for distance of 4 km and 100 km respectively. It is obvious that the impaired signal is fully recovered, not only for short propagation distances, but for a long distance as well.

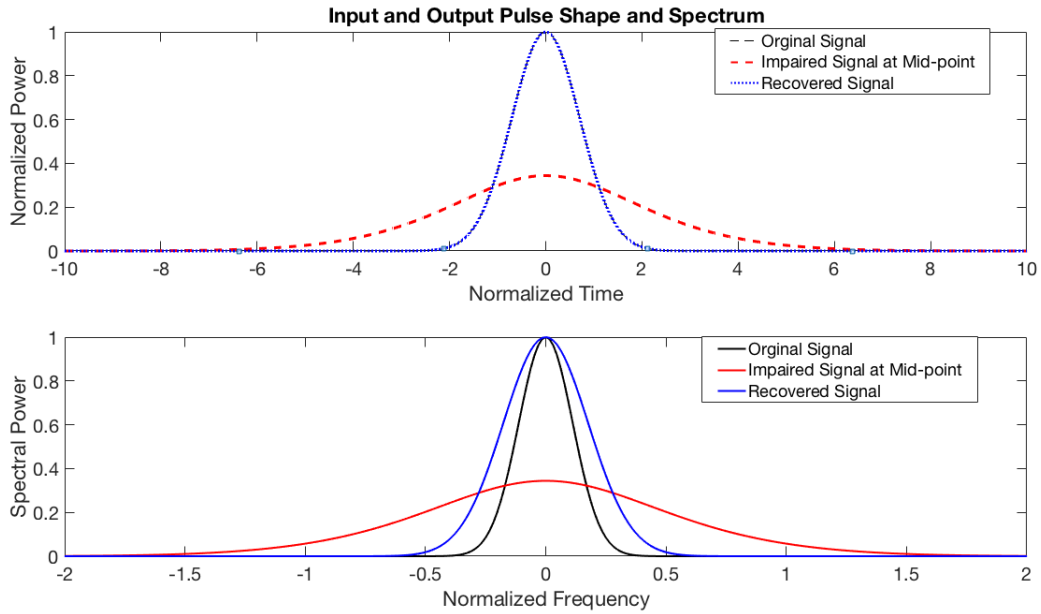

Figure 6-15: *Pulse transmission over 4 km with phase conjugation($\beta_2 = -20ps/(nm*km)$).*

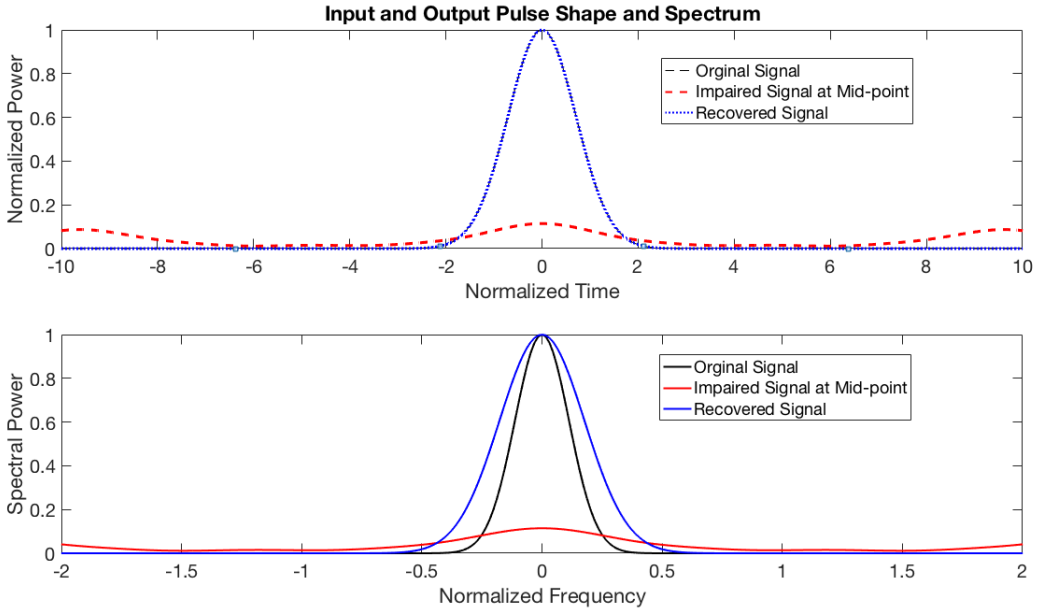

Figure 6-16: *Pulse transmission over 100 km with phase conjugation($\beta_2 = -20ps/(nm * km)$).*

The effect of increasing the propagation distance to 1000 km and 7500 km is shown in Fig. 6-17 and 6-18. Apparently, no matter how long the propagation distance is, the signal attenuation caused by chromatic dispersion and nonlinear effects can be fully recovered by optical phase conjugation.

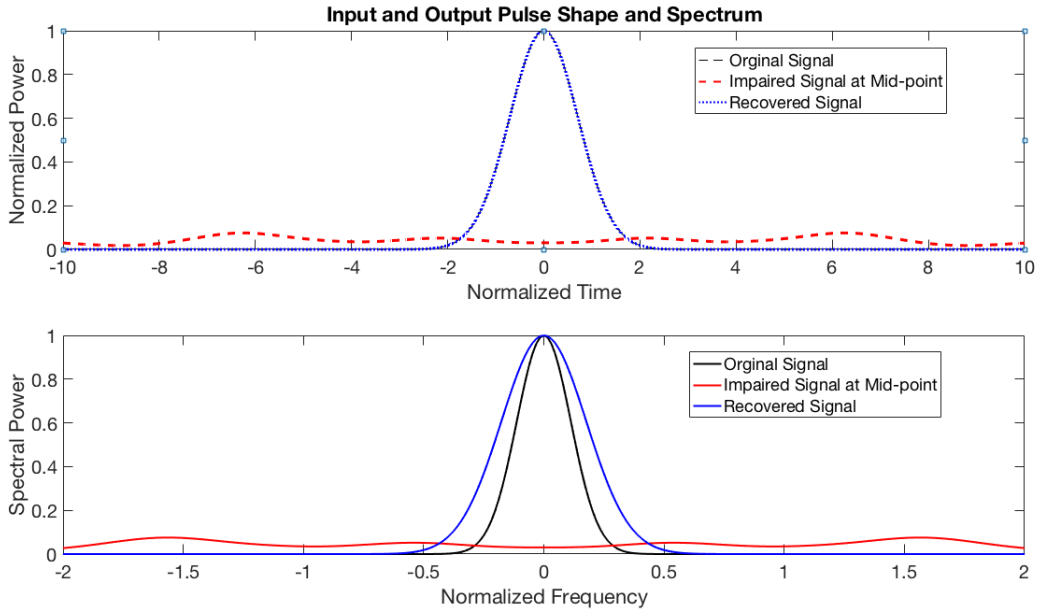

Figure 6-17: *Pulse transmission over 1000 km with phase conjugation*($\beta_2 = -20ps/(nm * km)$).

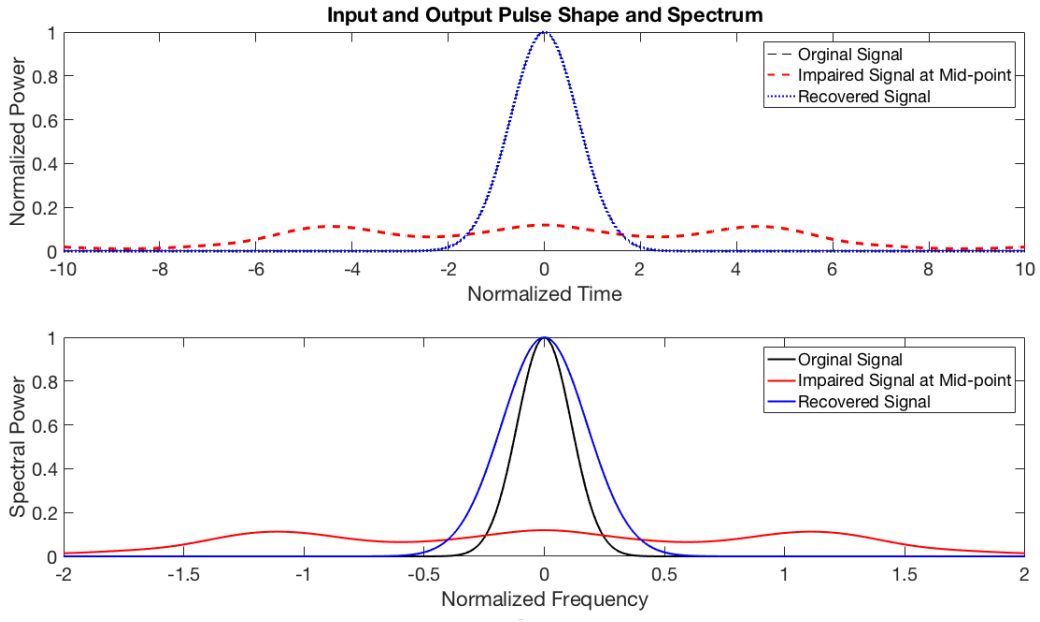

Figure 6-18: *Pulse transmission over 7500 km with phase conjugation*($\beta_2 = -20ps/(nm * km)$).

6.3.2 The Effects of Polarization

By introducing polarization into the simulation, the NLS equation needs to be rewritten for the propagation on both X and Y axes and the solutions become more complicated. In order to evaluate the effect of polarization and its combined effects with other factors, this simulation model will be modified. The results will be shown and discussed in the following chapters.

6.4 Summary

In this chapter, the simulation model is developed with the same algorithm as the emulator. The simulation results have been compared with the measurement result from the emulator and they are matched. Then, the simulation model is extended for longer fibre link simulation. Besides, an independent pulse simulation model has been developed as well, in order to study the pulse distortion caused by chromatic dispersion, nonlinear effects and polarization.

CHAPTER 7

POLARIZATION EFFECTS ON SIGNAL DISTORTION WITH NOISE

7.1 Background

Eye diagram has been proved to be a very useful tool to evaluate the impact to optical signal-to-noise (SNR) ratio from signal distortion. In the optical area, an optical eye diagram can also be used to evaluate the explicit effects of PMD and PDL on digital signalling.

Prior researches have been reported on the impact of PMD on optical signal-to-noise (OSNR) ratio [112, 113, 114, 115]. Most of these researches were carried out in real communication systems and PMD cannot be separated from other impact factors. In this case, a simulation model has the advantage of focusing on the pulse-distorting factor (PMD). It has the advantage of evaluating the performance of PMD compensation approach while no other factors are present. Such a simulation model has been programmed by amending the pulse simulation model built in the last part of this chapter.

In this chapter, in order to focus on the effect of signal distortion caused by PDL and PMD, eye diagrams were constructed using the following procedure. First, a three-continuous signal in the form of a sequence of three hyperbolic

secant shaped pulses was launched into an optical fibre that affected by PMD. Second, another signal in the same form but with a $T_0/2$ time delay was launched to form eyes, as shown in Fig. 7-1. Both signals were at the data rate of 10 Gb/s. The overlapped parts of the original pulses and the phase-shifting pulses formed eyes which can then be used to evaluate the signal distortion.

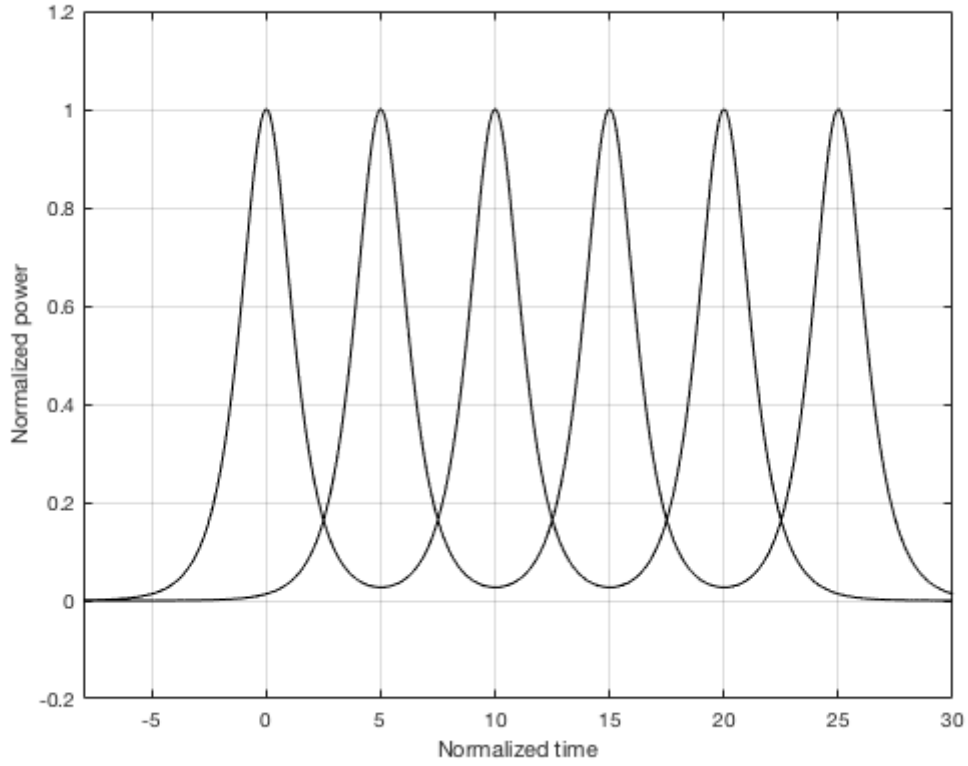

Figure 7-1: *Initial three-pulse sequence with the same three-pulse sequence overlapped after adding a 180 degree phase shift.*

7.2 Effect of PMD on Pulsed Signals over Short Distance (1km)

The effects of PMD on the pulse sequence shown in Fig. 7-1 was simulated initially by propagating it through a short fibre link of 1 km. White Gaussian

noise was added to the signal. In order to focus on the impact of just PMD, the simulation was loss-free but with no PDL and with chromatic dispersion set at -17 ps/km, which was the typical value at 1550 nm in ITU G.652 conventional single mode fibre [116]) . The same simulation was repeated multiple times. In each run a value of PMD was randomly selected from a Maxwellian distribution with mean value of 1 ps^2/km, and introduced into the link. The output signals with 50 dB Signal-to-Noise Ratio (SNR), 30 dB SNR and 20 dB SNR were shown in Fig. 7-2, Fig. 7-3 and Fig. 7-4 respectively. As can be seen, the PMD on its own did not cause much distortion to the eye diagrams. However the latter progressively closed when the SNR decreased, as expected, this gave confidence in the procedure for analysing the combined effects of PMD and thermal noise on degrading digital signalling. In Fig. 7-2 the eye-opening, calculated by numerically integrating the area of overlap of the two phase-shifted bit streams, is 95.3% when SNR=50 dB. The eye-opening decreases to 89.9% for a received SNR of 30 dB and falls further to just 45% when the received SNR is 20 dB.

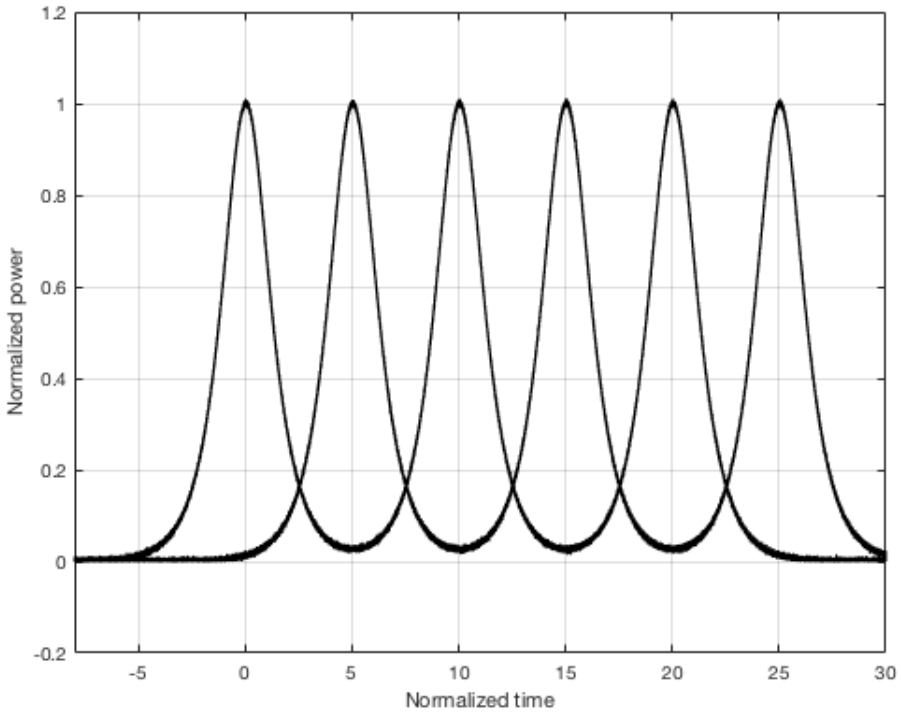

Figure 7-2: *Received signal (SNR=50 dB) at 1 km. Eye opening=95.3%.*

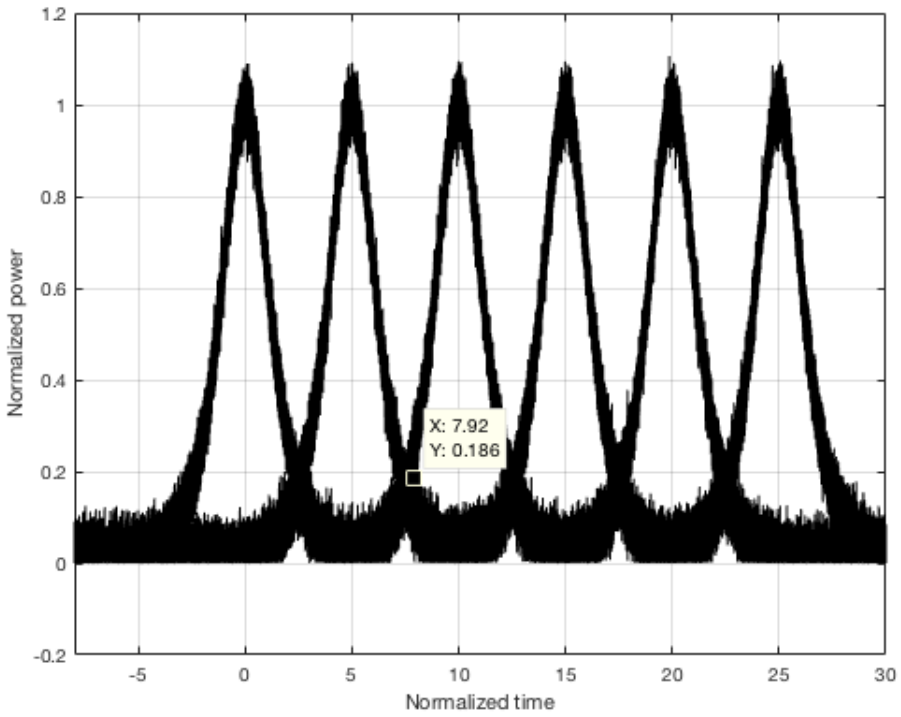

Figure 7-3: *Received signal (SNR=30 dB) at 1 km. Eye opening=89.9%.*

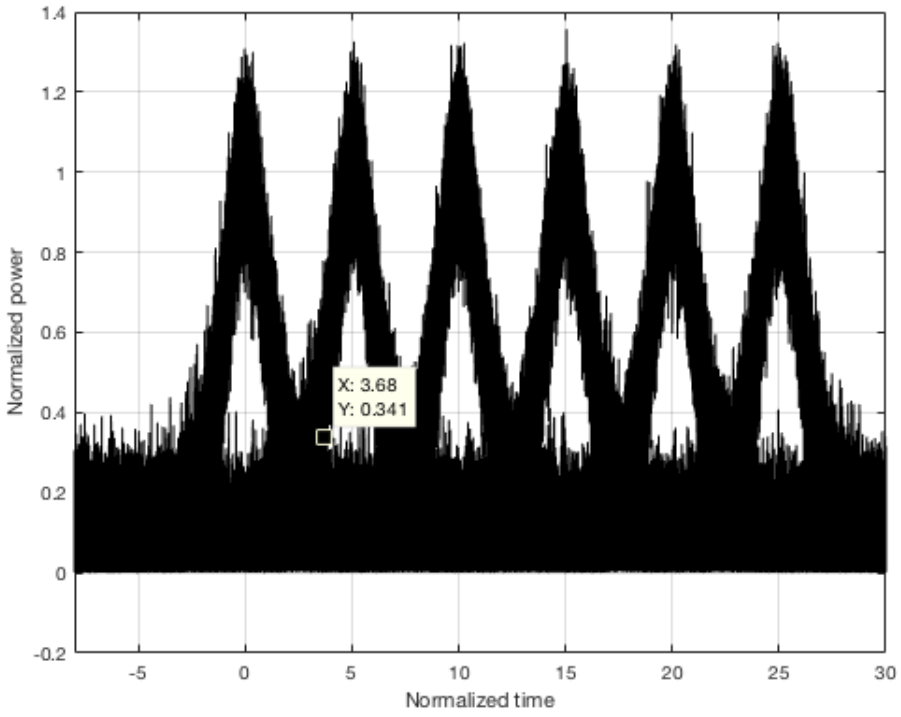

Figure 7-4: *Received signal (SNR=20 dB) at 1 km. Eye opening=45.0%.*

7.3 Effect of PMD on Pulsed Signals over Long Distances

The algorithm was then extended for long distance simulation in the following way. A 10 km-fibre-link was assumed as the basic element. The link consisted of 5 sections of fibre, with the lengths of 1 km, 2 km, 1 km, 5 km and 1 km. Each section had a random PMD (Maxwellian distribution, mean value=1 $ps/\sqrt{km}$). The output signals for arbitrarily inserted thermal noise equivalent to 50 dB Signal-to-Noise Ratio (SNR), 30 dB SNR and 20 dB SNR at the receiver are shown in Fig. 7-5, Fig. 7-6 and Fig. 7-7 respectively. With the increased transmission distance, the PMD impacts can be seen as jitter (as shown in Fig. 7-5 (b), one eye of Fig. 7-5 (a) was shown to make clear the thickness of the lines is mainly due to jitters not the added noise) on the phase which causes a decrease in the eye-opening with the fluctuation on the power peak position also causing a vertical decrease in the eye-opening. At 10 km, the eye has almost gone when the SNR was 20 dB or less. With a received SNR of 30 dB the eye-opening is reduced from 89.9% for 1 km SMF to 81.2% for 10 km SMF, due to the accumulated effect of PMD and thermal noise.

In the case of a received SNR of 50 dB, the eye opening is reduced from 95.3% to 83.1% when the fibre link length is increased from 1 km to 10 km. Thus, the impairment from PMD is almost equivalent to adding an extra 20 dB of noise over a propagation distance of just 10 km.

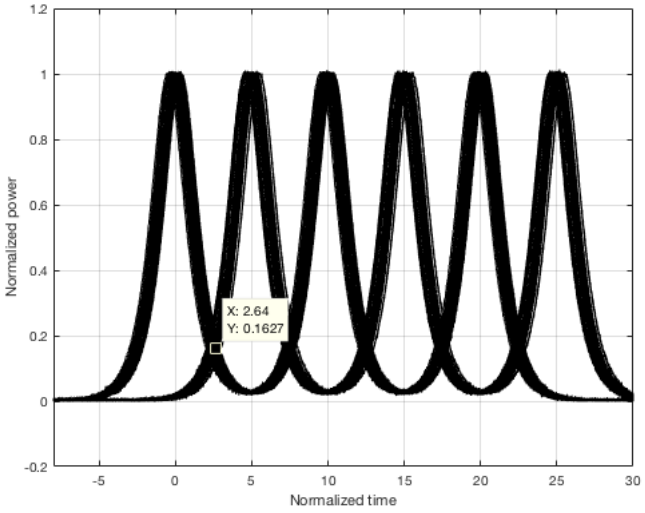

(a) Full pulse shapes.

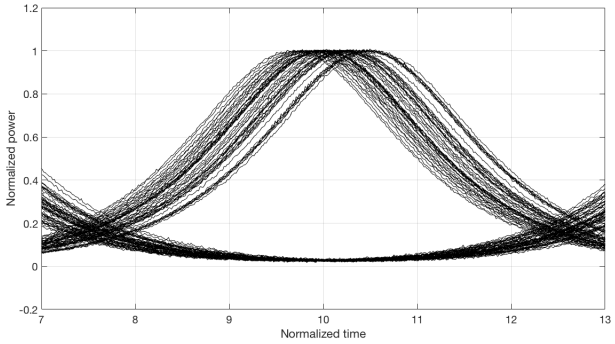

(b) Details of one eye.

Figure 7-5: *Received signal (SNR=50 dB) at 10 km. Eye opening=83.1%.*

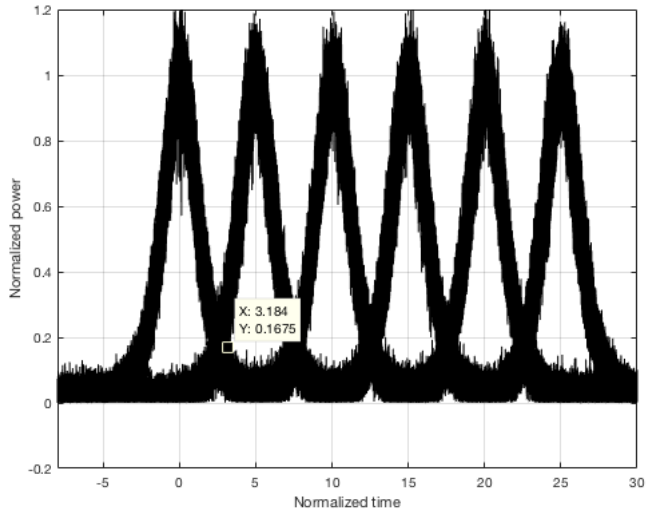

Figure 7-6: *Received signal (SNR=30 dB) at 10 km. Eye opening=81.2%.*

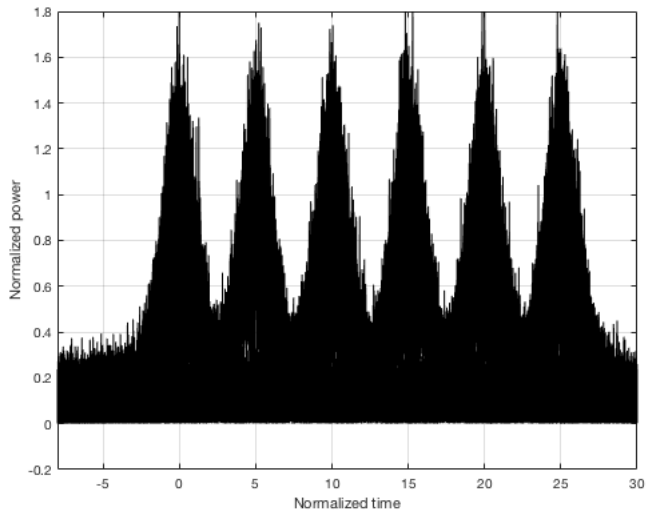

Figure 7-7: *Received signal (SNR=20 dB) at 10 km. Eye opening cannot be calculated.*

The 10 km fibre link was set as the basic fibre link in the following steps. By doubling the transmission distance to 20 km (2 times of the 10 km link), the closure of the eyes becomes even worse, as shown in Fig. 7-8 and Fig. 7-9. The eye opening with SNR=50 dB was still 73.6% for clear eye-opening, but with SNR=30 dB it is now just 30.4%, and too low for clear eye-opening.

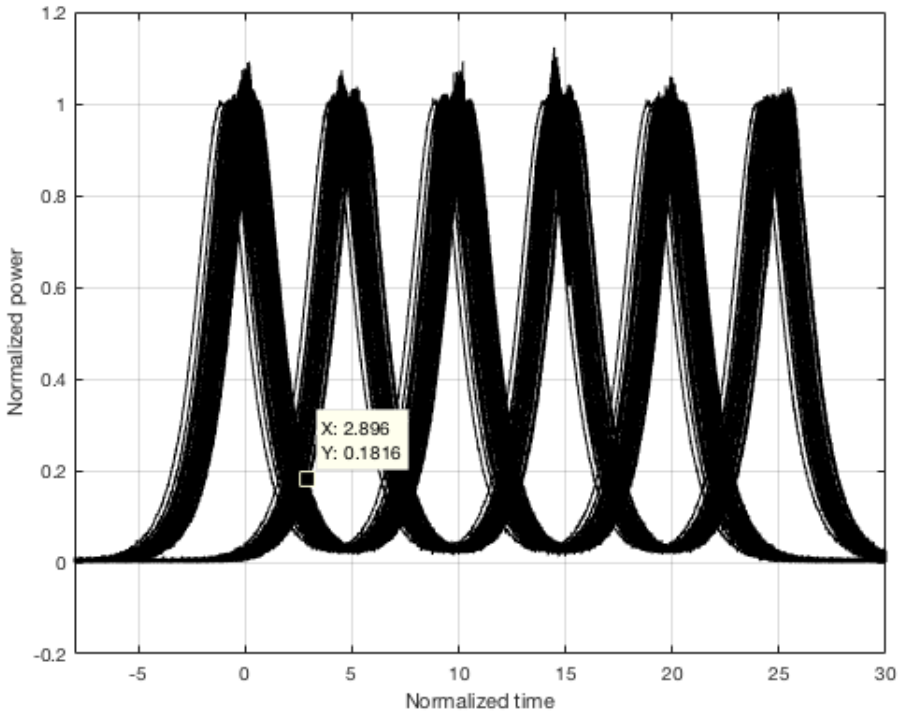

Figure 7-8: *Received signal (SNR=50 dB) at 20 km. Eye opening=73.6 %.*

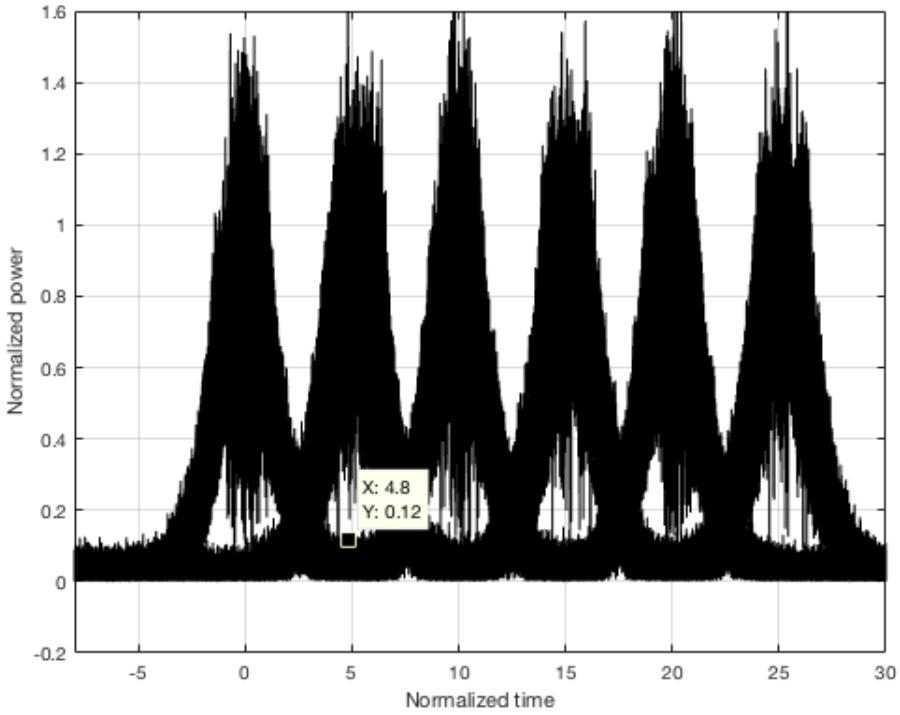

Figure 7-9: *Received signal (SNR=30 dB) at 20 km. Eye opening=30.4 %.*

When the distance increased to 30 km (3 times of the 10 km fibre link, shown in Fig. 7-10 and Fig. 7-11), the eye has closed when SNR=30 dB. When the distance increased to 40 km (4 times of the 10 km fibre link,shown in Fig. 7-12), the eye has almost closed even for a SNR =50 dB.

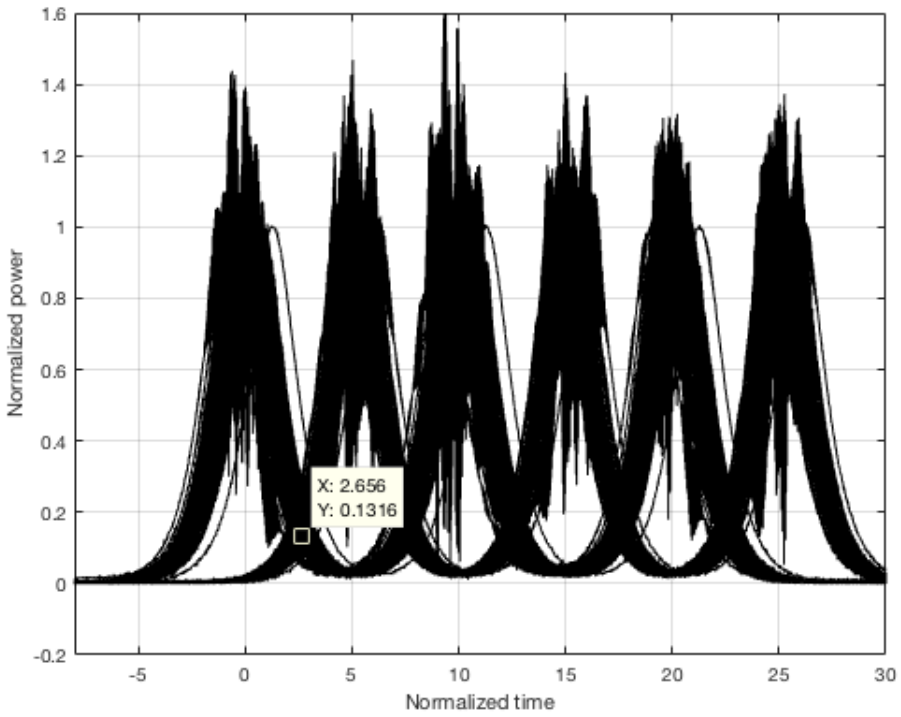

Figure 7-10: *Received signal (SNR=50dB) at 30km. Eye opening=59.9 %.*

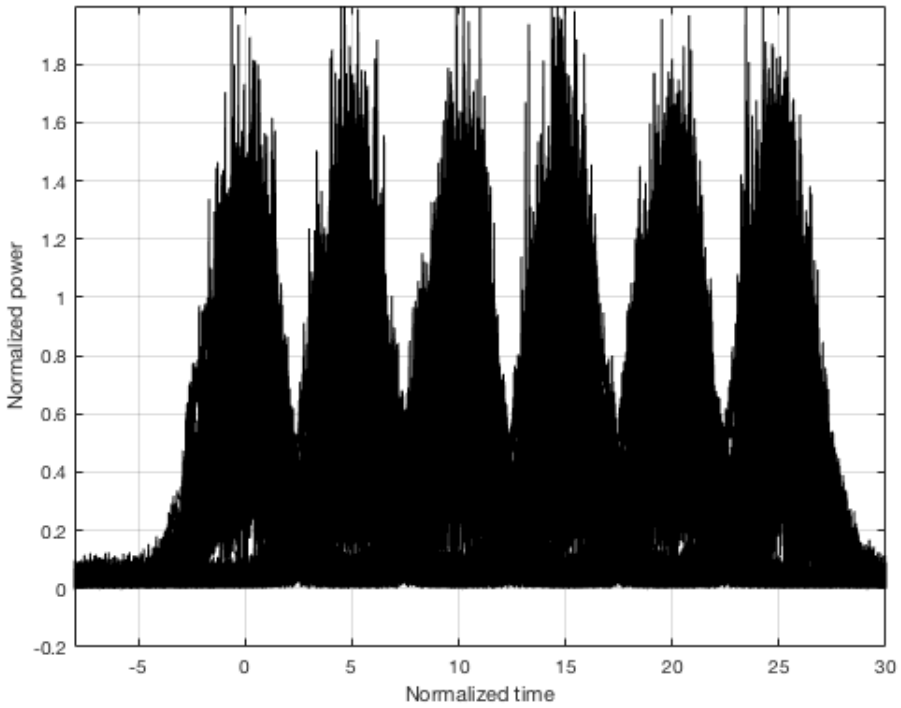

Figure 7-11: *Received signal (SNR=30dB) at 30km.*

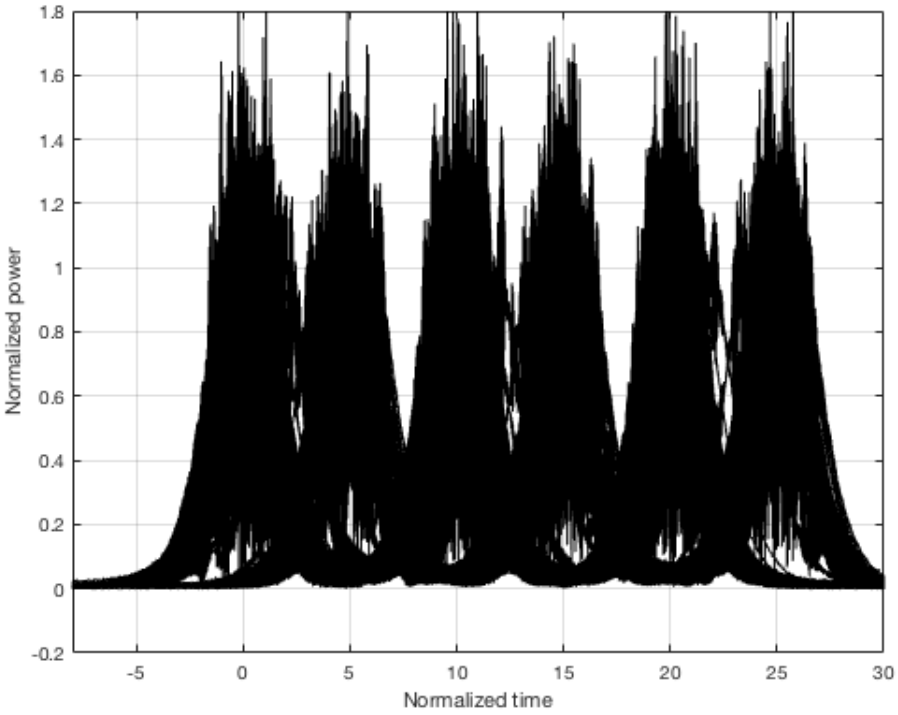

Figure 7-12: *Received signal (SNR=50dB) at 40km.*

Fig. 7-13 summarises the change in the percentage eye-opening of the simulated bit sequences with optical fibre link length for the three different SNR values.

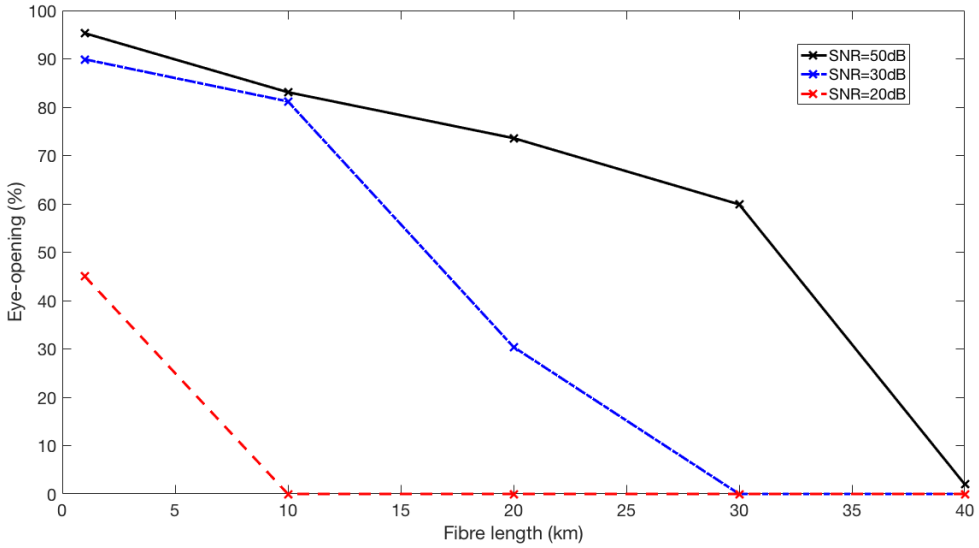

Figure 7-13: *Eye-opening evolution over distance at different SNR levels.*

7.4 Numerical Approach to Distortion Compensation

A numerical approach for both describing and reducing the effects of PMD on eye diagrams is now described. By recording the positions of each power peak in the eye diagrams, the central position and the average phase shifting can be calculated. The phase shifting from an average central position of the eyes of all the existing pulses and any further input pulses can be calculated and correspondingly compensated for with the effect that the jitter can be partly removed. This procedure assumes that the PMD statistics of the link to which it is being applied is known and that the effect of PMD on the eye diagram is larger than that of noise.

By applying this approach on the simulation with 10 km fibre link with different SNR levels, the results are shown in Fig. 7-14, 7-15 and 7-16. The eye-opening with SNR=50 dB enlarged from 83.1% to 93.7%, increased by 12.8%. When SNR=30 dB, it was enlarged from 81.2% to 86.7%, increased by 6.8%. However, it does not help much enough to reopen the eye with SNR=20 dB.

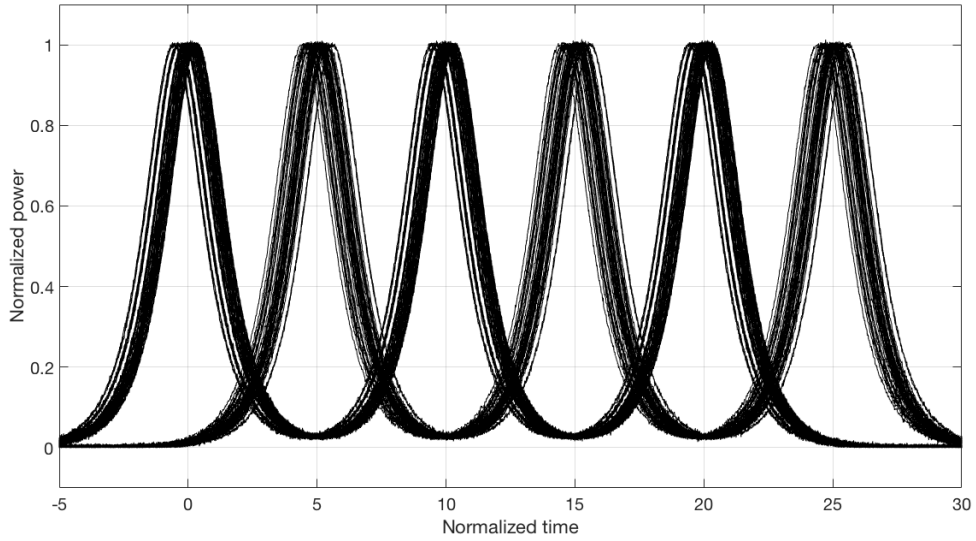

(a) Without jitter removal. Eye opening=83.1%.

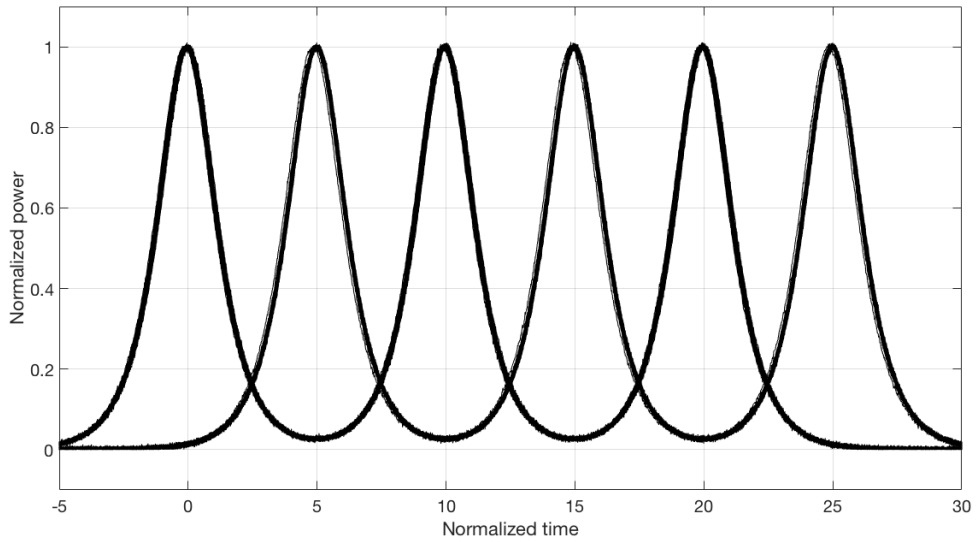

(b) With jitter removal. Eye opening=93.7%.

Figure 7-14: *Received signal (SNR=50 dB) at 10 km.*

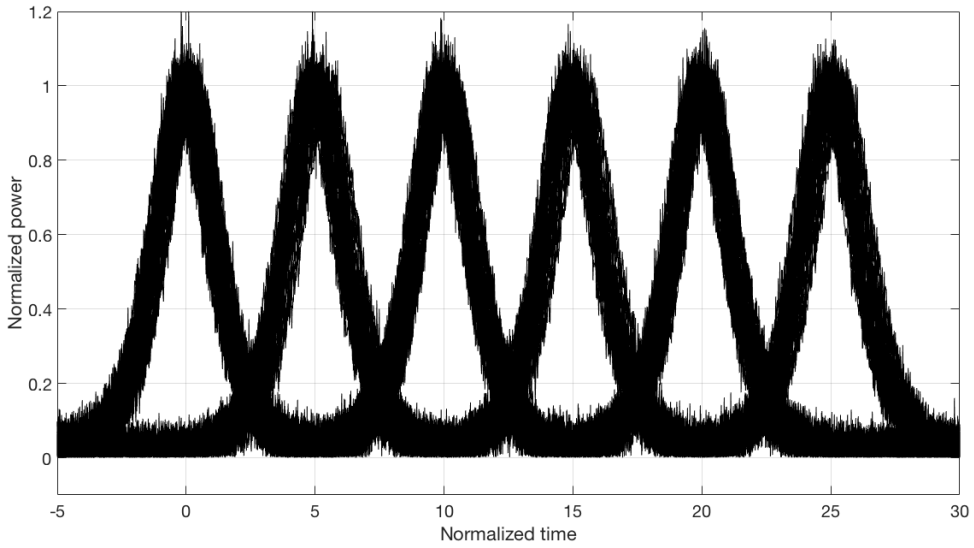

(a) Without jitter removal. Eye opening=81.2%.

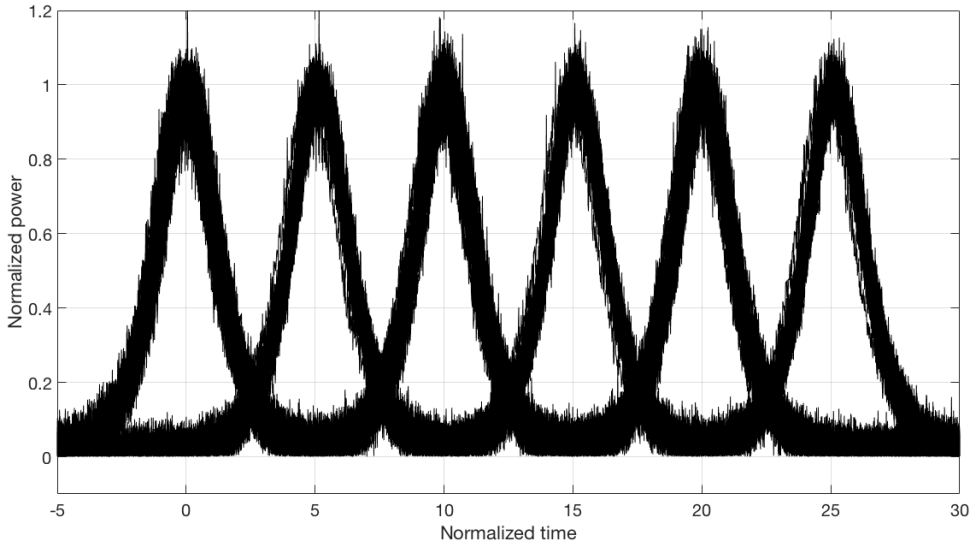

(b) With jitter removal. Eye opening=86.7%.

Figure 7-15: *Received signal (SNR=30 dB) at 10 km.*

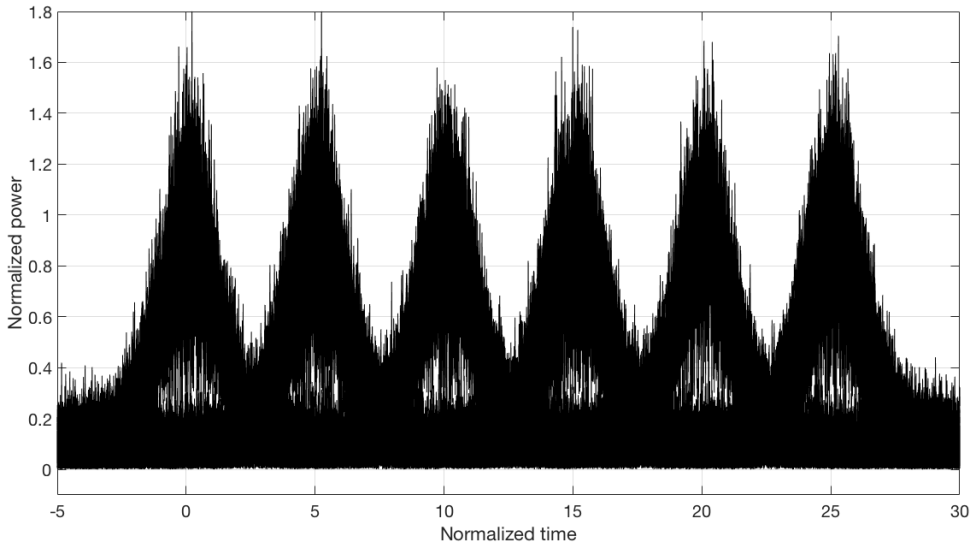

(a) Without jitter removal. Eye closed.

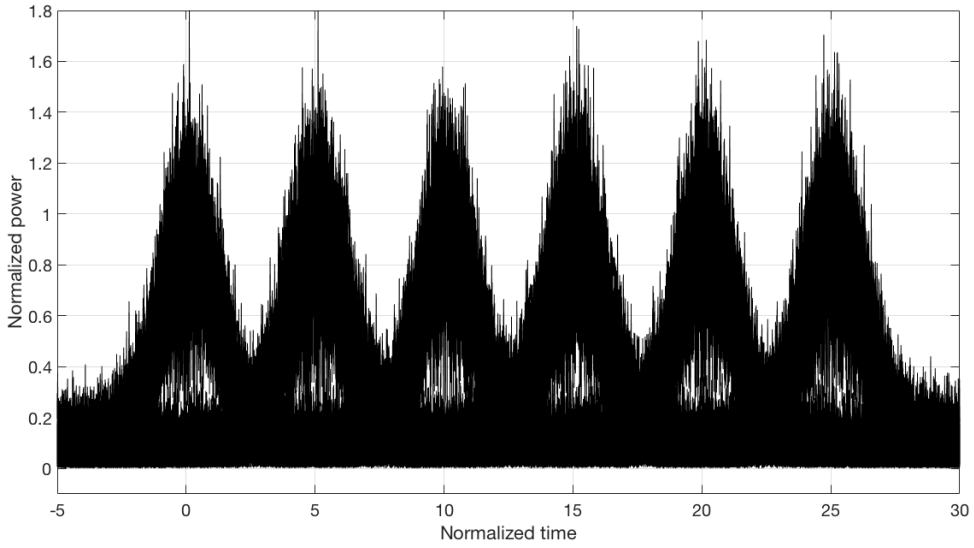

(b) With jitter removal. Eye still closed.

Figure 7-16: *Received signal (SNR=20 dB) at 10 km.*

To find out the scope for performance improved by this approach, simulations were run with SNR=50 dB for propagation distances of 20 km, 30 km and 40 km. The results are shown in Fig. 7-17, 7-18 and 7-19. The eye-opening at 20 km enlarged from 73.6% to 82.3%, increased by 11.8%. When it is at 30 km, it was enlarged from 59.9% to 76.8%, increased by 28.2%. However, it does not help much enough to reopen the eye at 40 km.

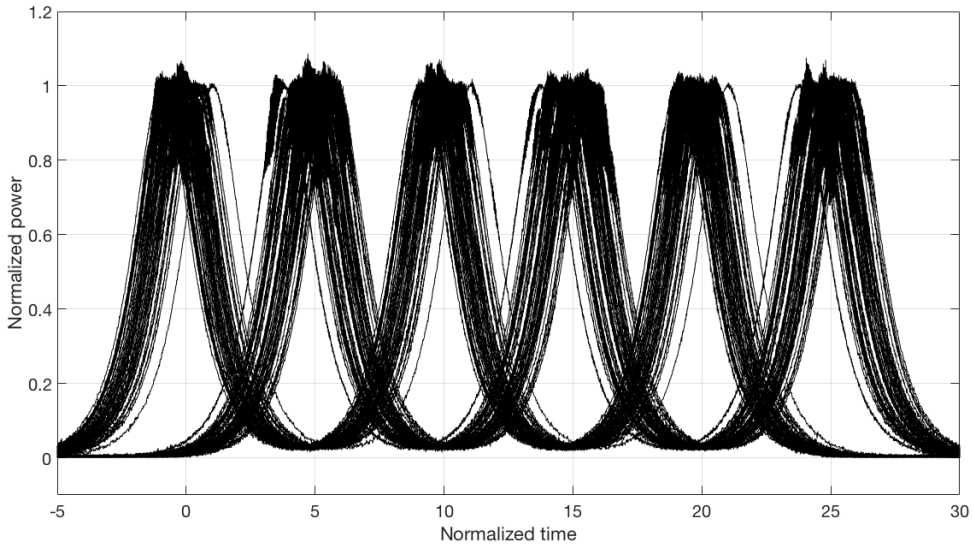

(a) Without jitter removal. Eye opening=73.6%.

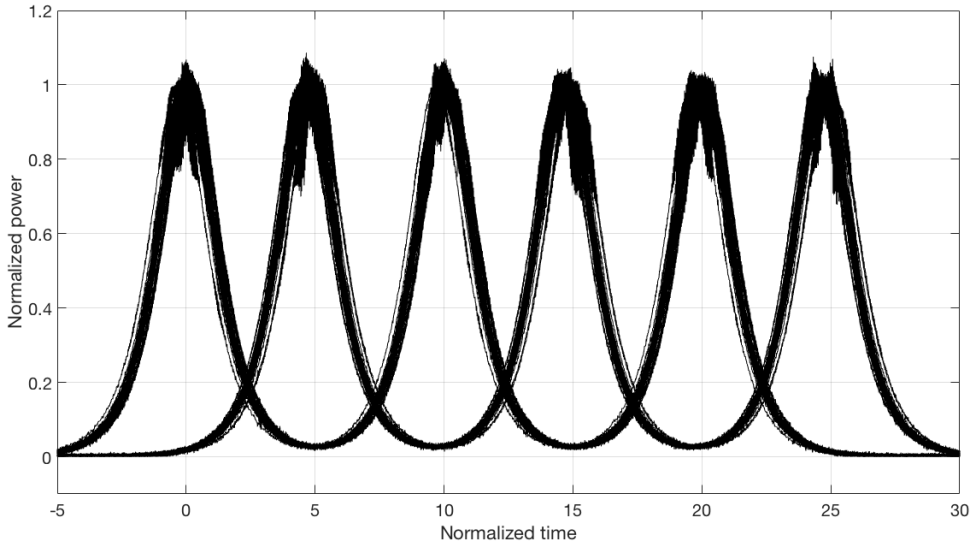

(b) With jitter removal. Eye opening=82.3%.

Figure 7-17: *Received signal (SNR=50 dB) at 20 km.*

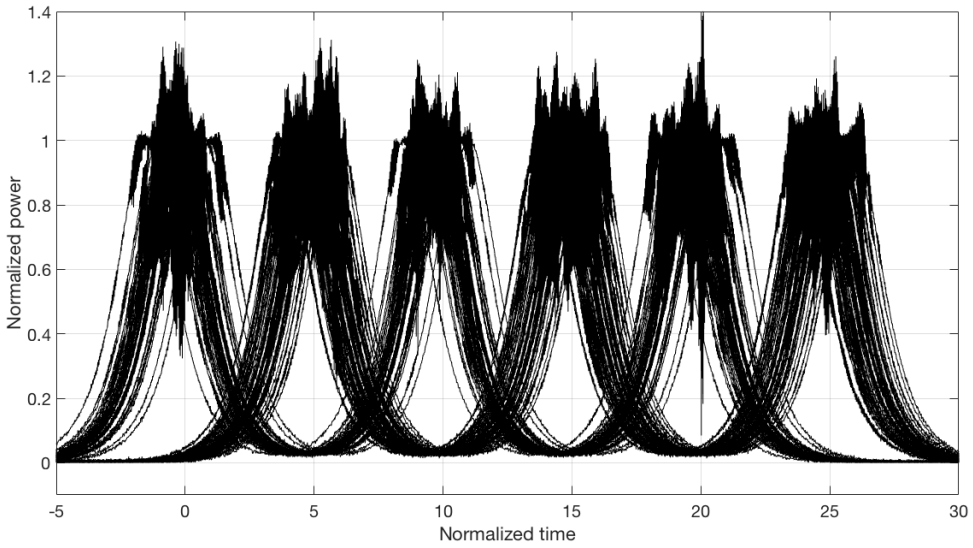

(a) Without jitter removal. Eye opening=59.9%.

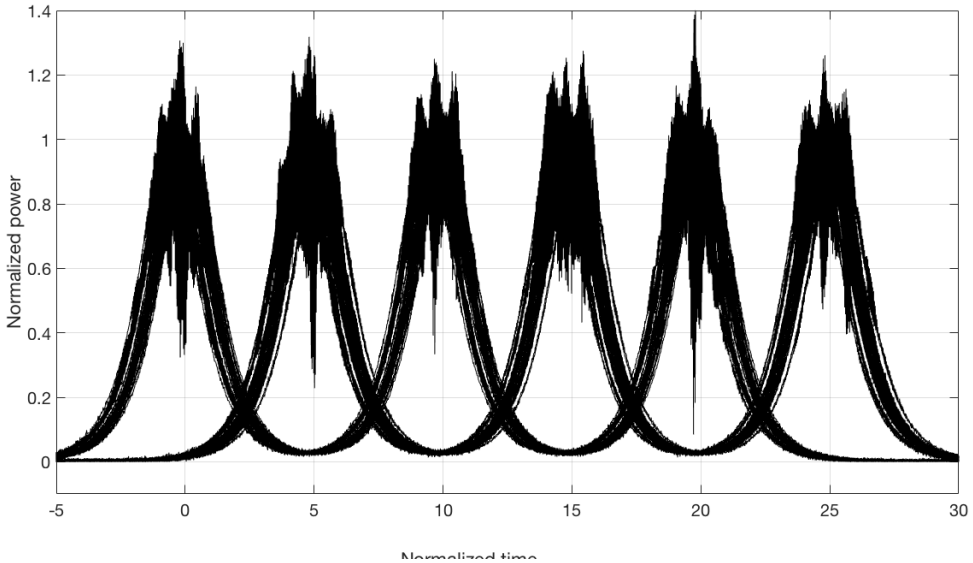

(b) With jitter removal. Eye opening=76.8%.

Figure 7-18: *Received signal (SNR=50 dB) at 30 km.*

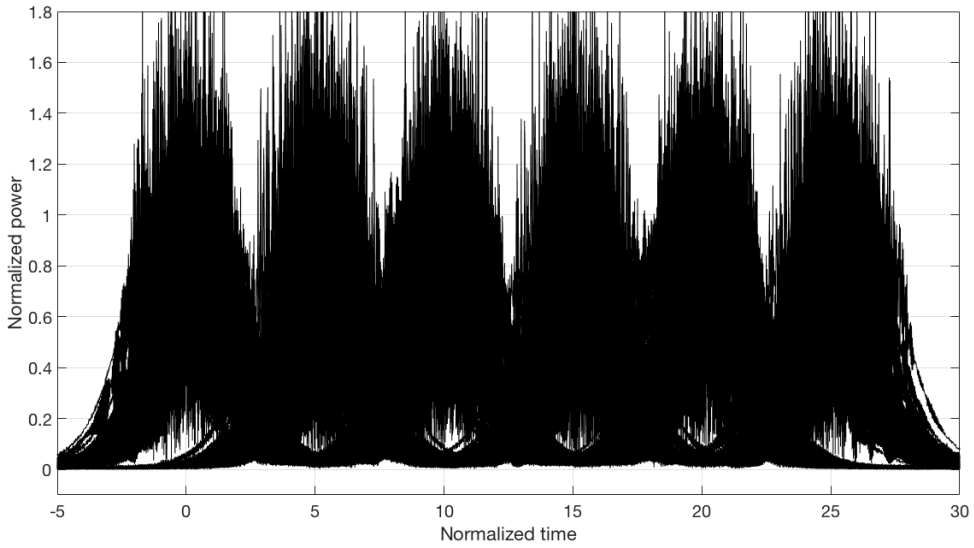

(a) Without jitter removal. Eye closed.

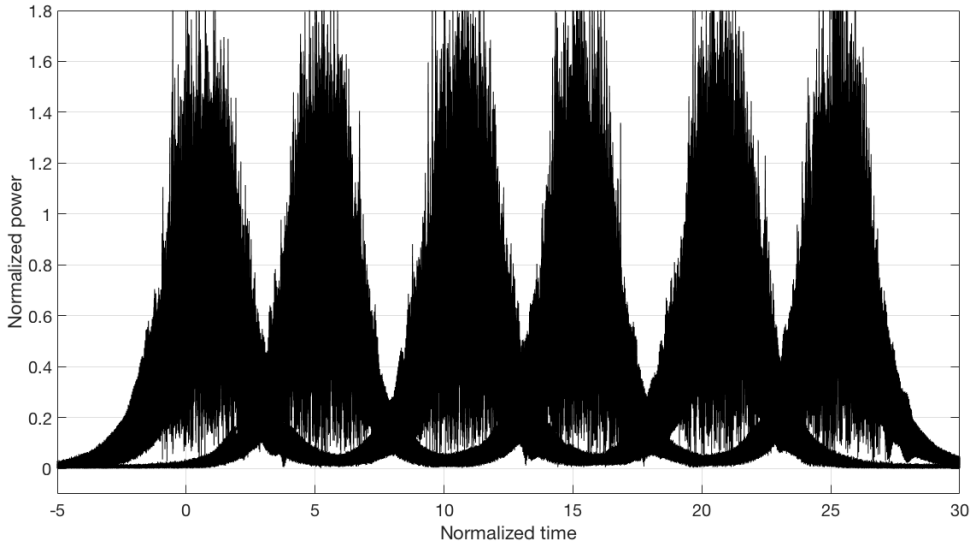

(b) With jitter removal. Eye closed.

Figure 7-19: *Received signal (SNR=50 dB) at 40 km.*

7.5 Discussion

Both PMD and thermal noise will impact the optical eye-opening but there are differences. PMD contributes horizontally by primarily reducing the eye width and thermal noise contributes vertically by primarily reducing the eye height. The effect of both PMD and noise accumulates over distance. As PMD introduces pulse jitter over long integration periods during which several spontaneous changes in PMD occur. The signal degradation from this effective jitter due to PMD quickly becomes dominant for high SNR as the fibre link length increases, with the effect that doped fibre amplifiers will not improve the bit rate performance. While this confirms established knowledge, the proposed eye-diagram approach provides a straightforward method for analysing the effect on PMD on digital signals.

Further, a simple post-reception numerical technique for mitigating the impact of PMD on bit stream using the known PMD statistics of a given optical fibre link has been demonstrated. When the propagation distance increased, the recovery rate can be increased by applying this procedure but the eye-opening still somewhat degraded. There is another interesting phenomenon that needs to be noticed, that there were fluctuations in the peak sections of the signals (i.e. spikes) like noise when the propagation distance increased. This will become a big issue when distance increases and leading to eye closing, and it is 40 km in this case. However, a better algorithm may improve the performance.

7.6 Summary

In this chapter, simulations were run to study the combined effects of PMD and noise. The results were shown in optical eye diagrams and were compared at different SNR level when the propagation distances were fixed, and at different propagation distances when the SNR was fixed. Moreover, a numerical approach of compensating the impact of PMD was provided. The results shown that this approach worked under certain conditions.

CHAPTER 8

COMBINED EFFECTS OF NONLINEARITY AND POLARIZATION MODE DISPERSION

8.1 Background

As discussed in the chapter describing the simulation experiments in the absence of polarization, the signal distortion caused by chromatic dispersion and nonlinearities can be restored by implementing optical phase conjugation (OPC). However, based on the Nonlinear Schrödinger Equations (NLS) (3.41), (3,42) and (3.43), polarization will introduce random factors into the nonlinear sections in these equations. In that case, OPC will no longer be able to restore the signal.

In this chapter, the combined effects of nonlinear and polarization was studied. A signal of 10 Gb/s in the form of hyperbolic secant shaped pulse was launched. Chromatic dispersion, nonlinearities and polarization mode dispersion (PMD) were included. Fibre attenuation and polarization dependent loss (PDL) were not included. Chromatic dispersion was set to $\beta_2 = -17ps/(nm \times km)$, which was the typical value at 1550 nm in ITU G.652 conventional single mode fibre [116]). The value of PMD in each 1 km fibre link was randomly selected from a Maxwellian distribution with mean value of 1 ps^2/km. The nonlinear coefficient was given by $\gamma = |\beta_2|/(P_0 T_0^2)$, where P_0 is the initial peak pulse power and T_0 is the pulse width. The initial pulse power was set to 1 mW. The basic

single mode fibre (SMF) link was set to 2 km (1 km × 2), which was constructed with 2 sections of 1 km SMF link connected with an optical phase conjugation (OPC) component, as shown in Fig. 8-1.

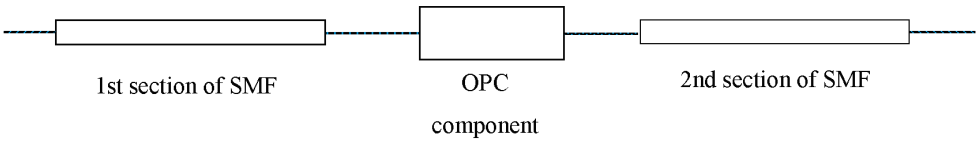

Figure 8-1: *Basic fibre link.*

The fibre specifications of the the fibre links in the following sections are shown in

Table 8.1: *Link specifications.*

Link No.	Input pulse FWHM (ps)	Peak power of input pulse (mW)	Length of 1st section of SMF (km)	Length of 2nd section of SMF (km)	Total link length (km)
1	50	1	1	1	2
2	50	1	10	10	20
3	50	1	25	25	50
4	50	1	50	50	100
5	50	1	100	100	200
6	50	1	200	200	400
7	50	2	50	50	100
8	50	4	50	50	100
9	50	2	100	100	200
10	50	4	100	100	200
11	50	2	200	200	400
12	50	4	200	200	400

8.2 Simulation with Fixed Input Power at Different Propagation Distance

The first set of simulations was run with the input power fixed at 1 mW. The first simulation was run with 2 km, which is the basic SMF link. The results are shown in Fig. 8-2. The result showed that at the mid-point of the fibre link (shown in blue solid line), the two pulse components on X and Y axis (also known as fast and slow pulses) experienced different rates of pulse spreading both in time domain (left column) and frequency domain (right column) due to the combined effects of nonlinearities and PMD. Chromatic dispersion also caused pulse spreading, but based on the NLS mentioned above, it is independent from PMD.

After the second half link, both of the X and Y components of the phase-conjugated pulse were fully recovered (red dashdot line). That included both the effects of chromatic dispersion and the combined effects of nonlinearities and PMD, when PMD was small enough to be neglected.

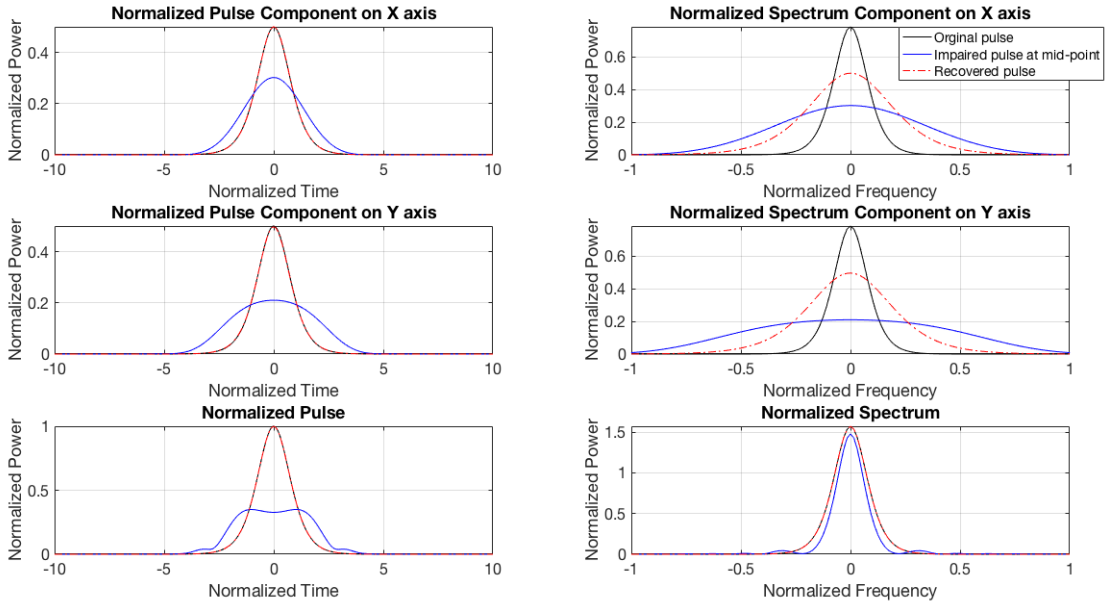

Figure 8-2: *Optical pulse in time domain (left) and frequency domain (right) for link 1 (length=2 km, power=1 mW).*

The following simulations were extending the fibre link while the input pulse power was fixed at 1 mW. The effect of increasing the length of SMF link from 2 km to 20 km is shown in Fig. 8-3. It can be seen that the pulse at the mid-point had been seriously distorted by chromatic dispersion and nonlinearities. However, as the PMD was still relatively small, the OPC could still almost fully recover the pulse at the receiver.

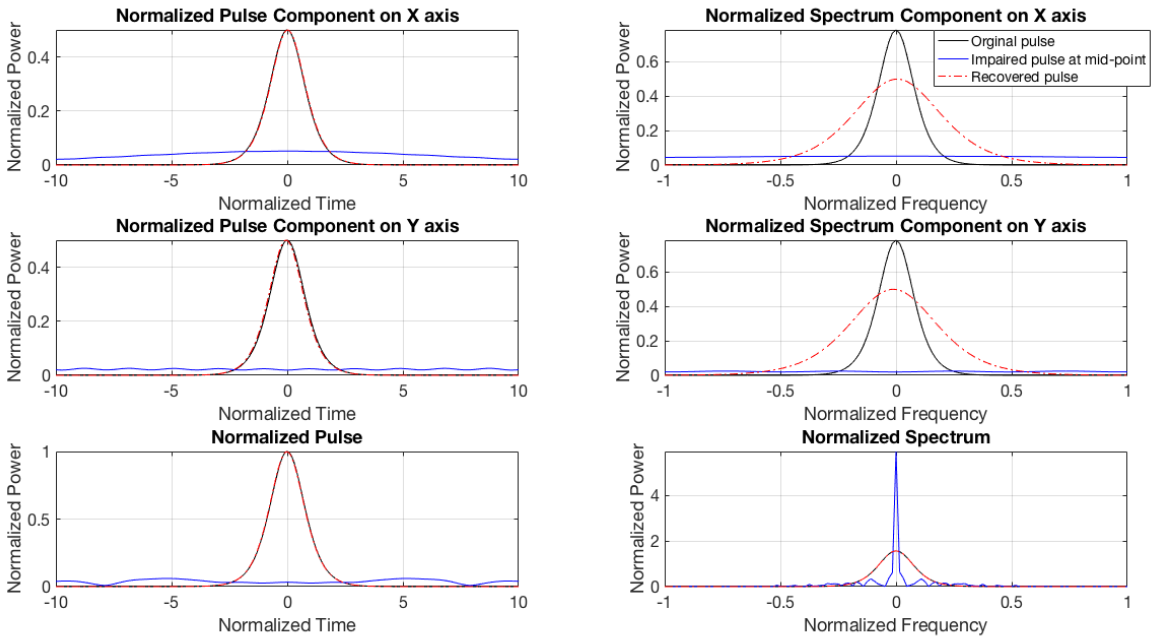

Figure 8-3: *Optical pulse in time domain (left) and frequency domain (right) for link 2 (length=20 km, power=1 mW).*

By increasing the SMF link to 50 km (shown in Fig. 8-4), the pulse shifting of the two components on the two axes of the recovered pulse were slightly observable. This effect was more noticeable in the frequency domain. This was the effect caused by accumulated PMD while the length of fibre link was increased, which was more observable when the fibre link was doubled to 100 km (shown in Fig. 8-5).

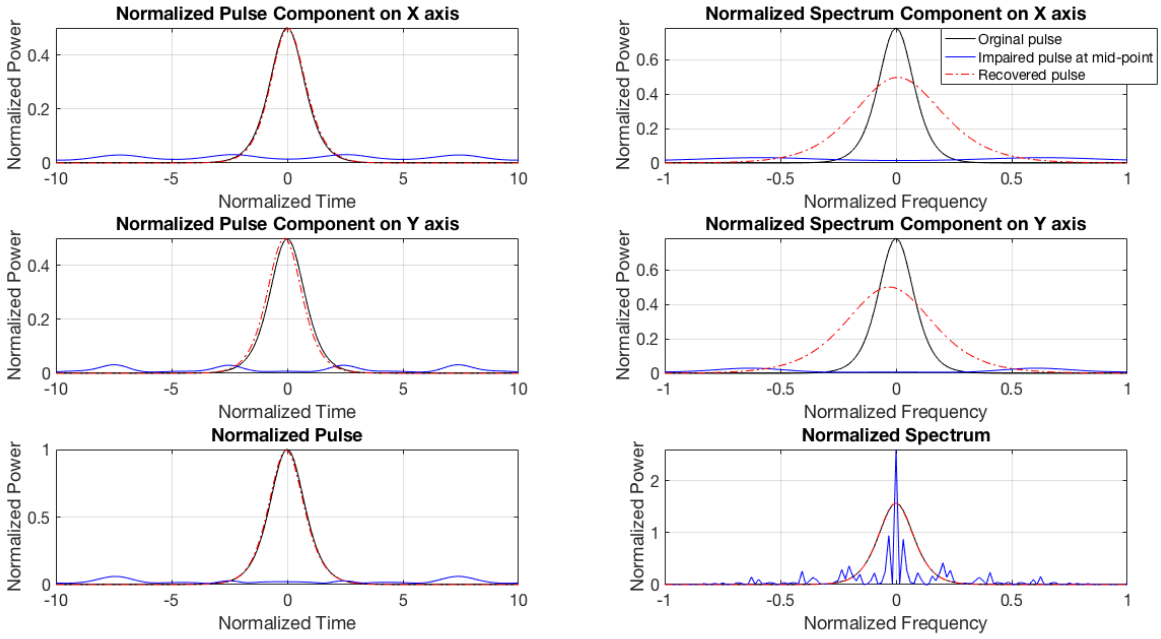

Figure 8-4: *Optical pulse in time domain (left) and frequency domain (right) for link 3 (length=50 km, power=1 mW).*

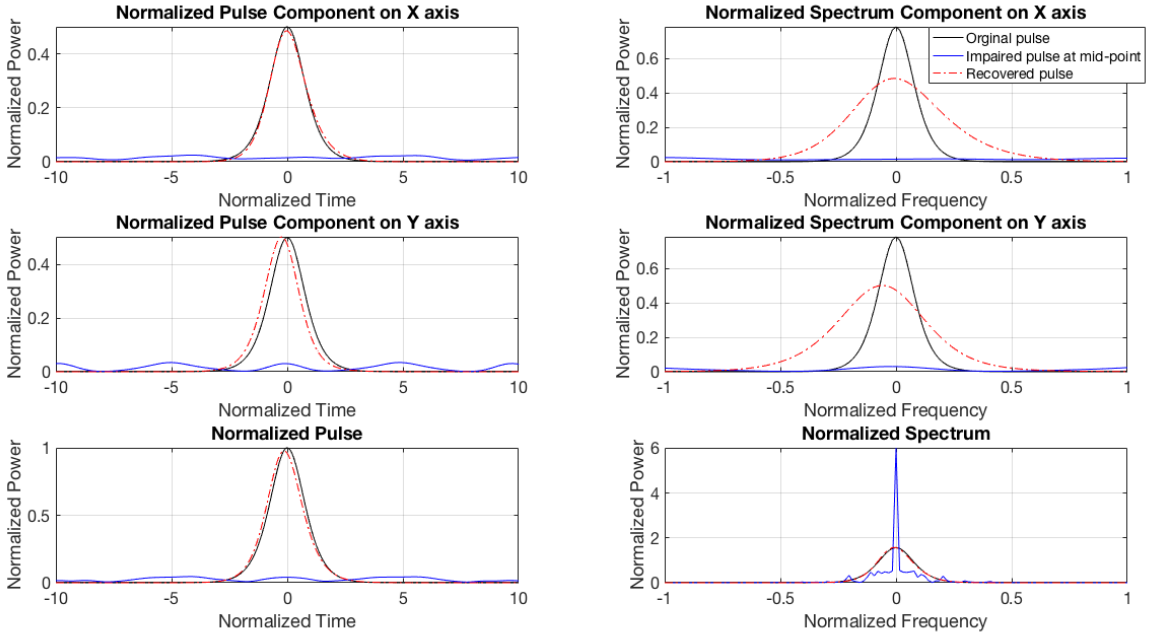

Figure 8-5: *Optical pulse in time domain (left) and frequency domain (right) for link 4 (length=100 km, power=1 mW).*

The effect of further increase in the SMF link to 200 km is shown in Fig. 8-6. The distortion of the pulse becomes more observable and can no longer be neglected. Moreover, a noticeable distortion on the left side of the Y components becomes apparent and a secondary peak begins to emerge on the right of the pulse. After doubling once more the fibre link to 400 km (shown in Fig. 8-7), it could be seen that multiple peaks form on both of the X and Y components in both time domain and frequency domain which lead to severe distortion of the pulse at the receiver end. A similar phenomenon was observed by N. Gisin and B. Huttner [17] as for the combined effects of PMD and PDL, however in simulations described in this chapter PDL was not included. This will be discussed at the end of this chapter.

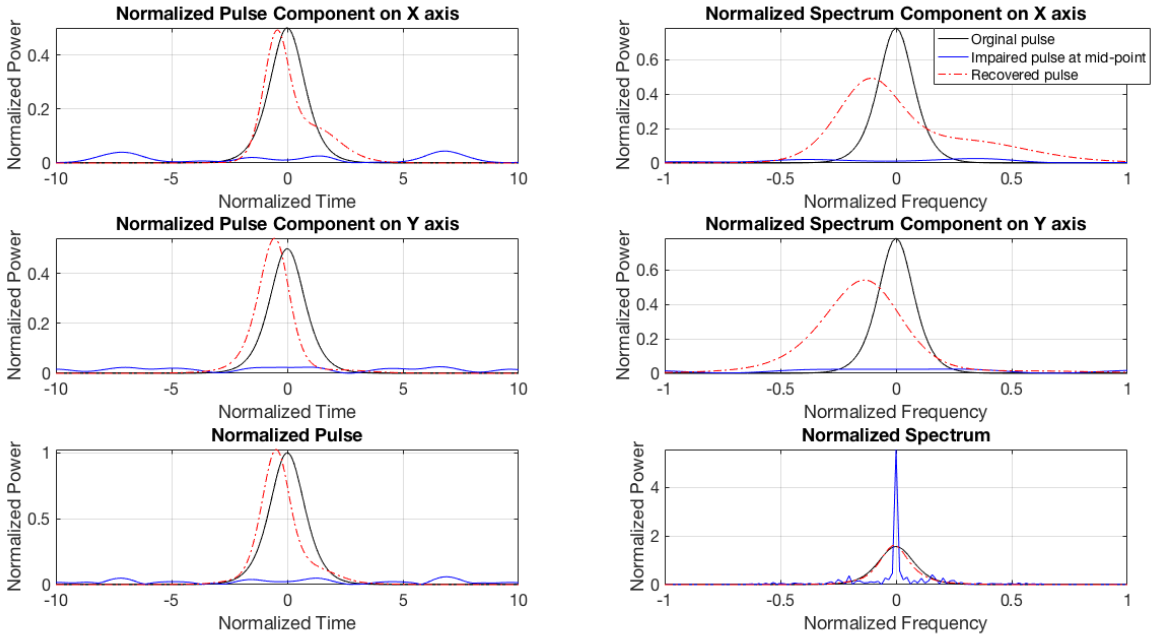

Figure 8-6: *Optical pulse in time domain (left) and frequency domain (right) for link 5 (length=200 km, power=1 mW).*

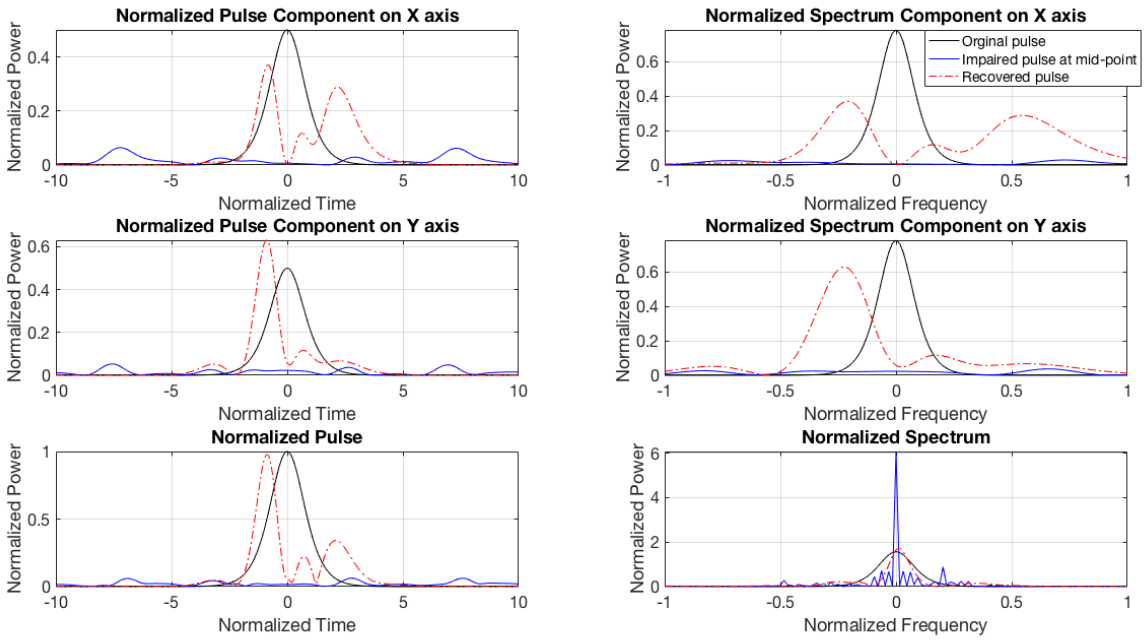

Figure 8-7: *Optical pulse in time domain (left) and frequency domain (right) for link 6 (length=400 km, power=1 mW).*

8.3 Effect of Different Input Power at Different Propagation Distance

Since the nonlinear effect is power-dependent, it is predicted that the combined effects of PMD and nonlinearity will become power-dependent. The simulation started with fibre link of 100 km as this was the minimum link length for which the effect of PMD was observable. The results for $P_0 = 2mW$ and $P_0 = 4mW$ are shown in Fig. 8-8 and 8-9. Comparing with Fig. 8-5, the difference between 2 mW and 1 mW can be ignored but when the power was increased to 4 mW, both of the components of the pulse had smaller pulse width but secondary peaks had formed. Previously this only became observable when the link length has increased to 200 km for an input pulse power of 1 mW. This indicates that higher input power can cause the dominant peak in both the time and frequency domains to narrow, which has the effect of making the PMD look worse.

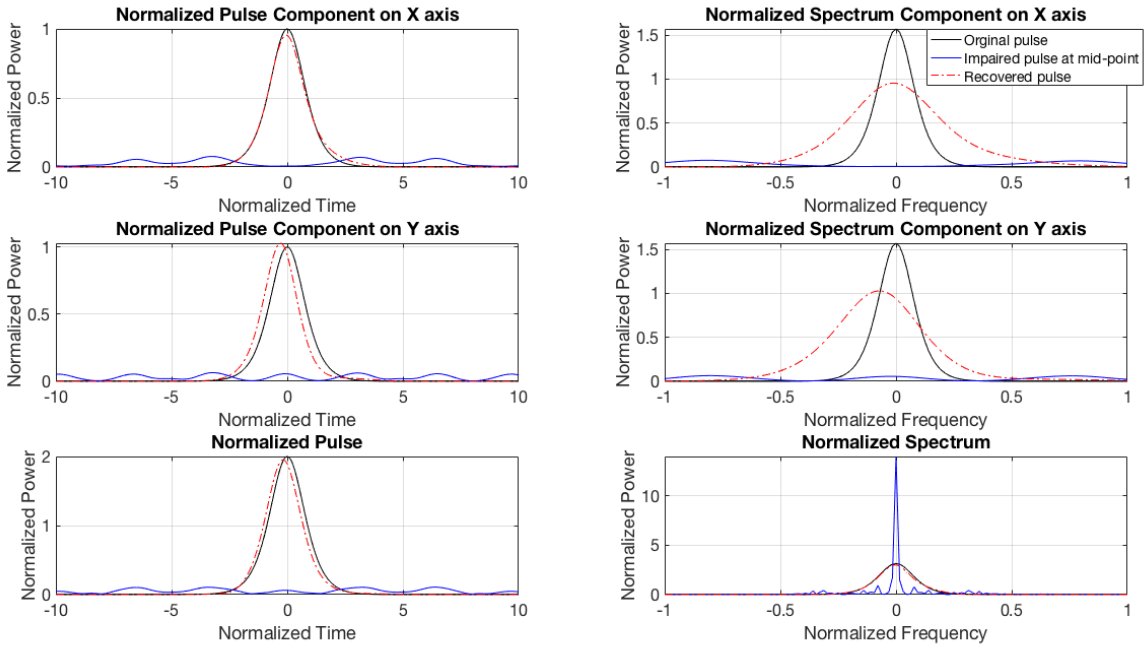

Figure 8-8: *Optical pulse in time domain (left) and frequency domain (right) for link 7 (length=100 km, power=2 mW).*

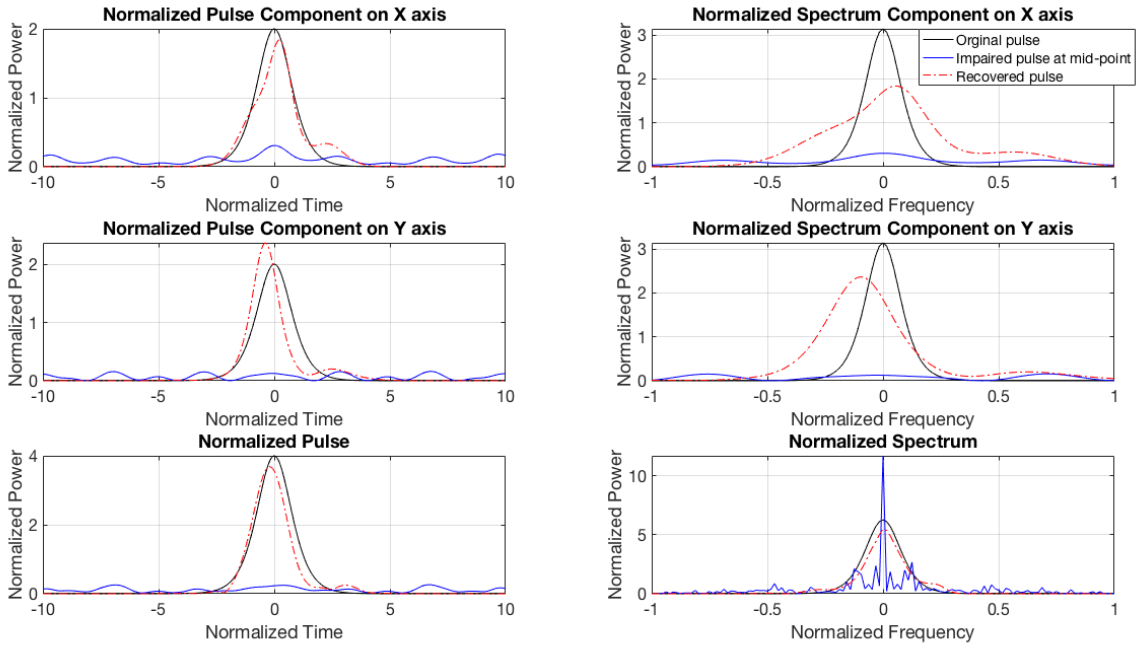

Figure 8-9: *Optical pulse in time domain (left) and frequency domain (right) for link 8 (length=1000 km, power=4 mW).*

The effect of doubling the input power once more to 4 mW for a 200 km link is shown in Fig. 8-10 and 8-11. Comparing with Fig. 8-6, second peaks appeared from 2 mW and became multiple peaks at 4 mW, which confirmed the conclusion made from the results from different input power at 100 km-fibre-link.

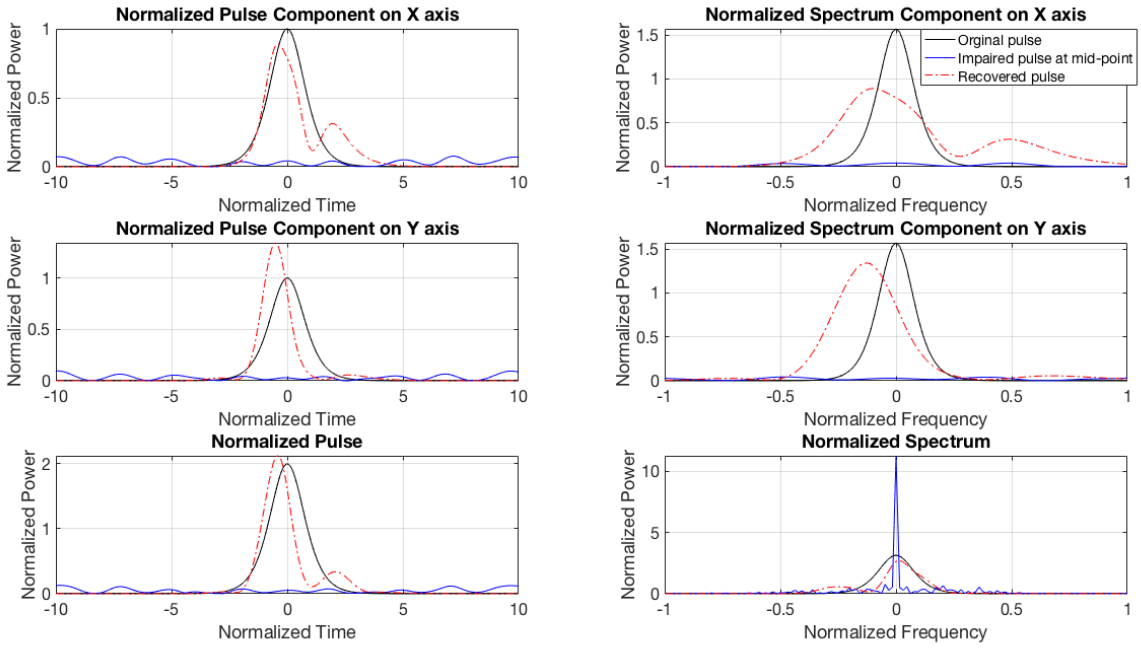

Figure 8-10: *Optical pulse in time domain (left) and frequency domain (right) for link 9 (length=200 km, power=2 mW).*

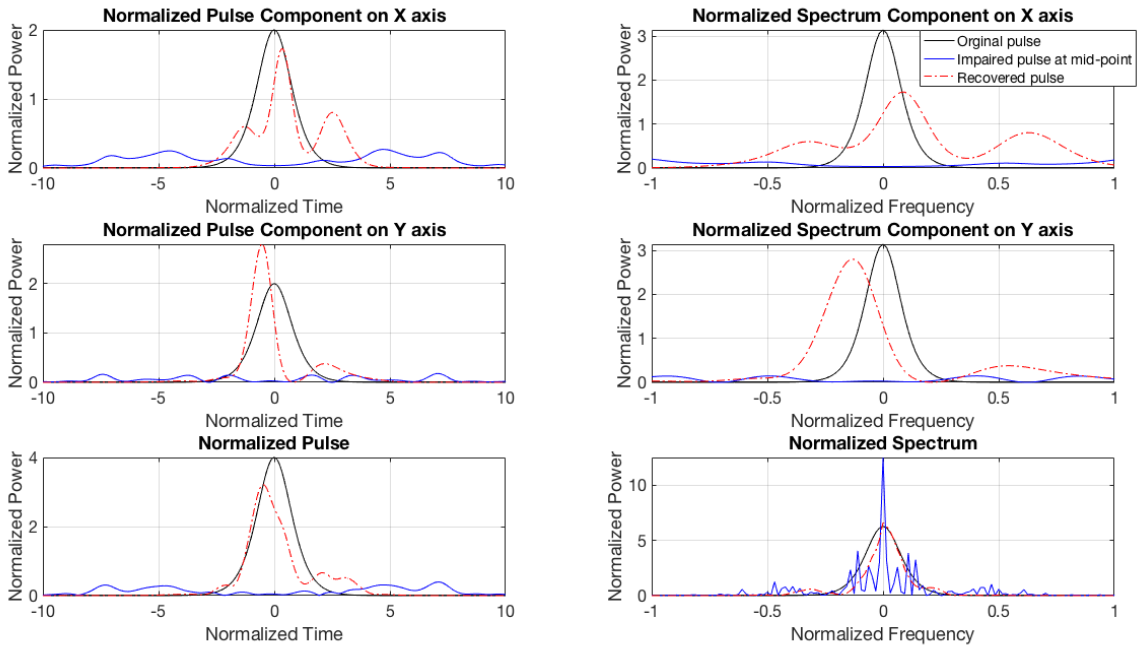

Figure 8-11: *Optical pulse in time domain (left) and frequency domain (right) for link 10 (length=200 km, power=4 mW).*

At 400 km, the pulse at the receiver was distorted into multiple peaks and the peak power dropped to about 70% of its original value when the input power increased to 2 mW. It became worse as the peak power dropped to about 60% of its original when the input power was 4 mW.

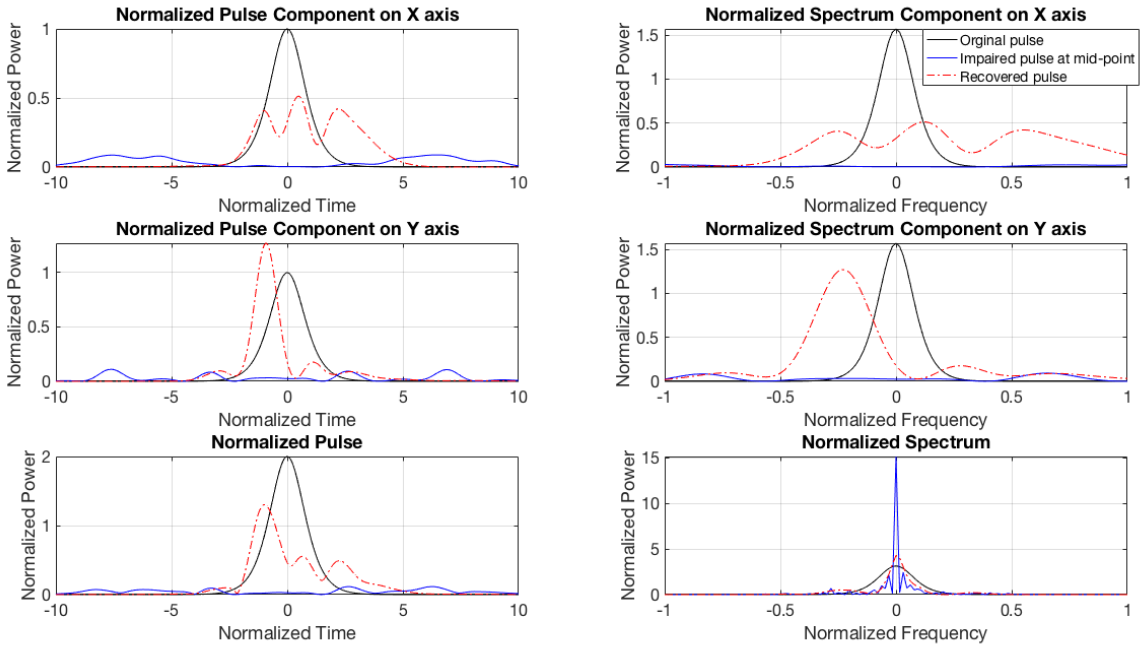

Figure 8-12: *Optical pulse in time domain (left) and frequency domain (right) for link 11 (length=400 km, power=2 mW).*

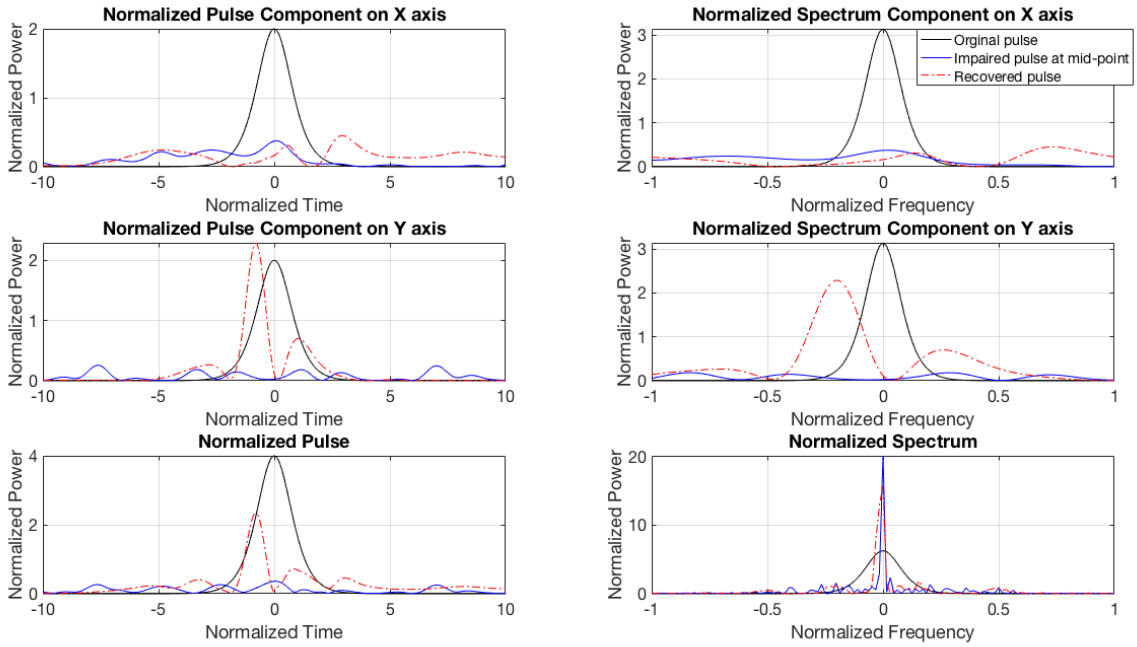

Figure 8-13: *Optical pulse in time domain (left) and frequency domain (right) for link 12 (length=400 km, power=4 mW).*

8.4 Discussion

As observed in Section 8.2, the combined effect of PMD and nonlinearities became severe as the PMD accumulates as the length of the SMF link increases. It is shown here that OPC can compensate the effects of pulse spreading caused by both chromatic dispersion and nonlinearity but it cannot recover the pulse while PMD is large.

Another phenomenon observed and mentioned in Section 8.2 is the combined effect of PMD and nonlinearity cause the pulse spreading into multiple peaks, which also observed in N. Gisin and B. Huttner's research of the combined effects of PMD and PDL. As a result of the combined effect of PMD and PDL, both the tilt angle and the amplitude of the state of polarization are changed, as shown in Fig. 8-14 (a). When PMD is the only polarization factor in the system, such as the simulation environment in this chapter, the angular is changed but the amplitude remains the same, as shown in Fig. 8-14 (b). In this case, if an attenuator with a certain setting was connected after the fibre link, the same result of the combined effect of PMD and PDL can be achieved. That means a section of PDL-free fibre followed by an attenuator can simulate the same result of a section of fibre with both PDL and PMD at the same time. The former setting will simulate the combined effect of PMD and PDL when PMD is the only random variable in the simulation, as long as the PDL statistics required is known. When known, the PDL parameters can be used to set up an attenuator to build a model that simulates the combined effect of nonlinearity and PMD, compared with one that simulates the combined effects of PMD and PDL.

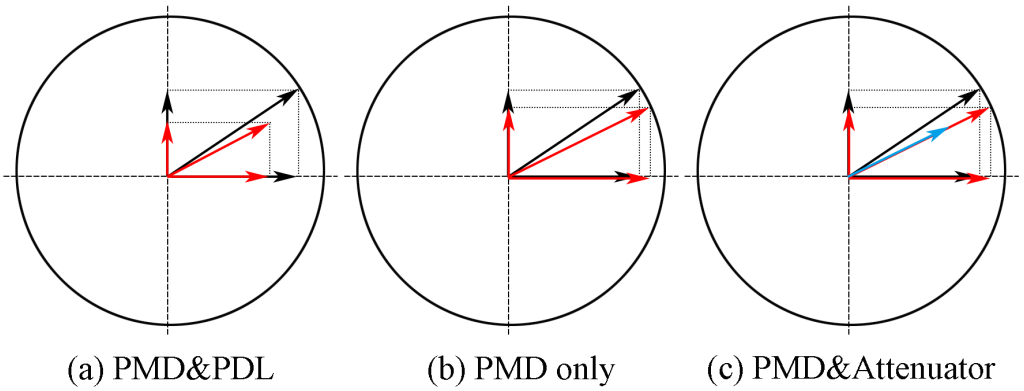

Figure 8-14: *The change of state of polarization under different conditions. (a) is the combined effect of PMD and PDL; (b) is PMD only; (c) is PMD with attenuator.*

As shown in Section 8.3, when the input power increased, the pulse width could be slightly reduced, but there was also a disadvantage that it enhanced the effect of PMD.

8.5 Summary

In this chapter, a simulation was run to study the combined effects of PMD and nonlinearity. A set of simulations were run to determine how accumulated PMD affected the system by varying the fibre link. Another set of simulations were run to determine how the input power affected the combined effects. An assumption based on the results was also provided to achieve the combined effects of PMD and PDL with only PMD components and attenuator.

CHAPTER 9

CONCLUSION AND FURTHER WORK

9.1 Conclusion

In this thesis, methods for analysing the performance limits imposed on optical fibre telecommunications by polarization dependent loss and polarization mode dispersion have been proposed and evaluated. First, a simplified PDL emulator with computer-driven polarization controllers and single mode fibres was built and its performance was evaluated. Polarization controllers are used as polarization components. Each controller has four independent paddles which can be rotated randomly through 180 degrees, so the controllers can provide an arbitrary state of polarization. Seven sections of 15 m-long single mode fibre were deployed as propagation media. The typical PDL value of 10 km single model fibre is less than 0.05 dB. As the fibre link is relatively short (105 m), the fibre can be considered as PDL-free media. Its novelty lies in the reduced number of polarization elements that are needed to achieve an accurate statistical distribution of PDL values.

As discussed in Chapter 5, when the randomness of the state of polarization variation is relatively small, such as in the case of one controller installed, or in the case of the controller's paddles being dependently rotated, the PDL statistics appear as a Gaussian distribution or even a reversed Maxwellian distribution.

The randomness of the state of polarization is increased in two ways. One is to set the paddles to rotate independently at their own random time interval, and the other is to increase the number of polarization controllers in the emulation system. Results show that the increasing of randomness of the state of polarization improves the PDL statistics. It was found that a PDL emulator with more controllers with independently rotated paddles generates a more stable Maxwellian distribution.

Another contribution of this emulator is that it proved that the positions within the link of the polarization components will affect the statistical result of PDL even the total fibre length is the same. This result was first found in the setting of two polarization controllers with 7 sections of 15-metre single mode fibre. Both of the controllers were set to random mode, which gave the emulator a random initial state of polarization. The measurement results show that the PDL mean value increases when the fibre length between the two controllers increases, until the length is approximately equal to the length of the fibre link connecting the second controller to the lightwave multimeter. After reaching the maximum, the PDL mean value starts to decrease when the fibre length between the two controllers keeps increasing.

However, the trend of the PDL value reversed when the first polarization controller was set to manual mode. This condition gave the emulator a fixed initial state of polarization by setting the paddles of the first polarization controller to the maximum value manually. The second polarization controller was still controlled by software in the random mode. Seven sections of 15-metre single mode fibre were deployed. The measurement results show that the PDL mean value decreases when the fibre length between the two controllers increases, until the lengths of the two sections of fibre (the one between the two controllers and the one connecting the second controller with the multimeter) are approximately equal. After reaching the minimum, the PDL mean value starts to increase when the fibre length between the two controllers keeps increasing.

More polarization variation was introduced by adding a third polarization controller into the emulation system. The first polarization controller's paddles were manually set to the maximum value. The second and the third controllers were set to random mode. Seven sections of 15-metre single mode fibre were

deployed. The measurement results confirm that when the input light with a fixed initial state of polarization, the PDL mean value of the system reaches its minimum value when the fibre lengths between each polarization components are approximately equal.

As discussed earlier, the emulator was built to enable a comparison between emulated results of PDL and those of a simulation algorithm and thereby provided a means of assessing the reliability of the latter. It was developed based on the Mueller matrix method, by simulating each of the polarization controller's paddles as a random Mueller matrix. In the simulation for repeating the emulation experiments (short-link fibre communication system), single mode fibre were considered as PDL-free components. With the same parameters as the emulator, the simulation mode gave similar PDL mean values in each case for the emulator with two polarization controllers and three controllers. The simulation results also confirm the trend that the PDL mean value of the system reach its minimum value when the fibre lengths between each polarization components are approximately equal.

The PDL effects of single mode fibre was considered when the simulation model was extended to simulate long fibre links. This excluded cases when optical amplifiers need to be introduced into the system as these introduce polarization dependent gain (PDG). Results show that the PDL does not linearly increase when the transmission distance increases. The typical PDL value of 10 km SMF is less than 0.05 dB, which is basically matched with the simulation result (0.0355 dB). In the simulation of 100 km SMF, one optical amplifier (EDFA) was added into the system. The simulation result is 0.309 dB. By increasing the transmission distance to 1,000 km (with 10 EDFAs), the simulation result is 0.798 dB (early measurement with a similar setting was less than 0.8 dB). By increasing the transmission distance to 7,500 km (with 75 EDFAs), the simulation result is 2.772 dB (early measurement was 2.6 dB). Results show that the PDG introduced by optical amplifiers is able to reduce the total PDL in the system.

An independent pulse propagation simulator was also developed to evaluate the signal distortion caused by chromatic dispersion, nonlinear effects and polarization during optical signal transmission, and the compensation contribution of optical phase conjugation (OPC) method. Results show that the pulse widening

caused by chromatic dispersion and nonlinear effect can be fully recovered with OPC.

After that, the simulator was altered to study the effects of polarization on signal distortion with noise. An optical eye diagram was formed as a measurement of the system performance. Results showed that PMD contributes horizontally by primarily reducing the eye width and thermal noise contributes vertically by primarily reducing the eye height. The effect of both PMD and noise accumulated over distance was quantitatively analysed.

In order to compensate the effect of PMD, a numerical approach was also provided. It works well to reduce the pulse jitter introduced by PMD to enlarge the eye width, but does not work on the closing of eye height introduced by noise.

This simulator was also altered to study the combined effects of nonlinearity and PMD. It revealed that when PMD is large enough, either accumulated over distance or introduced initially, the combined effect can distort the pulse which prevents OPC from recovering the pulse. It also reveals that increasing input power can slightly reduce the effect of nonlinearity but it can also enhance the effect of PMD.

9.2 Further Work

In the real communication systems, PMD and PDL are introduced by multiple environment factors. On one hand, the physical environment factors will lead to the external twisting and bending on fibre, which is emulated in this thesis. On the other hand, the temperature variation will lead to the internal tense variation of the fibre.

The variation of polarization in this emulator is only provided by the polarization controllers. That means the randomness of the polarization is temperature-irrelevant. In the next stage, it is recommended to introduce thermal devices to add temperature variation to the part or the whole fibre links. This will provide a more similar environment to the real systems and may be able to reduce the use of the number of the polarization controllers.

The simulation model of pulse propagation can be optimised in two ways. First, by introducing more factors, it can be used to research the combined effects between polarization with loss, gain and so on. The study can be carried on with both EDFAs and Raman amplifiers (RAs). The former has been simulated in the PDL simulation mode, which is proved to be a contribution to PDL. However, the amplified pulse of EDFAs is asymmetrical which means OPC is less effective in this case. On the other hand, RAs amplify a much better symmetrical pulse, which is a big advantage when OPC is applied.

By introducing a virtual polarization mode dispersion (PMD) compensation device, it can be used to study the compensation methods of PMD. This will required a reliable PMD measurement algorithm as well.

The simulation of the combined effect of PMD and PDL can be carried out by replacing the normal fibre with a combination of PDL-free fibre with attenuator. This may achieve the same results by reducing the random factor from 2 (PDL and PMD) to 1 (PMD only). The PDL's contribution can be simulated with the attenuator as long as the PDL statistics is know.

Another aspect of the PDL emulation and simulation that can be addressed is that SMF can be replaced by polarization-maintain fibre (PMF). Since PMF maintains the state of polarization during lightwave propagation, it will be easier to focus on the PDL variation of the polarization components.

BIBLIOGRAPHY

[1] V. Alwayn, "Fiber-optic technologies," *Retrieved March*, vol. 12, p. 2012, 2004.

[2] R. Ramaswami, "Optical fiber communication: From transmission to networking," *Communications Magazine, IEEE*, vol. 40, no. 5, pp. 138–147, 2002.

[3] F. Idachaba, D. U. Ike, and O. Hope, "Future trends in fiber optics communication," in *Proceedings of the World Congress on Engineering*, vol. 1, pp. 2–4, 2014.

[4] G. P. Agrawal, *Fiber-optic communication systems*, vol. 222. John Wiley & Sons, 2010.

[5] R. E. Nahory, T. P. Pearsall, and M. A. Pollack, "Growth and operation of a step-graded ternary iii-v heterojunction pn diode photodetector," Nov. 30 1976. US Patent 3,995,303.

[6] E. I. Ackerman and C. H. Cox, "Rf fiber-optic link performance," *Microwave Magazine, IEEE*, vol. 2, no. 4, pp. 50–58, 2001.

[7] E. Desurvire, D. Bayart, B. Desthieux, and S. Bigo, *Erbium-doped fiber amplifiers: Device and System Developments*, vol. 2. Wiley-Interscience, 2002.

[8] J.-P. Laude, *Wavelength division multiplexing*. Prentice-Hall, 1993.

[9] K. Fukuchi, T. Kasamatsu, M. Morie, R. Ohhira, T. Ito, K. Sekiya, D. Ogasahara, and T. Ono, "10.92-tb/s (273 x 40-gb/s) triple-band/ultra-dense wdm optical-repeatered transmission experiment," in *Optical Fiber Communication Conference*, Optical Society of America, 2001.

[10] A. Sano, H. Masuda, Y. Kisaka, S. Aisawa, E. Yoshida, Y. Miyamoto, M. Koga, K. Hagimoto, T. Yamada, T. Furuta, *et al.*, "14-tb/s (140 x 111-gb/s pdm/wdm) csrz-dqpsk transmission over 160 km using 7-thz bandwidth extended l-band edfas," in *Proceedings of ECOC*, vol. 6, pp. 1–2, 2006.

[11] R. Malhotra, S. Singh, H. Singh, and P. K. Luthra, "Analysis of intensity modulation and switched fault techniques for different optical fiber cables," *Computer and Information Science*, vol. 4, no. 5, p. p36, 2011.

[12] J. R. Taylor, *Optical solitons: theory and experiment*, vol. 10. Cambridge University Press, 1992.

[13] H. Kogelnik, R. M. Jopson, and L. E. Nelson, "Polarization-mode dispersion," *Optical Fiber Telecommunications IVB*, pp. 725–861, 2002.

[14] A. Willner and M. Hauer, "PMD emulation," *Journal of Optical and Fiber Communications Reports*, vol. 1, no. 3, pp. 181–200, 2004.

[15] S. Rashleigh and R. Ulrich, "Polarization mode dispersion in single-mode fibers," *Optics Letters*, vol. 3, no. 2, pp. 60–62, 1978.

[16] C. Poole and R. Wagner, "Phenomenological approach to polarisation dispersion in long single-mode fibres," *Electronics Letters*, vol. 22, no. 19, pp. 1029–1030, 1986.

[17] N. Gisin and B. Huttner, "Combined effects of polarization mode dispersion and polarization dependent losses in optical fibers," *Optics Communications*, vol. 142, no. 1, pp. 119–125, 1997.

[18] C. Xie, L. Mollenauer, and L. Moller, "Pulse distortion induced by polarization-mode dispersion and polarization-dependent loss in lightwave transmission systems," *Photonics Technology Letters, IEEE*, vol. 15, pp. 1073–1075, August 2003.

[19] L. Yan, B. Zhang, X. S. Yao, and A. Willner, "All-fiber PMD emulator with reduced number of polarization controllers between sections," in *Optical Fiber Communication Conference*, Optical Society of America, 2007.

[20] I. Lima Jr, R. Khosravani, P. Ebrahimi, E. Ibragimov, A. Willner, and C. Menyuk, "Polarization mode dispersion emulator," in *Optical Fiber Communication Conference, 2000*, vol. 3, pp. 31–33, IEEE, 2000.

[21] R. Noe, D. Sandel, M. Yoshida-Dierolf, S. Hinz, V. Mirvoda, C. Glingener, E. Gottwald, C. Scheerer, G. Fischer, T. Weyrauch, *et al.*, "Polarization mode dispersion compensation at 10, 20, and 40 gb/s with various optical equalizers," *Journal of lightwave Technology*, vol. 17, no. 9, p. 1602, 1999.

[22] J. Damask, "A programmable polarization-mode dispersion emulator for systematic testing of 10 gb/s PMD compensators," in *Optical Fiber Communication Conference, 2000*, vol. 3, pp. 28–30, IEEE, 2000.

[23] M. Hauer, Q. Yu, E. Lyons, C. Lin, A. Au, H. Lee, and A. E. Willner, "Electrically controllable all-fiber PMD emulator using a compact array of thin-film microheaters," *Lightwave Technology, Journal of*, vol. 22, no. 4, pp. 1059–1065, 2004.

[24] L. Yan, M. Hauer, Y. Shi, X. S. Yao, P. Ebrahimi, Y. Wang, A. E. Willner, and W. Kath, "Polarization-mode-dispersion emulator using variable differential-group-delay (DGD) elements and its use for experimental importance sampling," *Journal of lightwave technology*, vol. 22, no. 4, p. 1051, 2004.

[25] J. Damask, P. Myers, A. Boschi, and G. Simer, "Demonstration of a coherent PMD source," *Photonics Technology Letters, IEEE*, vol. 15, no. 11, pp. 1612–1614, 2003.

[26] T. G. Philbin, "Making geometrical optics exact," *Journal of Modern Optics*, vol. 61, no. 7, pp. 552–557, 2014.

[27] D. Keck, "Fundamentals of optical waveguide fibers," *IEEE Communications Magazine*, vol. 23, no. 5, pp. 17–22, 1985.

[28] M. Eve, "Multipath time dispersion theory of an optical network," *Optical and quantum electronics*, vol. 10, no. 1, pp. 41–51, 1978.

[29] A. W. Snyder and J. Love, *Optical waveguide theory*. Springer Science & Business Media, 2012.

[30] M. J. Adams, *An introduction to optical waveguides*, vol. 14. Wiley New York, 1981.

[31] P. Diament, *Wave transmission and fiber optics*. Macmillan, 1990.

[32] J. A. Arnaud, *Beam and fiber optics*. Elsevier, 2012.

[33] J. C. Palais, *Fiber optic communications*. Prentice Hall Englewood Cliffs, 1988.

[34] G. P. Agrawal, *Nonlinear fiber optics*. Springer, 2000.

[35] G. N. Watson, *A treatise on the theory of Bessel functions*. Cambridge university press, 1995.

[36] D. Marcuse, *Theory of Dielectric Optical Waveguides*. Academic press, 2012.

[37] J. A. Buck, *Fundamentals of optical fibers*. John Wiley & Sons, 2004.

[38] Y.-R. Shen, "The principles of nonlinear optics," *New York, Wiley-Interscience, 1984, 575 p.*, vol. 1, 1984.

[39] P. M. Morse and H. Feshbach, *Methods of theoretical physics*. Technology Press, 1946.

[40] J. P. Gordon, "Theory of the soliton self-frequency shift," *Optics letters*, vol. 11, no. 10, pp. 662–664, 1986.

[41] K. J. Blow and D. Wood, "Theoretical description of transient stimulated raman scattering in optical fibers," *IEEE Journal of Quantum Electronics*, vol. 25, no. 12, pp. 2665–2673, 1989.

[42] P. Mamyshev and S. V. Chernikov, "Ultrashort-pulse propagation in optical fibers," *Optics letters*, vol. 15, no. 19, pp. 1076–1078, 1990.

[43] S. V. Chernikov and P. V. Mamyshev, "Femtosecond soliton propagation in fibers with slowly decreasing dispersion," *JOSA B*, vol. 8, no. 8, pp. 1633–1641, 1991.

[44] A. W. Snyder and J. Love, *Optical waveguide theory*, vol. 190. Springer, 1983.

[45] T. Li, *Optical Fiber Communications: Fiber Fabrication*. Academic Press, 1985.

[46] D. Marcuse, "Light transmission optics," 1972.

[47] G. P. Agrawal and M. Potasek, "Nonlinear pulse distortion in single-mode optical fibers at the zero-dispersion wavelength," *Physical Review A*, vol. 33, no. 3, p. 1765, 1986.

[48] W. B. Davenport, W. L. Root, *et al.*, *An introduction to the theory of random signals and noise*. IEEE press New York, 1987.

[49] F. N. H. Robinson, "Noise and fluctuations in electronic devices and circuits," *Oxford, Clarendon Press, 1974. 252 p.*, vol. 1, 1974.

[50] N. Bloembergen, *Nonlinear optics*. World Scientific, 1996.

[51] P. N. Butcher and D. Cotter, *The elements of nonlinear optics*, vol. 9. Cambridge University Press, 1991.

[52] R. W. Boyd, "Nonlinear optics," 1992.

[53] C. R. Menyuk and A. Galtarossa, *Polarization mode dispersion*, vol. 1. Springer, 2005.

[54] C. De Angelis, A. Galtarossa, G. Gianello, F. Matera, and M. Schiano, "Time evolution of polarization mode dispersion in long terrestrial links," *Lightwave Technology, Journal of*, vol. 10, no. 5, pp. 552–555, 1992.

[55] P. Wai and C. Menyak, "Polarization mode dispersion, decorrelation, and diffusion in optical fibers with randomly varying birefringence," *Lightwave Technology, Journal of*, vol. 14, no. 2, pp. 148–157, 1996.

[56] R. G. Manohari and T. Sabapathi, "Analysis and reduction of polarization mode dispersion in an optical fiber," in *Recent Advancements in Electrical, Electronics and Control Engineering (ICONRAEeCE), 2011 International Conference on*, pp. 438–441, IEEE, 2011.

[57] O. Yurduseven, "PMD fundamentals and a general review of PMD compensation techniques," in *Telecommunications Forum (TELFOR), 2011 19th*, pp. 1612–1615, IEEE, 2011.

[58] J. Gordon and H. Kogelnik, "PMD fundamentals: Polarization mode dispersion in optical fibers," *Proceedings of the National Academy of Sciences*, vol. 97, no. 9, pp. 4541–4550, 2000.

[59] R. C. Jones, "A new calculus for the treatment of optical systems," *JOSA*, vol. 31, no. 7, pp. 500–503, 1941.

[60] B. L. Heffner, "Automated measurement of polarization mode dispersion using jones matrix eigenanalysis," *Photonics Technology Letters, IEEE*, vol. 4, no. 9, pp. 1066–1069, 1992.

[61] D. Penninckx and V. Morénas, "Jones matrix of polarization mode dispersion," *Optics Letters*, vol. 24, no. 13, pp. 875–877, 1999.

[62] A. Orlandini and L. Vincetti, "A simple and useful model for jones matrix to evaluate higher order polarization-mode dispersion effects," *Photonics Technology Letters, IEEE*, vol. 13, no. 11, pp. 1176–1178, 2001.

[63] H. Kogelnik, L. Nelson, J. Gordon, and R. Jopson, "Jones matrix for second-order polarization mode dispersion," *Optics Letters*, vol. 25, no. 1, pp. 19–21, 2000.

[64] V. Musara, W. T. Ireeta, L. Wu, and A. W. Leitch, "Polarization dependent loss complications on polarization mode dispersion emulation," *Optik-International Journal for Light and Electron Optics*, vol. 124, no. 18, pp. 3774–3776, 2013.

[65] W. H. McMaster, "Polarization and the stokes parameters," *American Journal of Physics*, vol. 22, no. 6, pp. 351–362, 1954.

[66] H. Dong, P. Shum, M. Yan, J. Zhou, G. Ning, Y. Gong, and C. Wu, "Generalized mueller matrix method for polarization mode dispersion measurement in a system with polarization-dependent loss or gain," *Optics express*, vol. 14, no. 12, pp. 5067–5072, 2006.

[67] Y. Zhu, E. Simova, P. Berini, and C. P. Grover, "A comparison of wavelength dependent polarization dependent loss measurements in fiber gratings," *IEEE Transactions on Instrumentation and Measurement*, vol. 49, no. 6, pp. 1231–1239, 2000.

[68] J. N. Damask, "Properties of polarization-dependent loss and polarization-mode dispersion," *Polarization Optics in Telecommunications*, pp. 297–384, 2005.

[69] L. E. Nelson, C. Antonelli, A. Mecozzi, M. Birk, P. Magill, A. Schex, and L. Rapp, "Statistics of polarization dependent loss in an installed long-haul wdm system," *Opt. Express*, vol. 19, pp. 6790–6796, Mar 2011.

[70] A. Mecozzi and M. Shtaif, "The statistics of polarization-dependent loss in optical communication systems," *IEEE Photonics Technology Letters*, vol. 14, no. 3, pp. 313–315, 2002.

[71] B. Huttner, C. Geiser, and N. Gisin, "Polarization-induced distortions in optical fiber networks with polarization-mode dispersion and polarization-dependent losses," *IEEE Journal of Selected Topics in Quantum Electronics*, vol. 6, no. 2, pp. 317–329, 2000.

[72] C. D. Poole and J. Nagel, "Polarization effects in lightwave systems," *Optical Fiber Telecommunications IIIA*, pp. 114–161, 1997.

[73] C. Gardiner, *Stochastic methods*. Springer-Verlag, Berlin–Heidelberg–New York–Tokyo, 1985.

[74] C. Sulem and P.-L. Sulem, *The nonlinear Schrödinger equation: self-focusing and wave collapse*, vol. 139. Springer, 1999.

[75] T. Kato, "Nonlinear schrödinger equations," in *Schrödinger operators*, pp. 218–263, Springer, 1989.

[76] E. M. Dianov, P. Mamyshev, and A. Prokhorov, "Nonlinear fiber optics," *Quantum electronics*, vol. 18, no. 1, pp. 1–15, 1988.

[77] G. Agrawal, *Applications of nonlinear fiber optics*. Access Online via Elsevier, 2001.

[78] R. A. Fisher, *Optical phase conjugation*. Access Online via Elsevier, 1983.

[79] V. V. Shkunov and B. I. Zeldovich, "Optical phase conjugation," *Scientific American*, vol. 253, pp. 54–59, 1985.

[80] A. Yariv, D. Fekete, and D. M. Pepper, "Compensation for channel dispersion by nonlinear optical phase conjugation," *Optics Letters*, vol. 4, no. 2, pp. 52–54, 1979.

[81] A. Corchia, C. Antonini, A. D'Ottavi, A. Mecozzi, F. Martelli, P. Spano, G. Guekos, and R. Dall'Ara, "Mid-span spectral inversion without frequency shift for fiber dispersion compensation: a system demonstration," *Photonics Technology Letters, IEEE*, vol. 11, no. 2, pp. 275–277, 1999.

[82] A. Mecozzi, G. Contestabile, F. Martelli, L. Graziani, A. D'Ottavi, P. Spano, R. Dall'Ara, J. Eckner, F. Girardin, and G. Guekos, "Optical spectral inversion without frequency shift by four-wave mixing using two pumps with orthogonal polarization," *Photonics Technology Letters, IEEE*, vol. 10, no. 3, pp. 355–357, 1998.

[83] A. technologies, *Agilent 83433A Lightwave Transmitter User's Guide*.

[84] A. technologies, *Agilent 11894A Polarisation Controller User, Programming and Service Guide*.

[85] H. Packard, *Operating and Programming manual HP8153A Lightwave Multimeter*, second ed.

[86] G. Foschini and C. Poole, "Statistical theory of polarization dispersion in single mode fibers," *Lightwave Technology, Journal of*, vol. 9, no. 11, pp. 1439–1456, 1991.

[87] F. Curti, B. Daino, G. De Marchis, and F. Matera, "Statistical treatment of the evolution of the principal states of polarization in single-mode fibers," *Lightwave Technology, Journal of*, vol. 8, no. 8, pp. 1162–1166, 1990.

[88] F. Bruyere, "Impact of first-and second-order PMD in optical digital transmission systems," *Broadband Superhighway: Noc'96*, vol. 1, p. 312, 1996.

[89] J. M. Hammersley, D. C. Handscomb, and G. Weiss, "Monte carlo methods," *Physics today*, vol. 18, p. 55, 1965.

[90] M. J. Meyer, "Monte carlo simulation with java and c+," 2003.

[91] A. Doucet, N. De Freitas, N. Gordon, *et al.*, *Sequential Monte Carlo methods in practice*, vol. 1. Springer New York, 2001.

[92] D. Pathria and J. L. Morris, "Pseudo-spectral solution of nonlinear schrödinger equations," *Journal of Computational Physics*, vol. 87, no. 1, pp. 108–125, 1990.

[93] L. R. Watkins and Y. R. Zhou, "Modeling propagation in optical fibers using wavelets," *Lightwave Technology, Journal of*, vol. 12, no. 9, pp. 1536–1542, 1994.

[94] M. Ismail and S. Alamri, "Highly accurate finite difference method for coupled nonlinear schrödinger equation," *International Journal of Computer Mathematics*, vol. 81, no. 3, pp. 333–351, 2004.

[95] T. R. Taha and M. J. Ablowitz, "Analytical and numerical aspects of certain nonlinear evolution equations iv. numerical, modified korteweg-de vries equation," *Journal of Computational Physics*, vol. 77, no. 2, pp. 540–548, 1988.

[96] R. Hardin and F. Tappert, "Siam rev," *Chronicle*, vol. 15, p. 423, 1973.

[97] J. W. Cooley and J. W. Tukey, "An algorithm for the machine calculation of complex fourier series," *Mathematics of computation*, vol. 19, no. 90, pp. 297–301, 1965.

[98] M. Feit, J. Fleck Jr, and A. Steiger, "Solution of the schrödinger equation by a spectral method," *Journal of Computational Physics*, vol. 47, no. 3, pp. 412–433, 1982.

[99] Agilent Technologies, *Polarization-dependent loss measurements using modular test system configurations*, 1996. 11896-2.

[100] M. Taylor, "Observation of new polarization dependence effect in long haul optically amplified system," *IEEE photonics technology letters*, vol. 5, no. 10, pp. 1244–1246, 1993.

[101] Y. Sun, I. T. Lima, H. Jiao, J. Wen, H. Xu, H. Ereifej, G. M. Carter, and C. R. Menyuk, "Study of system performance in a 107-km dispersion-managed recirculating loop due to polarization effects," *IEEE Photonics Technology Letters*, vol. 13, no. 9, pp. 966–968, 2001.

[102] H. Haunstein and H. Kallert, "Influence of PMD on the performance of optical transmission systems in the presence of PDL," in *Optical Fiber Communication Conference*, p. WT4, Optical Society of America, 2001.

[103] S. Jansen, D. Van Den Borne, P. Krummrich, S. Spalter, G.-D. Khoe, and H. De Waardt, "Long-haul dwdm transmission systems employing optical phase conjugation," *IEEE journal of selected topics in Quantum electronics*, vol. 12, no. 4, pp. 505–520, 2006.

[104] J. Jiang, D. Richards, S. Oliva, P. Green, and R. Hui, "PMD and PDL monitoring of traffic-carrying transatlantic fibre-optic system," *Electronics Letters*, vol. 45, no. 2, p. 123, 2009.

[105] L. E. Nelson, C. Antonelli, A. Mecozzi, M. Birk, P. Magill, A. Schex, and L. Rapp, "Statistics of polarization dependent loss in an installed long-haul wdm system," *Optics express*, vol. 19, no. 7, pp. 6790–6796, 2011.

[106] L. E. Nelson, G. Zhang, M. Birk, C. Skolnick, R. Isaac, Y. Pan, C. Rasmussen, G. Pendock, and B. Mikkelsen, "A robust real-time 100g transceiver with soft-decision forward error correction [invited]," *Journal of Optical Communications and Networking*, vol. 4, no. 11, pp. B131–B141, 2012.

[107] Agilent Technologies, *Polarization-dependent loss measurements using modular test system configurations*. Product Note 11896-2.

[108] R. Hardin, "Applications of the split-step fourier method to the numerical solution of nonlinear and variable coefficient wave equations," *SIAM rev.*, no. 15, p. 423, 1973.

[109] R. A. Fisher and W. K. Bischel, "Numerical studies of the interplay between self-phase modulation and dispersion for intense plane-wave laser pulses," *Journal of Applied Physics*, vol. 46, no. 11, pp. 4921–4934, 1975.

[110] T. R. Taha and M. I. Ablowitz, "Analytical and numerical aspects of certain nonlinear evolution equations. ii. numerical, nonlinear schrödinger equation," *Journal of Computational Physics*, vol. 55, no. 2, pp. 203–230, 1984.

[111] L. Zhang and Q. Chang, "A conservation numerical scheme for nonlinear schrödinger equation," *Chin. J. Comput. Phys.*, vol. 16, no. 16, pp. 661–668, 1999.

[112] J. Lee, D. Jung, C. Kim, and Y. Chung, "Osnr monitoring technique using polarization-nulling method," *Photonics Technology Letters, IEEE*, vol. 13, pp. 88–90, January 2001.

[113] Y. Lize, L. Jeng-Yuan Yang, S. Christen, A. Xiaoxia Wu, R. Nuccio, F. Teng Wu, F. Willner, F. Kashyap, and F. Seguin, "Simultaneous and independent monitoring of osnr, chromatic and polarization mode dispersion for nrz-ook, dpsk and duobinary," pp. 1–3, IEEE, March 2007.

[114] L.-S. Yan, X. Yao, Y. Shi, and A. Willner, "Simultaneous monitoring of both optical signal-to-noise ratio and polarization-mode dispersion using polarization scrambling and polarization beam splitting," *Lightwave Technology, Journal of*, vol. 23, pp. 3290–3294, October 2005.

[115] J. Lee, H. Choi, S. Shin, and Y. Chung, "A review of the polarization-nulling technique for monitoring optical-signal-to-noise ratio in dynamic wdm networks," *Lightwave Technology, Journal of*, vol. 24, pp. 4162–4171, November 2006.

[116] "Characteristics of a single-mode optical fibre and cable," tech. rep., Telecommunication standardization sector of ITU, June 2005.